1997

Characterization of Monomer-Containing Monolayer Films on Au Surfaces.

Robert J. Willicut
Louisiana State University and Agricultural & Mechanical College

INFORMATION TO USERS

This manuscript has been reproduced from the microfilm master. UMI films the text directly from the original or copy submitted. Thus, some thesis and dissertation copies are in typewriter face, while others may be from any type of computer printer.

The quality of this reproduction is dependent upon the quality of the copy submitted. Broken or indistinct print, colored or poor quality illustrations and photographs, print bleedthrough, substandard margins, and improper alignment can adversely affect reproduction.

In the unlikely event that the author did not send UMI a complete manuscript and there are missing pages, these will be noted. Also, if unauthorized copyright material had to be removed, a note will indicate the deletion.

Oversize materials (e.g., maps, drawings, charts) are reproduced by sectioning the original, beginning at the upper left-hand corner and continuing from left to right in equal sections with small overlaps. Each original is also photographed in one exposure and is included in reduced form at the back of the book.

Photographs included in the original manuscript have been reproduced xerographically in this copy. Higher quality 6" x 9" black and white photographic prints are available for any photographs or illustrations appearing in this copy for an additional charge. Contact UMI directly to order.

UMI

A Bell & Howell Information Company
300 North Zeeb Road, Ann Arbor MI 48106-1346 USA
313/761-4700 800/521-0600

CHARACTERIZATION OF MONOMER-CONTAINING MONOLAYER FILMS ON Au SURFACES

A Dissertation

Submitted to the Graduate Faculty of the
Louisiana State University and
Agricultural and Mechanical College
in partial fulfillment of the
requirements for the degree of
Doctor of Philosophy

in

The Department of Chemistry

by
Robert J. Willicut
B.S., Angelo State University, 1992
December, 1997

Dedication

This thesis is dedicated to:

my mom, Mary Douglas

my dad, Gary Douglas

my sister, Christine Willicut

you are all living proof of what can be done with the support of a loving family

to my lovely and talented wife,

Jenny

your support, love, and endurance made it happen

to my little boy,

Jeffrey Ryan

you make this work a little less important - and rightly so

And to my adopted mom,

Linda Dickson

Acknowledgements

It is a privilege to acknowledge the part that my research advisor, Robin McCarley, has played in the successful completion of this thesis. His wisdom, intelligence, and more importantly, his foresight, have all contributed greatly to the exposure that I and this work have received. I feel that I know a great deal more about specific, perhaps even esoteric, areas of chemistry due to my stay at LSU under Rob. Most important, though, I have been given the confidence in my own abilities to explore any area - a gift applicable not just to research, but to every aspect of life.

I have been truly blessed with wonderful friends and acquaintances while pursuing this degree. Chief among them are James Flanagan, Daryl Williams, and Jack Davies. Without you guys, I would probably have finished, but certainly not with the depth of experience and happiness I enjoy today. Thank you all for the fishing trips, barbecues, tailgate parties, late night parties, and crucial support that comes from an intimate understanding of a graduate students' life. Wherever I go, there will never be another king's hour.

The faculty and staff in the chemistry department have also contributed in great measure to the completion my project. Barbara, Dawn, Danielle, Wanda, Benn, Letty and the rest of the office crew: you made it ten times easier to get things done. You will always deserve better wherever you go. The analytical professors: you've built (and are still building) a vigorous new program - thank you for making it easier to find a job.

Dr. Mark McLaughlin and Dr. Alfonso Davila: thank you both for helping a synthetically-challenged analytical chemist at the dawn of his stay here - I wouldn't have been able to clear the gate without your help. Tracy McCarley deserves special thanks for her help with Mass Spectroscopy issues and for her effortless ability to cheer me up just by talking. (soon to be Dr.) Melissa Cameron: thank you for watching "da baby," and loaning me your husband for the occaisonal fishing trip - remember Kirk, "chicks dig the car."

Many other friends have made the stay here enjoyable. I would like to thank the McCarley group: Sonya Caston, C.J. DuBois, Ben Boussert, Paul Moberg, Cory Schomburg, Alyssa Henry, and Dave Dunaway (retired). It looks like we all learned something from each other. It's all about "group."

Table of Contents

List of Tables

List of Figures

List of Abbreviations

$(CH)_x$	poly(acetylene)
$(SN)_x$	poly(sulfurnitride)
11-SOL	11-hydroxyundecanethiol
2,5-PyC_6SH	2,5-dimethyl-ω-(*N*-pyrrolyl)hexanethiol
ATR-IR	attenuated total reflectance infrared spectroscopy
AuO_x	gold oxide
CFM	chemical force microscopy
CME	chemically modified electrode
δ	in-plane deformation mode (in infrared spectroscopy)
DCM	dichloromethane
DMF	dimethyl formamide
DMSO	dimethyl sulfoxide
E_{bias}	electrical bias between tip and sample (in STM)
ECP	electrically conducting polymer
$E_{faradaic}$	electrical bias needed to initiate reaction (in STM)
EI	electron ionization
EtOH	absolute ethanol
Fc	ferrocene
FTIR	fourier transform infrared
GC	gas chromatography

GC/MS	gas chromatograph/mass spectrometer
HF	hydrofluoric acid
IR	infrared
IRE	internal reflection element
IRRAS	infrared reflection-absorption spectroscopy
L-B	Langmuir-Blodgett
LFM	lateral force microscopy
MeCN	acetonitrile
MS	mass spectra
OCP	organic conducting polymer
PC	propylene carbonate
Ph_3P	triphenyl phosphine
PyC_xSH	ω-(*N*-pyrrolyl)alkanethiol
$PyC_{10}SH$	ω-(*N*-pyrrolyl)decanethiol
$PyC_{10}S/Au$	$PyC_{10}SH$-modified Au surface
PyC_6SH	ω-(*N*-pyrrolyl)hexanethiol
PyC_6S/Au	PyC_6SH-modified Au surface
PyC_5SH	ω-(*N*-pyrrolyl)pentanethiol
PyC_5S/Au	PyC_5SH-modified Au surface
Q	charge (in cyclic voltammetry)
RA	reflection-absorption
SA	self-assembly

SAM	self-assembled monolayer
SCE	saturated calomel electrode
SEM	scanning electron microscopy
SPM	scanning probe microscopy
SSCE	sodium saturated calomel electrode
STM	scanning tunneling microscopy
TBAP	tetra-n-butyl ammonium perchlorate
TIC	total ion chromatogram
TLC	thin layer chromatography
υ	stretching mode (in infrared spectroscopy)
VRA-RMA	versatile reflection accessory with retro-mirror attachment
ω	out-of-plane deformation mode (in infrared spectroscopy)
XPS	X-ray photoelectron spectroscopy
$X_{pyrrole}$	mole fraction of pyrrole-containing molecule in solution

Abstract

Exploration into the nature of ultrathin, surface-confined films capable of electronic conduction has been the primary purpose of this dissertation. Specifically, the confinement of pyrrole monomer to Au surfaces through organosulfur linkages has been investigated. The synthesis of these new ω-(*N*-pyrrolyl)alkanethiols is described herein. Cyclic voltammetry was utilized in this work to polymerize the monolayers and characterize the resulting films. Voltammetric analysis yielded currents in the correct potential region for poly(*N*-alkylpyrrole) charging/discharging. Other electrochemical studies revealed the ability of strong nucleophiles and electroinactive diluents to quench surface-confined polymer formation though they did not affect oxidation of the monomer. Exchange experiments performed with an electroactive thiol in solution indicated a much higher degree of monolayer stability to desorption *after* electrochemical polymerization of the monolayer.

Infrared reflection-absorption spectroscopy (IRRAS) and X-ray photoelectron spectroscopy (XPS) were used to characterize the structural changes in the monolayer upon electrochemical polymerization. Infrared analysis yielded the loss of all pyrrole ring absorbance bands upon polymerization due to changes in the absorption cross-section of the resulting pyrrole units. Additional infrared studies on surface-confined oligomers indicated that some band intensity could be seen for the shorter chains. In agreement with literature reports on bulk species, the infrared intensities of oxidized (conducting) oligomers was higher than undoped oligomers of similar length. IRRAS analysis of the methylene stretching region for the alkane chains showed no change in

band intensity indicating no loss of material from the surface. This was confirmed by integrating nitrogen and sulfur abundances on pristine and electrochemically oxidized surfaces using XPS.

Microscopic investigations were carried out using various scanning probe microscopy (SPM) techniques but were hampered by the sensitivity of these monolayers to oxygen and airborne contaminants. These monolayers were also studied using physical and scanning electron microscopy (SEM) techniques. Pyrrole-terminated SAMs on Au electrodes were found to significantly increase the adhesion of thick poly(pyrrole) films to the electrode surface.

Chapter 1

Ultrathin Films on Au Electrodes

The ultimate goal of this work is to restrict the formation of a conducting polymer to a two-dimensional film in order to control the chemical, physical, and electrical properties of the surface to which it is attached. Our intention is to modify a metal electrode surface with a monomer-containing monomolecular layer and polymerize the monomer units in the film to each other in the absence of additional solution-phase monomer. This work will lead to fundamental insights into the dynamics of the coupling monomers that will allow us to synthetically tailor conducting polymer monolayers for different applications.

1.1 Chemically Modified Electrodes

The field of chemically modified electrodes (CMEs) has been an active area of research since the pioneering work of Hubbard[1] and Murray[2] in the early 1970s. Modification of an electrode is generally performed to enhance or change certain properties of that electrode. CMEs have been utilized[3] in catalysis, sensing, electrochromic displays, and the study of long-distance electron transfer events across dielectric media of controlled thickness. Passivation of metal surfaces to inhibit corrosion is yet another example of the practical uses of CMEs.

Modification of electrode surfaces can be performed to yield surfaces with a variety of chemical functionalities. Deposition of monomer-containing molecules on electrode surfaces is currently an active area of research. The interest in this type of

electrode modification originates from the wide range of useful surface properties encompassed by the resulting polymer films. From the work done so far, the research can be subdivided into different regimes of polymer thickness: thick films (0.05 to 5 μm), thin films (5-50 nm), and ultrathin (monolayer and submonolayer) films. Useful experiments have also been performed with the thicker films (vide infra). The work described in this thesis, though, is primarily concerned with the fabrication and characterization of ultrathin polymer films on an electrode surface in an effort to understand changes in the interfacial properties of a substrate modified with such a film. A strong interest also exists, in this report and others, in exploring the change in properties of a polymer upon going from the bulk material to an ultrathin film with thickness approaching molecular dimensions.

There are two basic ways to coat an electrode with an extremely thin polymer film - deposition of a solution-formed polymer onto an electrode, Figure 1.1, or polymerization of a monomer that has been pre-adsorbed onto the electrode surface, Figure 1.2. The pre-adsorption of a monomer onto an electrode surface produces a highly controlled and well-defined amount of material that is available for polymerization. Further, the regular spatial arrangement of monomeric centers can result in a uniform coating of polymer. Deposition of polymer from solution phase differs in this respect due to the possibility for preferential nucleation and growth of polymer at defect sites on the surface resulting in a discontinuous film (see Figure 1.1).

Upon electrochemical polymerization of solution-phase monomers, the resulting polymer chains can do one of two things. Polymer growth can result in

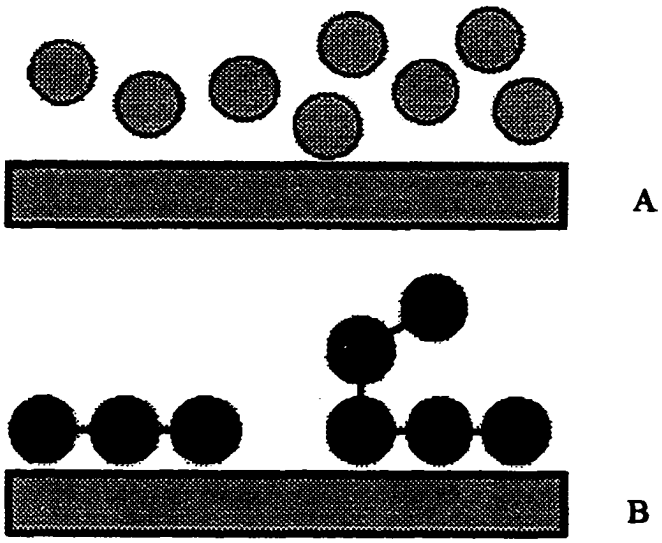

Figure 1.1 **Cartoon depicting polymerization of solution-phase monomer (A) to form a polymeric layer (B) on a smooth surface.**

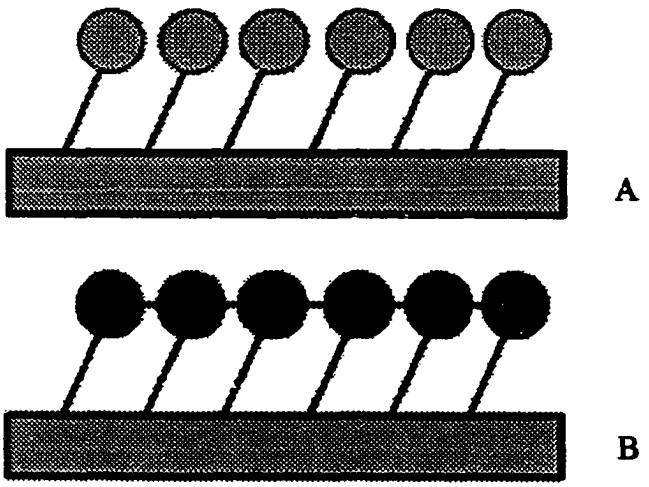

Figure 1.2 **Cartoon depicting polymerization of surface-confined monomer (A) to form a thin polymeric layer (B) on a smooth surface.**

immediate nucleation of the chains on the surface at the point of polymerization or delayed nucleation away from the site of their production. This latter effect is the result of diffusion of the polymer chains away from their activation point until chain growth renders the polymer insoluble and it nucleates on the surface. Behavior of the type described above can complicate the fabrication of polymeric features when extremely small feature sizes are desired. Monomers that have been immobilized on the surface prior to polymerization should prevent this "diffusional broadening." For the aforementioned reasons, we will discuss here the formation of ultrathin polymer films from pre-adsorbed monomer monolayers on metal electrode surfaces.

1.2 Formation of Anchored Organic Monolayers

1.2.1 Langmuir-Blodgett (L-B) Techniques

One way to form monolayer and multilayer assemblies[4] on surfaces is the use of Langmuir-Blodgett (L-B) techniques. L-B techniques utilize amphiphilic molecules spread at a gas/liquid interface (typically air/water) from a solvent that is immiscible with the liquid phase (sub-phase). The disordered amphiphilic layer is compressed together by increasing the surface pressure of the molecules in a special trough to form close-packed assemblies. The molecules can then be transferred to hydrophobic or hydrophilic substrates to form films with various structures.

L-B films benefit from strong interchain interactions that allow films with a high degree of order to be fabricated. One serious drawback of L-B films, however, is their relatively poor adherence to the underlying substrate - an important issue when a thin film device has stringent longevity requirements. Low film adherence also restricts the

use of L-B films in solvents[4] that are able to decrease the interchain interactions and cause removal of the layer(s) from the surface.

1.2.2 Self-Assembly (SA) Techniques

Monolayers can also be formed on solid substrates using a technique called self-assembly. Spontaneous formation of monolayers on solid surfaces can occur if the assembling molecule contains a moiety that can bind strongly to the substrate and another moiety that is capable of undergoing strong intermolecular attractions.[4] The use of self-assembled monolayers[5] (SAMs) has proven to be an excellent way to anchor molecules onto various types of surfaces.[6] One of the most heavily studied of these anchor/substrate combinations is that of organosulfur compounds on Au.[4] The first example of such monolayers was described by Allara and Nuzzo[7] who noted that Au substrates exposed to *n*-alkyl disulfides underwent changes in their surface wettability from a very hydrophilic surface to that resembling a very hydrophobic surface. It was later found that *n*-alkanethiols bind strongly to and self assemble on the coinage metals giving rise to highly ordered monomolecular structures.[8] Au substrates are the most commonly used because sulfur has been shown to bind strongly to Au[4] and Au supports no stable oxide.[9] The degree of packing of the molecules, that is the order of the alkane chains, is dependent on the van der Waals radius of the largest chemical functionality present in the molecule and the lattice spacing of the crystalline substrate. Thus, *n*-alkanethiols (terminal methyl group) yield monolayers on Au that are highly ordered and relatively free of defects.

Alkanethiol SAMs on Au and Ag have been extensively studied due to various fundamental processes that can be explored with their close-packed, fairly rugged structure. Alkanethiols are believed to self assemble onto Au surfaces with the loss of the sulfhydryl proton and subsequent formation of a bond between the sulfur and the metal.[10] The sulfur headgroup forms an adlattice on Au(111) with a $\sqrt{3}$ x $\sqrt{3}$ R30° orientation[11] as shown in the cartoon in Figure 1.3. In order to maximize van der Waals interactions in alkanethiol SAMs on Au(111), the alkane chains are tilted ca. 30° from the surface normal as shown by infrared spectroscopic measurements.[12] The close-packed nature of the molecules has also been shown to passivate the electrode surface[13] thereby lowering the access of solution-phase redox probes to the underlying metal. The potential of organothiol monolayers for the inhibition of corrosion of metal surfaces through a similar mechanism is currently being explored.[14]

1.2.3 Chemically Functionalized Alkanethiol SAMs - Toward Immobilized Monomers

Besides their reproducible and rugged structure, the real strength of SAMs fabricated from thiols on gold is their ability to be synthetically functionalized to form a variety of useful interfaces.[4] A great deal of research has gone into fundamental and technological studies of organothiols containing simple tail groups like -OH, -COOH, and $-CF_3$; all of which are fairly simple extensions of the methyl-terminated thiols. Facile ω-functionalization has allowed for interesting studies involving changes in surface wettability and interfacial effects on lubrication and wear,[15] among many others, to be performed.

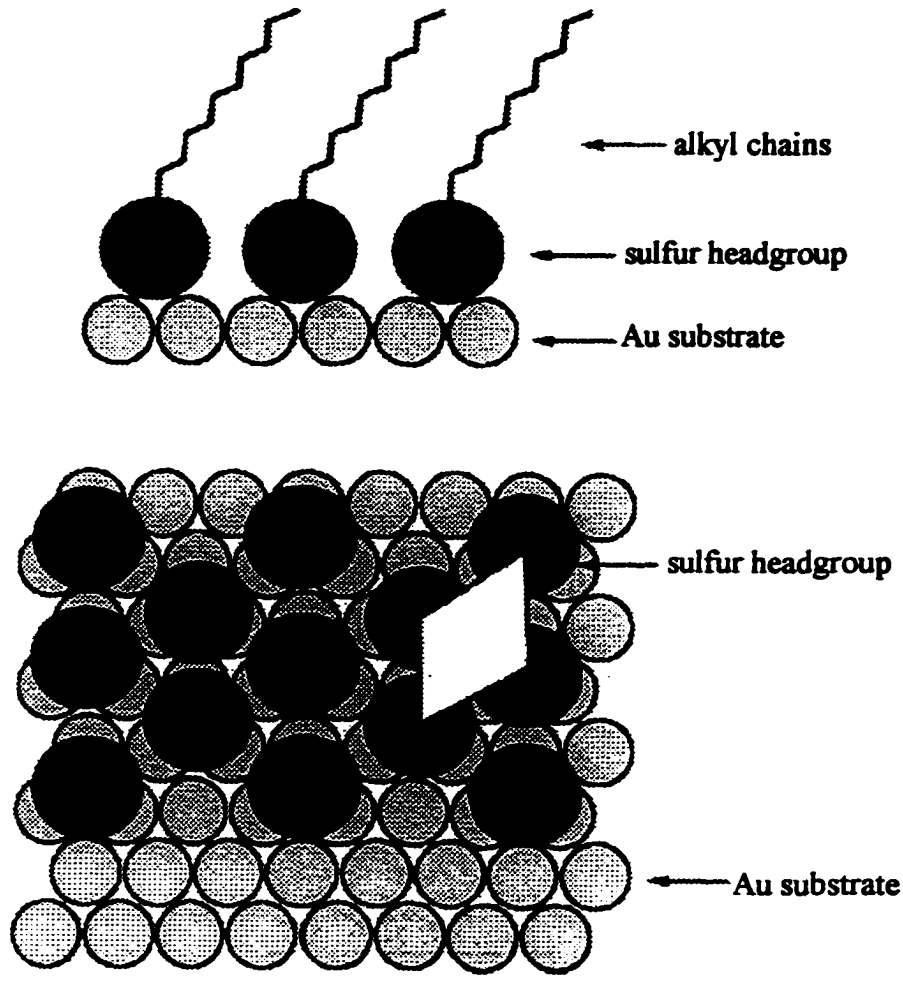

Figure 1.3 **Packing of *n*-alkanethiols on a Au(111) substrate.**

The synthetic modification of alkanethiol SAMs is not limited to the more simple chemical functionalities mentioned above. More exotic endgroups have been attached to alkanethiols in an attempt to achieve certain fundamental and technological goals. The range of endgroups used thus far includes molecules that complex other molecules such as porphyrins[16] and cyclodextrins.[17] These "binding type" monolayers

have been used in investigations of surface-confined donor-acceptor chemistry and as selective redox barriers, respectively. Smaller aromatic functionalities like ferrocene[18] and pyridine[19] have also been used as monolayer endgroups in order to study electron transfer events in controlled environments and as sensors for trace metal determination. There exist many other examples of the complex chemistries that can be developed using synthetic techniques to modify self-assembling molecules.[6]

From the discussion above concerning adsorbed monomers on surfaces, it is logical to synthetically modify an alkanethiol to contain a monomer endgroup. The variety of useful chemical functionalities that can be incorporated into SAMs is extensive in comparison to those moieties that can be used in L-B films. Due to the fact that amphiphilic molecules are required for good L-B film formation, synthetic modification of molecules to create useful properties can sometimes impair their ability to form good films. SAMs of alkanethiols on Au do not suffer in this respect as long as functionalization does not introduce a chemical moiety that can compete strongly with the sulfur for binding sites on the Au surface.

Several interesting monomeric monolayers have already been placed on Au surfaces in an attempt to form ultrathin polymer films. One example is the use of diacetylene-containing organosulfur monolayers.[20] These monolayers have been synthesized by both Batchelder et al.[21] and Kim and Crooks[22] and shown to polymerize laterally upon exposure to UV light.[21] The applications of these poly(diacetylene) monolayers include ultrathin resists for photopatterning[23] and adhesion-enhancing

layers for composite thin films.[24] One of the most useful traits of these types of polymeric films is their excellent resistance to removal from the underlying surface in very harsh environments. This trait would be very important for their use in the fabrication of sensors. A more recent report by Peanasky and McCarley[25] describes the ability of ω-olefin-terminated monolayers to polymerize laterally upon exposure to γ-rays. All of these efforts are excellent proof-of-concept experiments that demonstrate the ability to form ultrathin polymeric layers from immobilized monomer precursors using various protocols for monomer activation.

Formation of nanostructured polymers are another possible application of the types of monolayers discussed above. Polymeric monolayers have the potential to allow the controlled fabrication of stable structures with sizes approaching molecular dimensions. Toward these ends, a monoatomic layer of organic material only 4 Å thick was recently formed by Ozaki et al.[26] from a diacetylene-containing precursor. A layer this thin and contiguous would be extraordinarily difficult to fabricate without using a pre-adsorbed monolayer containing the monomer sites.

The main goal of this thesis is to present work involving the synthesis of monomer-containing electrically conducting polymer (ECP) precursor molecules pre-adsorbed onto an electrode surface and their use in the formation of ultrathin polymer films. In addition to the motivations listed above, ultrathin ECP films could be useful in the formation of conducting features on nanoscopic size scales - a result that has been unattainable by other methods.

1.3 Introduction to and History of Electrically Conducting Polymers

Electrically conducting polymers are generally regarded as non-metallic polymers that exhibit metal-like conductivities. In actuality, most ECPs have conductivity values falling somewhere between metallic conductors and doped semi-conductors (ca. $10^7\ \Omega^{-1}\ cm^{-1}$ to $10^{-1}\ \Omega^{-1}\ cm^{-1}$). Organic and inorganic materials that can conduct electricity have been intensely studied since the 1960s. Many reasons exist, from both fundamental and technological standpoints, for the development and use of materials of this nature. In particular, organic conductors are attractive due to the ability to custom design their electrical properties[27] through synthetic manipulations of their structure. Other reasons for their study include low cost, replacement of environmentally unfriendly conductors (heavy metals) in batteries, and use in applications requiring lightweight or mechanically flexible conducting components.[28] All of these reasons, plus the desire to understand the fundamental physical processes involved in the conduction of electricity in non-metallic systems, have driven this area of research.

Although organic materials completely dominate the ECP field, research in this area actually began with the discovery that the inorganic material poly(sulfurnitride), denoted as $(SN)_x$, was able to conduct electricity.[29] The conductivity value of this material, $2 \times 10^3\ \Omega^{-1}cm^{-1}$, generated significant interest in developing this inorganic polymer as a possible alternative to metallic conductors. Unfortunately, the shortcomings of this material could not be overcome even with the extensive work conducted on $(SN)_x$. The polymeric material and its precursors were explosive, and

many of the gas-phase dopants used to increase the conductivity of the polymer were hazardous chemicals. Probably the most significant problem with this polymer, however, was the inability to synthetically manipulate its structure and therefore its properties.

Soon after the discovery of $(SN)_x$, an *organic* polymer that conducted electricity was developed. Poly(acetylene), denoted as $(CH)_x$, was shown to conduct electricity poorly in 1961,[30] but in 1973 Shirakawa et al. were able to form[31] poly(acetylene) films with higher conductivities and metallic lusters. This accomplishment marked the beginning of an entirely new class of materials called organic conducting polymers (OCPs). An extensive amount of work was performed on poly(acetylene),[32] and in 1977 a method was developed for doping poly(acetylene) to form highly conducting films.[33] Further efforts eventually lead to methods to form poly(acetylene) that pushed its conductivity as high as $10^5\ \Omega^{-1}cm^{-1}$ - a value better than Cu on a volume basis.[34]

Despite the many advantages poly(acetylene) had over the $(SN)_x$ system, problems with the environmental and thermal stability of the doped and undoped polymer proved extremely difficult to overcome. Poly(acetylene), in both the doped and undoped states was found to react irreversibly with H_2O and/or O_2 to form non-conductive products. As a direct result of the intense research on poly(acetylene), a new type of conducting polymer was soon discovered.

In 1979 Diaz and Kanazawa[35] were able to achieve the electroxidative polymerization of pyrrole monomer at a Pt electrode in non-aqueous solvent to form

conductive films that could be removed from the electrode surface. Such films of poly(pyrrole) were found to be highly conductive and mechanically flexible. The electrochemically formed poly(pyrrole) films developed by Diaz and Kanazawa had high conductivities (greater than 100 $\Omega^{-1}cm^{-1}$) and were a shiny blue-black in appearance. This pioneering work built upon previous efforts by Dall'Olio et al.[36] who had found that pyrrole could be oxidized at a Pt electrode in 1M H_2SO_4 to yield a brittle film with a conductivity of 8 $\Omega^{-1}cm^{-1}$. Also, Gardini had discovered[37] in 1973 that pyrrole could be chemically oxidized to form a conducting black powder, now commonly referred to as "pyrrole black."

Although lower in conductivity than poly(acetylene), poly(pyrrole) was perceived as containing greater potential for actual commercial use primarily due to the fact that it had a much higher degree of environmental and thermal stability.[38] The polymer did not thermally degrade until almost 250 °C[39] and was stable for months in air when doped.[27] Research concerned with electrochemically produced poly(pyrrole) films became extraordinarily active in the 1980s when studies on the effects of solvent, electrolyte, monomer concentration, and presence of O_2 and H_2O were carried out. Experiments were also done to form films with a range of conductivities by using pyrrole derivatives[40,41] and co-monomers.[42]

Poly(pyrrole) films, however, had some drawbacks. They were insoluble in virtually all solvents and they were amorphous, making it very difficult to characterize their properties using standard polymer analysis techniques. Investigations into other heteroaromatic compounds as an attempt to solve these problems soon led to polymers

based on thiophenes.[43] Poly(thiophene) was formed in an analogous electroxidative manner to poly(pyrrole) but the oxidation potential of the monomer was much higher,[27] leading to a greater number of defects in the polymer chains. The resulting poly(thiophene) films were about as stable and conductive as poly(pyrrole) films, but their material properties were not superior enough to make them a viable alternative to poly(pyrrole) films for most applications.

Other poly(aromatic) systems were also thoroughly investigated. This research yielded a host of new conducting polymers, including, but not limited to, poly(*p*-phenylene),[44] poly(*p*-phenylene vinylene),[45] poly(*p*-phenylene sulfide),[46] and poly(aniline).[47] Each of these polymers showed promise in different areas, but none of them appeared to be superior to the poly(heterocyclic) polymers.

1.4 Choice of Monomer to be Utilized

Poly(pyrrole) was chosen as the OCP to be investigated in this work for several reasons. With the exception of poly(acetylene), poly(pyrrole) is the most studied of the vast number of OCPs. Much is now known about the mechanism of electronic conduction in poly(pyrrole) although the structure responsible for this conduction is still not well understood. Poly(pyrrole) is also one of the most air-stable OCPs which makes it ideal for constructing a very thin film having a high surface area to volume ratio. Poly(pyrrole) films on electrode surfaces have the advantage over poly(acetylene)-based polymers that doping and de-doping of the polymer can be controlled by more precise electrochemical means. In the work described here, we wish to make monolayers of monomer on Au surfaces and subsequently

electrochemically polymerize them anodically. For the Au substrate that will be used to support and activate the surface-confined monomer monolayer, poly(pyrrole) is superior to poly(thiophene) because the sulfur group in the thiophene ring has been shown to adsorb on gold[48] and possibly compete for alkanethiol adsorption sites. Another important reason to choose poly(pyrrole) over poly(thiophene) is that the oxidation potential needed to activate the thiophene monomer is high enough to induce electroxidative desorption of the thiol from the Au surface[13] as well as cause oxidation of Au.

Another important consideration when monomer choice was being made for this project was that thick, bulk-deposited poly(pyrrole) films had a history of successfully being made or incorporated into technologically important items. Thick poly(pyrrole) films have been used as solid-state battery cathodes,[49] electrolytic capacitors,[50] gas separation membranes,[51] and gas sensors,[52] to name just a few technological applications. Other uses include immobilization of redox centers,[53] controlled ion release,[54] and templates for deposition of minerals.[55] In addition, poly(pyrrole) films aid in the deposition of Cu onto printed circuit boards[56] and have been used in the production of commercially available shapable conducting sheets.[57] It should be stressed that all of these examples utilize relatively thick (μm) poly(pyrrole) films. As previously stated, it will be the purpose of this work to construct ultrathin, *monolayer* films of poly(pyrrole) from a surface-confined monomer.

1.5 Various Confined Polymer Systems

The use of monolayer films of monomers as precursors for *conducting polymer* formation has not been intensively studied. There are only a handful of reports prior to our work described here demonstrating the utility of thin, surface-confined polymer layers on surfaces; *all* of these examples were based on the use of L-B films.[58-60] Previous to the work described here, there had been no reports of the use of a self-assembled monomer monolayer to form conducting polymer *monolayers*.

A few examples were found in the literature concerning surface immobilization of monomers capable of forming conducting polymer monolayers but *all* of these studies focused on the use of these monomer SAMs to modify the characteristics of thicker polymer films subsequently deposited from solution onto the modified surfaces. Monolayers were formed from an alkoxysilane pyrrole[61] and a thiol-terminated 2,5-bis(pyrrolyl)thiophene[62] on Si/SiO_2 and Au surfaces, respectively. Another group reported the use[63] of a monolayer of *p*-aminothiophenol on gold as an effective adhesion promoter for the deposition of bulk poly(aniline). All of these studies focused on the differences in the characteristics of the thick, deposited films and made no attempt to study the monolayer itself to see if conducting polymer could be formed in the restricted plane of the monolayer. That is to say, none of the studies reported successful formation of a conducting polymer monolayer.

Other examples of polymerizations involving ECP monomers in restricted environments are available in the literature. In many ways, the goals of this work share common origins with several other groups currently investigating the synthesis of small

isolated conducting polymer fragments in general, and poly(pyrrole) in particular. The interest in doing this stems from the fact that the way in which the properties of a bulk material change as the amount of material becomes microscopic can be fundamentally and technologically enlightening. An example unrelated to this research area is so-called "quantum dots." These quantum dots are small clusters of semiconductors, such as CdS, that are fabricated in different sizes. As the diameter of the quantum dots falls below ca. 10 nm, the optical properties become dependent on the quantum dot diameter.

Most of the work done on poly(pyrrole) has focused on the synthesis of small, discrete aggregates of polymer. A desire to exert exquisite spatial control over a conducting material, i.e. the formation of "molecular wires," is one reason the work described here and in other labs is being pursued. Another possible focus of this work is learning enough about the formation of tiny conducting polymer deposits so as to control the order of the polymer chains making up the deposit.

Studying the effect that confined polymerizations have on the orientation of the polymer chains (and thus the conductivity and optical properties) within a small deposit has been approached in several ways. Martin's group has focused primarily on the synthesis of poly(pyrrole) and poly(aniline) inside nanoporous membranes of various types and sizes (pores five nm to several hundred nm in diameter).[64] These membranes allow the synthesis of poly(pyrrole) fibrils (solid cylinders) and tubules (hollow cylinders) of controlled diameter. Various analytical techniques were applied to determine that highly ordered poly(pyrrole) chains accounted for various[65] portions of

the fibrils with a resulting increase in conductivity over similarly-sized, but randomly oriented, poly(pyrrole) deposits. Wu et al.[66] have utilized the same type of technique to make poly(pyrrole) strands only 3 nm in diameter - a feat that would be difficult to accomplish without restricting the free volume available for polymerization.

Encapsulation of poly(pyrrole) in zeolite channels to limit polymer deposit size has also been done by Bein and Enzel,[67] Millar et al.,[68] and Larsen et al.[69] Successful polymerization of poly(pyrrole) into these channels was confirmed using various analytical methods. In addition, dissolution of the zeolites with HF resulted in the collection of the deposited polymer followed by subsequent analysis with IR. The collected poly(pyrrole) resembled the bulk compound spectroscopically and had a conductivity of 1×10^{-4} $\Omega^{-1}cm^{-1}$. The above studies are an excellent foray into the construction of "customized" organic conducting polymers for various uses.

The previously described synthesis and characterization of nanometer-sized poly(pyrrole) deposits was motivated by several different factors. One of the largest, though, was the desire to increase the conductivity of poly(pyrrole) through a forced ordering of the polymer chains. A highly conductive poly(pyrrole) deposit is a desirable goal because a highly conductive organic polymer displaying excellent environmental stability has yet to be made.

Technological goals of the work described in this thesis will include enhancing the adhesion of thick poly(pyrrole) films on Au, increasing the stability of monolayers toward premature removal from the surface, and forming templates suitable for the fabrication of nanometer-sized conducting features. Fundamental goals will include

characterizing the structural changes occurring in the film before and after electrochemical polymerization with infrared spectroscopy, scanning probe microscopy techniques, and various other surface analysis techniques. The attempts we have made to synthesize monolayers of monomer, convert the monomer to conducting polymer and characterize the resulting films, along with some applications of those films, follow in the main body of this thesis.

1.6 References

1) Lane, R. F.; Hubbard, A. T. *J. Phys. Chem.* **1973**, *77*, 1401.

2) Moses, P. R.; Wier, L.; Murray, R. W. *Anal. Chem.* **1975**, *47*, 1882.

3) Murray, R. W.; Ewing, A. G.; Durst, R. A. *Anal. Chem.* **1987**, *59*, 379A.

4) Ulman, A. *An Introduction to Ultrathin Organic Films from Langmuir-Blodgett to Self-Assembly*; Academic: San Diego, 1991.

5) Bigelow, W. C.; Pickett, D. L.; Zisman, W. A. *J. Coll. Sci.* **1946**, *1*, 513.

6) Zhong, C.-J.; Porter, M. D. *Anal. Chem.* **1995**, *67*, 709A.

7)Nuzzo, R. G.; Allara, D. L. *J. Am. Chem. Soc.* **1983**, *105*, 4481.

8) Whitesides, G. M.; Laibinis, P. E. *Langmuir* **1990**, *6*, 87.

9) Somorjai, G. A. *Chemistry in Two Dimensions - Surfaces*; Cornell University Press: Ithaca, NY, 1982.

10) Widrig, C. A.; Chung, C.; Porter, M. D. *J. Electroanal. Chem.* **1991**, *310*, 335.

11) Camillone, N.; Chidsey, C. E. D.; Liu, G.-Y.; Scoles, G. *J. Phys. Chem.* **1993**, *98*, 3503.

12) Porter, M. D.; Bright, T. B.; Allara, D. L.; Chidsey, C. E. D. *J. Am. Chem. Soc.* **1987**, *109*, 3559.

13) Finklea, H. O.; Avery, S.; Lynch, M.; Furtsch, T. *Langmuir* **1987**, *3*, 409.

14) Feng, Y.; Teo, W.-K.; Siow, K.-S.; Gao, Z.; Tan, K.-L.; Hsieh, A.-K. *J. Electrochem. Soc.* **1997**, *144*, 55.

15) Ulman, A. *Chemtech* **1995**, 22.

16) Akiyama, T.; Imahori, H.; Sakata, Y. *Chem. Lett.* **1994**, *8*, 1447.

17) He, P. G.; Ye, J. N.; Fang, Y. Z.; Sutzuki, I.; Osa, T. *Electroanalysis* **1997**, *9*, 68.

18) Creager, S. E.; Rowe, G. K. *Anal. Chim. Acta* **1991**, *246*, 233.

19) Turyan, I.; Mandler, D. *Anal. Chem.* **1997**, *69*, 894.

20) Tieke, B.; Wegner, G.; Naegele, D.; Ringsdorf, H. *Angew. Chem. Int. Ed. Engl.* **1976**, *15*, 764.

21) Batchelder, D. N.; Evans, S. D.; Freeman, T. L.; Häussling, L.; Ringsdorf, H.; Wolf, H. *J. Am. Chem. Soc.* **1994**, *116*, 1050.

22) Kim, T.; Crooks, R. M. *Tetrahedron Lett.* **1994**, *35*, 9501.

23) Chan, K. C.; Kim, T.; Schoer, J. K.; Crooks, R. M. *J. Am. Chem. Soc.* **1995**, *117*, 5875.

24) Kim, T.; Crooks, R. M.; Tsen, M.; Sun, L. *J. Am. Chem. Soc.* **1995**, *117*, 3963.

25) Peanasky, J. S.; McCarley, R. L. *submitted to Langmuir* **1997**.

26) Ozaki, H.; Kasuga, M.; Tsuchiya, T.; Funaki, T.; Mazaki, Y.; Aoki, M.; Masuda, S.; Harada, Y. *J. Chem. Phys.* **1995**, *103*, 1226.

27) Skotheim, T. A. *Handbook of Conducting Polymers*; Marcel Dekker: New York, 1986; Vol. 1.

28) Miller, J. S. *Adv. Mater.* **1993**, *5*, 587.

29) Walatka, V. V.; Labes, M. M.; Perlstein, J. H. *Phys. Rev. Lett.* **1973**, *31*, 1139.

30) Hatano, M.; Kambara, S.; Okamoto, S. *J. Polym. Sci.* **1961**, *51*, 526.

31) Shirakawa, H.; Ito, T.; Ikeda, S. *Polym. J. (Tokyo)* **1973**, *4*, 460.

32) Ito, T.; Shirakawa, H.; Ikeda, S. *J. Polym. Sci. Chem. Ed.* **1974**, *12*, 11.

33) Shirakawa, H.; Louis, E. J.; MacDiarmid, A. G.; Chiang, C. K.; Heeger, A. J. *J. Chem. Soc. Chem. Commun.* **1977**, 578.

34) Krieger, J. *Chem. Eng. News.* **1987**, 20.

35) Diaz, A. F.; Kanazawa, K. K. *J. Chem. Soc., Chem. Commun.* **1979**, 635.

36) Dall'Olio, A.; Dascola, Y.; Varacco, V.; Bocchi, V. *C. R. Acad. Sci.* **1968**, *C267*, 433.

37) Gardini, G. P. *Adv. Heterocyclic Chem.* **1973**, *15*, 67.

38) Ferraro, J. R.; Williams, J. M. *Introduction to Synthetic Electrical Conductors*; Academic: New York, 1987.

39) Kanazawa, K. K.; Diaz, A. F.; Geiss, R. H.; Gill, W. D.; Kwak, J. F.; Logan, J. A.; Rabolt, J. F.; Street, G. B. *J. Chem. Soc., Chem. Commun.* **1979**, 854.

40) Street, G. B.; Clarke, T. C.; Geiss, R. H.; Lee, V. Y.; Nazzal, A.; Pfluger, P.; Scott, J. C. *J. Phys. Paris Colloq.* **1983**, *C3*, 599.

41) Salmon, M.; Diaz, A. F.; Logan, A. J.; Krounbi, M.; Bargon, J. *Mol. Cryst. Liq. Cryst.* **1982**, *83*, 265.

42) Kanazawa, K. K.; Diaz, A. F.; Krounbi, M. T.; Street, G. B. *Synth. Met.* **1981**, *4*, 119.

43) Kossmehl, G.; Chatzitheodorou, G. *Makromol. Chem. Rapid Commun.* **1981**, *2*, 551.

44) Ivory, D. M.; Miller, G. G.; Sowa, J. M.; Shacklette, L. W.; Chance, R. R.; Baughman, R. H. *J. Chem. Phys.* **1979**, *71*, 1506.

45) Wnek, G. E.; Chien, J. C. W.; Karasz, F. E.; Lillya, C. P. *Polym. Commun.* **1979**, *20*, 1443.

46) Rabolt, J. F.; Clarke, T. C.; Kanazawa, K. K.; Reynolds, J. R.; Street, G. B. *J. Chem. Soc. Chem. Commun.* **1980**, 347.

47) Diaz, A. F.; Logan, J. A. *J. Electroanal. Chem.* **1980**, *111*, 111.

48) Li, T., T.-T.; Weaver, M. J. *J. Am. Chem. Soc.* **1984**, *106*, 1233.

49) Kakuda, S.; Momma, T.; Osaka, T.; Appetechi, G. B.; Scrosati, B. *J. Electrochem. Soc.* **1995**, *142*, L1.

50) Miller, J. S. *Adv. Mater.* **1993**, *5*, 671.

51) Kunugi, Y.; Watt, E. J.; Freeman, N. J. *The Analyst* **1992**, *117*, 1265.

52) Gustaffson, G.; Lundström, I.; Liedberg, B.; Wu, C. R.; Inganäs, O.; Wennerström, O. *Synth. Met.* **1989**, *31*, 163.

53) Curran, D.; Grimshaw, J.; Perera, S. D. *Chem. Soc. Rev.* **1991**, *20*, 391.

54) Pyo, M.; Maeder, G.; Kennedy, R. T.; Reynolds, J. R. *J. Electroanal. Chem.* **1994**, *368*, 329.

55) Frostman, L. M.; Bader, M. M.; Ward, M. D. *Langmuir* **1994**, *10*, 576.

56) Gottesfeld, S.; Uribe, F. A.; Armes, S. P. *J. Electrochem. Soc.* **1992**, *139*, L14.

57) Wernet, W. *Synth. Met.* **1990**, *41-43*, 843.

58) Yang, X. Q.; Chen, J.; Hale, P. D.; Inagaki, T.; Skotheim, T. A.; Okamoto, Y.; Samuelson, L.; Tripathy, S.; Hong, K.; Rubner, M. F.; denBoer, M. L. *Synth. Met.* **1989**, *28*, C251.

59) Rosner, R. B.; Rubner, M. F. *Chem. Mater.* **1994**, *6*, 581.

60) Rikukawa, M.; Rubner, M. F. *J. Mater. Sci., Pure Appl. Chem.* **1994**, *A31*, 793.

61) Simon, R. A.; Ricco, A. J.; Wrighton, M. S. *J. Am. Chem. Soc.* **1982**, *104*, 2031.

62) Kowalik, J.; Tolbert, L.; Ding, Y.; Bottomley, L.; Vogt, K.; Kohl, P. *Synth. Met.* **1993**, *55*, 1171.

63) Rubinstein, I.; Rishpon, J.; Sabatani, E.; Redondo, A.; Gottesfeld, S. *J. Am. Chem. Soc.* **1990**, *112*, 6135.

64) Martin, C. R. *Acc. Chem. Res.* **1995**, *28*, 61.

65) Cai, Z.; Lei, J.; Liang, W.; Menon, V.; Martin, C. R. *Chem. Mater.* **1991**, *3*, 960.

66) Wu, C.-G.; Bein, T. B. *Science* **1994**, *264*, 1757.

67) Bein, T.; Enzel, P. *Angew. Chem. Int. Ed. Engl.* **1989**, *28*, 1692.

68) Millar, G. J.; McCann, G. F.; Hobbis, C. M.; Bowmaker, G. A.; Cooney, R. P. *J. Chem. Soc., Faraday Trans.* **1994**, *90*, 2579.

69) Larsen, G.; Haller, G. L.; Marquez, M. *J. Phys. Chem.* **1992**, *96*, 4145.

Chapter 2

Synthesis of Pyrrole-Functionalized Monomers Capable of Self-Assembly

2.1 Introduction

The generally facile synthesis of alkanethiols with modified tailgroups was one of the driving factors for choosing a thiol-on-gold approach to building very thin layers of monomer.[1] The commercial availability of mono- and di-substituted hydroxy- and bromo-alkanes opens up a wide variety of methods to synthesize alkanethiols with various groups at the end of the chain. This work focuses on the synthesis of alkanethiols with terminal pyrrole groups.

The first question addressed was the choice of positions on the pyrrole ring to utilize for attachment to the alkane chain terminus. The 2 and 5 positions on the pyrrole ring were disregarded immediately since they are the positions that lead to the most conductive form of poly(pyrrole).[2] This leaves the 1, 3, and 4 positions as possibilities with positions three and four being equivalent. Pyrrole-based polymers derived from monomers substituted in either the 1 or 3 position are considerably less conductive than the unsubstituted monomer species.[3] The decrease in conductivity of either 1- or 3-substituted poly(pyrroles) approaches 3-4 orders of magnitude. With this factor being nearly equal for the 1- or 3-substituted pyrroles, matters of orientation of the pyrrole ring with respect to the plane of the substrate were considered next.

It was thought from a simple geometric analysis that any attachment point on the ring that allowed a more planar and linear placement of the 2 and 5 positions of adjacent rings with respect to each other would increase the efficiency of the

polymerization reaction. A cartoon depicting the arrangement of 1- and 3-substituted pyrroles adsorbed on a smooth surface is shown in Figure 2.1. In the event that the alkyl chains exhibited a low degree of order, little difference was predicted in the two places for substitution on the pyrrole rings. The 1-position was chosen, however, assuming that a moderate to high degree of order might be present in the longer alkane chain spacer analogues (> 10 carbons). In this case, substitution that resulted in a symmetrical monomer would allow for the possibility of coplanar ring alignment even when the alkyl chains were rigidly locked in place.

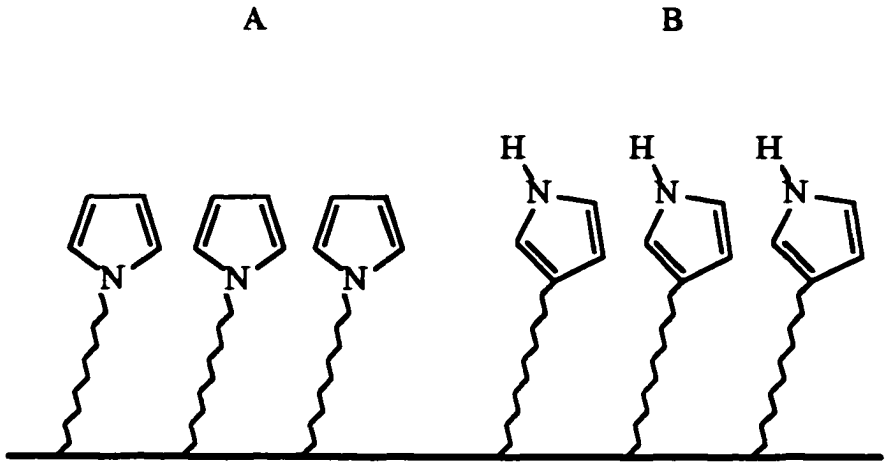

Figure 2.1 **Possible arrangements for (A) 1-substituted and (B) 3-substituted pyrroles on a planar surface.**

The length of the alkyl tether between the sulfur headgroup and the pyrrole tailgroup was also an important consideration. It has been shown that *n*-alkanethiols with short alkane portions (<9 carbons) form relatively disordered or "floppy" monolayers on Au and Ag.[4] Longer chain alkanethiols, however, form more ordered,

even semi-crystalline monolayers due to increased van der Waals interactions between the C-H groups making up the alkane backbone.

It was decided that several chain lengths would be synthesized to cover a range of possible effects of order in the monolayer. The first pyrrolyl alkanethiol would consist of a six-carbon chain. This length should be sufficient to allow some intermolecular interaction for monolayer stability while allowing a considerable amount of "floppiness" at the chain terminus. Due to the possible strain in the resulting polymer, it was determined that a certain amount of freedom of the pyrrole groups would be needed to facilitate coupling of the immobilized monomers.

2.2 Synthesis of ω-(*N*-pyrrolyl)-1-bromoalkanes

The first step towards (mercaptoalkyl)pyrrole synthesis was the addition of a bromoalkyl chain to the *N*-terminus of pyrrole. Such a modification of pyrrole was carried out based on a literature procedure[5] in a one-step, S_N2 reaction as depicted in Figure 2.2. Pyrrole was first purified by filtering through a short neutral alumina column until a clear, light-yellow liquid was obtained. To a 50 mL round bottom flask was added 9.48 g (141 mmol) of purified pyrrole followed by purging with Ar for 10-15 minutes. To a 500 mL round bottom flask, 100 g (410 mmol) of dibromohexane was added and purged with Ar for 15 minutes. Dimethyl formamide (DMF) was chosen as the reaction solvent due to the fact that polar, aprotic solvents are known to increase the reactivity of nucleophiles in S_N2 reactions[6] and thus increase the reaction rate. Thirty-five mL of DMF, previously purged with Ar and dried over 3 Å sieves, was cannulated into the round bottom containing the dibromide.

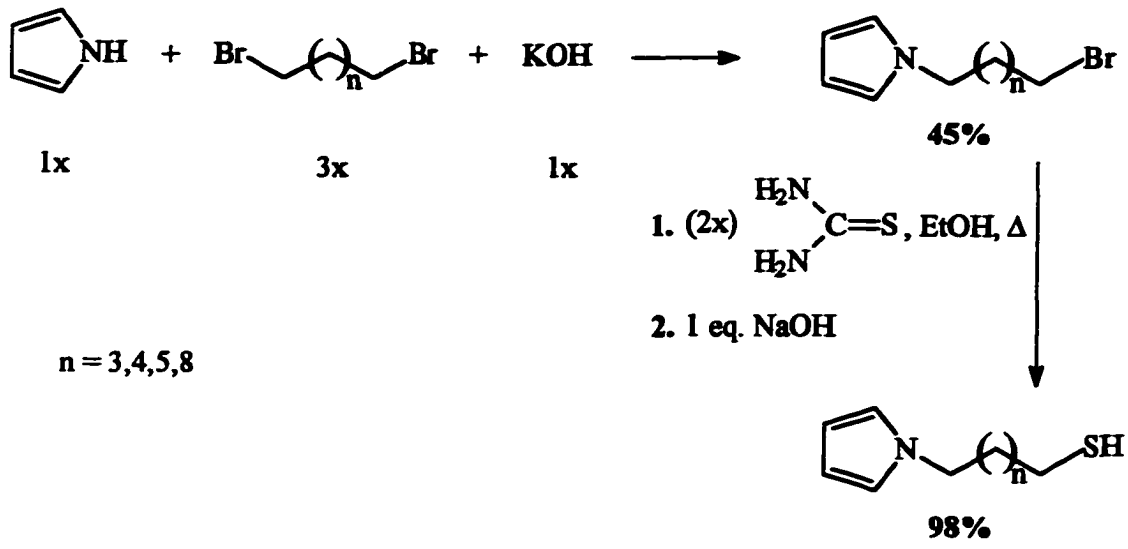

Figure 2.2 **Synthetic route for formation of ω-(*N*-pyrrolyl)alkanethiols.**

To a 500 mL reaction vessel equipped with a reflux condenser and stirbar, 5.67 g (142 mmol) of finely ground NaOH was added. During this process, the apparatus was kept under a dry Ar atmosphere, and purging continued for 10-15 minutes. At this point the dibromohexane in DMF was cannulated into the 500 mL reaction vessel and allowed to mix thoroughly. The degassed pyrrole was then cannulated slowly (ca. 20 drops/minute) into the reaction vessel. The Ar-purge was removed and the flask was covered with aluminum foil. The reaction initially gave off a small amount of heat and was allowed to proceed overnight.

A 1-mL aliquot of the reaction mixture was taken after 16 hours to check the progress of the reaction. An equal volume of 18 MΩ cm water was added to the aliquot and then extracted with one mL of diethyl ether. The ether was injected into the GC/MS to monitor the disappearance of the pyrrole peak at 2.7 minutes and the

growth of a new peak at 11.2 minutes. Fragmentation patterns of the new peak from the GC/MS were analyzed to confirm the formation of the (bromoalkyl)pyrrole. MS (EI) *m/z* [relative intensity] 229 [6.6, (M^+)], 150 [48.4, $(M\text{-}Br)^+$], 81 [100, $(C_5H_7N)^+$], 80 [94.6, $(C_5H_6N)^+$], 67 [15.1, $(C_4H_4N)^+$]. The peaks at 81, 80, and 67 are strong indicators of *N*-alkylated pyrrole rings.[7]

Once the reaction was complete, extraction of the organic portion of the reaction mixture was performed. Two volumes of 18 MΩ cm water were added to the DMF mixture which was then extracted with diethyl ether (4 x 100 mL). The ether washes were combined and then washed with 18 MΩ cm water (3 x 45 mL) to remove any DMF extracted into the ether. Several grams of anhydrous magnesium sulfate ($MgSO_4$) were then added to the ether portion to remove any residual water. The ether was subsequently filtered through 15 μm filter paper, degassed and stored under Ar or nitrogen at reduced temperatures. GC/MS was run again on the purified ether portion to confirm extraction of the (bromoalkyl)pyrrole and the starting material. Crude yield of the product was 42% by GC.

Column chromatography with 240-400 mesh silica gel 60 as the stationary phase and petroleum ether as the mobile phase was utilized to purify the product. Approximately 10 mL of dry silica gel was used for every 100 mg of mixture to be purified on a 30 mm column. It was found from thin layer chromatography (TLC) that the product moved extremely slowly ($R_f < 0.1$) under the solvent conditions while the dibromohexane moved much more quickly (R_f ca. 0.8). This allowed relatively large samples to be separated by column chromatography.

A 2 mL portion of the crude mixture was added to a column and fractions of various sizes were collected and monitored by TLC for the appearance of the (bromoalkyl)pyrrole product using a mixed iodine/silica gel developing chamber. Once the (bromoalkyl)pyrrole began to elute, the eluent was gradually switched to 90:10 petroleum ether:diethyl ether mobile phase using 100 mL additions of solvent with one percent incremental increases in the diethyl ether content (v/v). The increase in the polarity of the mobile phase caused the product to elute much faster. Those fractions containing product spots on the TLC plates were checked by GC/MS to confirm the presence and purity of the product. The purer fractions were added together and checked again by GC/MS. A second column on the combined fractions was needed to separate the product from traces of the dibromide well enough to proceed with the next reaction. The middle fractions of this column, with the highest purity, were combined and stored under Ar- or N_2-purged ether at reduced temperatures. Before use, the ether was removed from the (bromoalkyl)pyrrole under reduced pressure to yield a reddish-orange oil. The purity of the bromide exceeded 95% by GC with the five percent impurity content composed of several very small peaks on the lower retention side of the (bromoalkyl)pyrrole peak.

2.3 Synthesis of ω-(*N*-pyrrolyl)hexanethiol

2.3.1 Attempted Synthesis Using NaHS/DMSO Mixture

The conversion of the pure ω-(*N*-pyrrolyl)bromohexane to the thiol was first attempted using a literature procedure that focused on the use of -SH as a nucleophile.[8] Thus, the approach here involves reacting 6-(*N*-pyrrolyl)-1-bromohexane with saturated sodium hydrosulfide (NaHS) dissolved in a dimethyl sulfoxide (DMSO):water

mixture. Under these conditions, the hydrosulfide is an excellent nucleophile that can attack the ω-carbon in a S_N2 reaction to displace the bromide and give the thiol.

Conversion of the 6-(*N*-pyrrolyl)-1-bromohexane to the thiol was attempted using the following procedure. Pure (bromoalkyl)pyrrole was dissolved in 10 mL of dry DMSO. The (bromoalkyl)pyrrole/DMSO mixture was dripped via an addition funnel into a saturated NaHS solution in 80%/20% DMSO/H_2O (v/v) over approximately 30 min. The reaction was immediately worked up by adding 100 mL of H_2O and extracting with ether (8 x 75 mL). The ether was dried with $MgSO_4$ and evaluated by GC/MS. The total ion chromatogram (TIC) displayed peaks identified as the thiol, dialkyl sulfide, and dialkyl disulfide. The two sulfides were insoluble at low temperatures (-80 °C). The mixture in ether was brought to this temperature, allowed to form a precipitate, and then filtered through 15 μm filter paper three times. The purity of the thiol was better than 99.2% by GC/MS. The solvent was evaporated leaving the thiol as a clear, yellow liquid. MS (EI) *m/z* [relative intensity] 185 and 183 [4.7 and 1.6, (M^+)], 150 [26.4, $(M\text{-}SH)^+$], 81 [100, $(C_5H_7N)^+$], 80 [73.2, $(C_5H_6N)^+$], 68 [12.7, $(C_4H_5N)^+$], 67 [10.8, $(C_4H_4N)^+$].

This method was not chosen as the most suitable for two reasons. First, the thiol quickly transformed into the disulfide thereby lowering the yield of the more desirable thiol and adding extra purification steps to the procedure. Second, it was found that DMSO was nearly impossible to completely remove from the thiol once formed.

2.3.2 Synthesis Using Thiourea in Absolute Ethanol

The use of another thiolating reagent, thiourea, was found in the literature.[9] In the presence of a good leaving group, thiourea will replace that group by forming an isothiouronium salt. This salt is stable to hydrolysis in absolute ethanol and thus disulfide formation is no longer a noticeable side reaction. Once formation of the isothiouronium salt is complete, the thiol is easily formed by hydrolytic cleavage of the salt with strong base.

To 1.47 g (6.4 mmol) of degassed 6-(*N*-pyrrolyl)-1-bromohexane in a 100 mL, 3-neck round bottom flask fitted with a Hg bubbler and condenser was added 0.976 g (12.8 mmol) of thiourea. Approximately 20 mL of degassed ethanol was added to this mixture, which was then purged with N_2 or Ar for 15 minutes. Once the thiourea and 6-(*N*-pyrrolyl)-1-bromohexane had dissolved, foil was wrapped around the round bottom flask which was then heated using a heating mantle. Formation of the isothiouronium salt was complete in roughly four hours, as evidenced by the disappearance of the 6-(*N*-pyrrolyl)-1-bromohexane spot in the TLC. One equivalent of NaOH as a 10% solution (0.28 g NaOH in 3 mL H_2O) in degassed 18 MΩ cm water was then added to the mixture. The reaction was heated at reflux for four hours.

Upon cooling to room temperature, an equal volume of 18 MΩ cm water was added to the mixture and acidified to pH = 1 with hydrochloric acid in order to facilitate formation of the thiol. Appearance of the thiol was monitored by the appearance of a new spot in the thin layer chromatograms. Once this spot was observed, a 1-mL aliquot of the reaction mixture was withdrawn, mixed with an equal volume of 18 MΩ cm water, and extracted with one mL of diethyl ether for GC/MS

analysis. A 1-μL injection of the ether layer yielded only one peak in the ion chromatogram with *m/z* = 183 equal to the parent mass. Additional peaks corroborated this assessment. MS (EI) *m/z* [relative intensity] 183 [23.2, (M^+)], 150 [61.1, $(M-SH)^+$], 81 [100, $(C_5H_7N)^+$], 80 [77.3, $(C_5H_6N)^+$], 68 [19.2, $(C_4H_5N)^+$], 67 [16.3, $(C_4H_4N)^+$].

Extraction of the reaction mixture with ether (4 x 45 mL) was followed by 18 MΩ cm water washes (3 x 50 mL) to remove any remaining ethanol, drying with $MgSO_4$, and filtering through 15 μm filter paper. GC/MS indicated that the purity of the thiol was greater than 97%. For all of the different *N*-substituted pyrrolyl thiols discussed, the general procedure for synthesis of the ω-(*N*-pyrrolyl)hexanethiol was used.

2.4 Synthesis of 2,5-dimethyl-ω-(*N*-pyrrolyl)hexanethiol

Another synthesis was performed in order to make a pyrrolyl alkanethiol whose preferred ring positions for polymerization were blocked. The blockage of the 2 and 5 carbons of the pyrrole ring with methyl groups would prevent oxidative linking at these preferred sites and could have important effects on studies of the surface-confined polymerization reactions discussed later. As previously mentioned, polypyrrole does contain some β,β'-coupling defects along the polymer chain - proof that polymerization can occur through the less favored positions on the ring. On the surface the blocked molecule would have fewer ring sites to polymerize through thereby reducing the probability of two rings coupling together. It was thought that perhaps the dynamics of the chains would preclude linking under these conditions and allow this compound to be compared spectroscopically to the less-hindered analogues. Reducing the number of

ring linkages also implies a lower polymer chain length which could also have an affect on the resulting spectra due to reduced charge delocalization.

Synthesis of 6-(*N*-2,5-dimethylpyrrolyl)-1-bromohexane was initially attempted using a procedure similar to the one for 6-(*N*-pyrrolyl)-1-bromohexane but using 2,5-dimethyl pyrrole as the starting material instead of pyrrole. This reaction was found to proceed but with low yields (<5%) as a result of steric hindrance from the two methyl groups. An alternate way to make this compound was to generate the 6-(*N*-2,5-dimethylpyrrolyl)-1-bromohexane from 6-(*N*-2,5-dimethylpyrrolyl)-1-hydroxyhexane. It is known that (hydroxyalkyl)pyrroles can be formed using a Knorr-Paal condensation as described in the literature.[10,11] The terminal alcohol can then be converted to the thiol after the attachment of a suitable leaving group in place of the alcohol.

The synthesis proceeded as depicted in Figure 2.3. To a 100 mL round bottom flask containing 4.02 g (34.4 mmol) of solid 6-amino-1-hexanol under an Ar atmosphere was added dropwise 3.99 g (35 mmol) of 2,5-hexanedione while stirring. The mixture was allowed to react for 5 hours yielding a clear, orange liquid. A small aliquot of this liquid was dissolved in DCM to give an approximately 4 mg/mL solution and then injected into the GC/MS. The TIC exhibited a single peak centered at 11.9 minutes with a fragmentation pattern consistent with 6-(*N*-2,5-dimethylpyrrolyl)-1-hydroxyhexane. MS (EI) ***m/z*** [relative intensity] 195 [36, (M^+)], 180 [8.3, $(M\text{-}CH_3)^+$], 178 [3.6, $(M\text{-}OH)^+$], 109 [83.4, $(C_7H_{11}N)^+$], 108 [100, $(C_7H_{10}N)^+$], 94 [37.7, $(C_6H_8N)^+$].

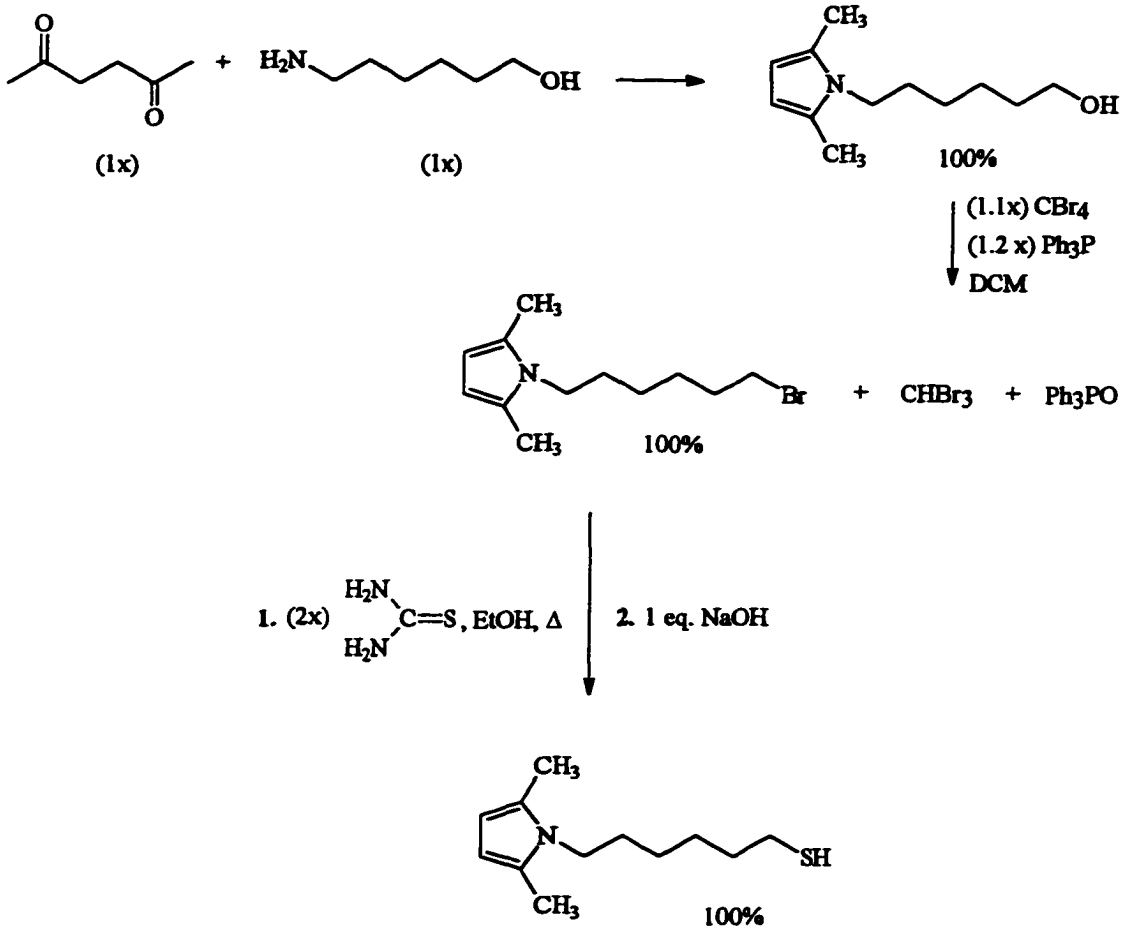

Figure 2.3 **Synthetic route to 6-(*N*-2,5-dimethylpyrrolyl)-1 mercaptohexane.**

Conversion of the alcohol to the bromide was achieved by following the literature.[12] To 13.3 g (40.1 mmol) of carbon tetrabromide (CBr_4) in 10 mL of DCM in a 250 mL round bottom flask was added 6.26 g (32.1 mmol) of 6-(*N*-2,5-dimethylpyrrolyl)-1-hydroxyhexane. To this mixture was added 12.5 g (47.7 mmol) of triphenyl phosphine (Ph_3P) in small portions. The reaction mixture bubbled briefly and was allowed to stir for 30 minutes under Ar. GC/MS analysis of an aliquot dissolved in DCM demonstrated complete conversion of all the components to

6-(*N*-2,5-dimethylpyrrolyl)-1-bromohexane, tribromomethane ($CHBr_3$), and triphenyl phosphine oxide (Ph_3PO). MS (EI) *m/z* [relative intensity] 259 and 257 [10.6 and 11.3, (M^+)], 178 [32.0, $(M\text{-}Br)^+$], 109 [72.1, $(C_7H_{11}N)^+$], 108 [100, $(C_7H_{10}N)^+$], 94 [35.9, $(C_6H_8N)^+$].

A large portion of the triphenyl phosphine oxide was removed by rotoevaporating all of the DCM, dissolving the resulting red solid in a minimum amount of acetonitrile (MeCN) (ca. 2.5 mL), and then extracting the mixture with hexane.[13] The hexane extracts were added together then covered and placed in a freezer overnight at ca. -20 °C in air. White crystals that had slowly formed in the beaker were filtered through 15 μm filter paper the next day. Analysis of the filtrate by GC/MS indicated the presence of only bromoform and the desired product. Column chromatography was performed on the remaining mixture using 52 mL of dry silica gel for every 1.9 g of the mixture and hexane as the mobile phase. Approximately 225 mL fractions were collected from the column and Fraction 5 was found to contain all of the product while bromoform was found in the first two fractions. Fraction 5 was rotoevaporated to yield 1.38 g (5.4 mmol) of product. This product was converted to the thiol as described above in 100% yield to give the dimethyl-blocked *N*-alkylated pyrrolyl thiol as shown by GC/MS. MS (EI) *m/z* [relative intensity] 211 [39, (M^+)], 178 [44.9, $(M\text{-}SH)^+$], 109 [66.3, $(C_7H_{11}N)^+$], 108 [100, $(C_7H_{10}N)^+$], 94 [40.0, $(C_6H_8N)^+$].

2.5 Experimental

2.5.1 Chemicals

Triphenyl phosphine, carbon tetrabromide, 6-amino-1-hexanol, 2,5-hexanedione, and thiourea were all ACS grade from Aldrich and were used as received. Semiconductor grade NaOH (Aldrich), analytical grade DMF (Mallinckrodt), absolute ethanol (Aaper), nanograde petroleum ether (Mallinckrodt), analytical grade anhydrous ether (Mallinckrodt), and reagent grade hydrochloric acid (EM Sciences) were all used as received. Dibromopentane, dibromohexane, dibromoheptane, and dibromodecane were all purchased from Aldrich and filtered through 15 μm filter paper (Whatman) before use. All flash columns were made with 240-400 mesh silica gel 60 (Alltech). Pyrrole was from Aldrich and was purified before use (vide supra).

2.5.2 GC/MS Analysis

GC/MS analyses were carried out on a Hewlett-Packard 5890 series II gas chromatograph interfaced to a Hewlett-Packard 5971A quadrapole mass selective detector. The capillary column in the GC was a 20 m x 1.80 μm (film thickness) DB-5 column (J & W, Folsom, CA). All GC/MS samples were run with the same method consisting of a 2 minute hold at 40 °C followed by a temperature ramp of 20 °C/minute up to 280 °C where the temperature was held until 25 minutes of time had elapsed. The GC used He as the carrier gas at a head pressure of 20 psi. High purity water (18 MΩ cm) was provided by a Nanopure purification system (Barnstead) using a distilled water feed and a pre-filter reverse osmosis system.

2.6 References

1) Ulman, A. *An Introduction to Ultrathin Organic Films from Langmuir-Blodgett to Self-Assembly*; Academic: San Diego, **1991**.

2) Skotheim, T. A. *Handbook of Conducting Polymers*; Marcel Dekker: New York, **1986**; Vol. 1.

3) Diaz, A. F.; Castillo, J.; Kanazawa, K. K.; Logan, J. A.; Salmon, M.; Fajardo, O. *J. Electroanal. Chem.* **1982**, *133*, 233.

4) Porter, M. D.; Bright, T. B.; Allara, D. L.; Chidsey, C. E. D. *J. Am. Chem. Soc.* **1987**, *109*, 3559.

5) Dehaen, W.; Hassner, A. *J. Org. Chem.* **1991**, *56*, 896.

6) Solomons, T. W. G. *Organic Chemistry*; 5th ed.; John Wiley & Sons, Inc.: New York, **1992**.

7) Jones, R. A.; Bean, G. P. *The Chemistry of Pyrroles*; Academic Press: New York, **1977**; Vol. 34.

8) Vasil'tsov, A. M.; Trofimov, B. A.; Amosova, S. V. *J. Org. Chem. USSR* **1983**, *19*, 1197.

9) Patai, S., Ed.; *Chemistry of the Thiol Group*; Wiley: New York, **1974**.

10) Buu-Hoï, N. P.; Xuong, N. D.; Gazave, J. M. *J. Org. Chem.* **1955**, *20*, 639.

11) Hazlewood, S. J.; Hughes, G. K.; Lions, F. *J. P. R. Soc. NSW* **1937**, 92.

12) Kocienski, P. J.; Cernigliaro, G.; Feldstein, G. *J. Org. Chem.* **1977**, *42*, 353.

13) Strongin, R., *private communication*, **1997**.

Chapter 3

Electrochemical Formation and Analysis of Poly(*N*-1-mercaptoalkyl)pyrroles: From Bulk to Surface-Confined Polymers

3.1 Electrochemical Formation and Doping of Poly(pyrrole) Derived From Unsubstituted Solution-Phase Monomer

Poly(pyrrole) films can typically be formed at electrode surfaces by electrochemical oxidation of pyrrole monomer dissolved in suitable electrolyte solutions.[1] One electron oxidation of pyrrole results in an unstable radical cation which can couple with another pyrrole radical cation or neutral monomer to form a dimer. Due to extended conjugation, the oxidation potential of the dimer is lower than the monomer by ca. 0.25 V.[2] Under these potential conditions, the dimer is oxidized and thus couples with other dimers or monomers. This process continues, leading to polymer of a molecular weight which renders it insoluble.

The length of a typical poly(pyrrole) chain thus formed is difficult to determine due to the intractability of the material. It is generally agreed that the chain length needed to achieve maximum conductivity can be rather short.[3] Poly(pyrrole), however, displays the lack of solubility in most solvents that is typically more indicative of a longer, higher molecular weight polymer. Electrochemical oxidation of an α,α '-tritio-β,β '-dimethyl pyrrole[4] yielded a value of 100-1000 units in the average polymer chain as determined by the radioactivity of the tritiated α-groups remaining after polymerization, recalling from Chapter 2 that polymerization takes place primarily through the α-positions on the pyrrole ring. Effects of chain length on the conductivity

of the resulting polymer are difficult to estimate due to the lack of knowledge concerning "average" polymer structure.

Electrochemical oxidation of pyrrole to form poly(pyrrole) consumes 2.25-2.33 electrons per equivalent[5] which can be broken down into two faradaic components - monomer oxidation and polymer doping. The monomer loses two electrons and two protons upon oxidation and coupling to two other pyrrolyl units, Figure 3.1, resulting in a predominantly α,α '-linked polymer. α,β and β,β ' linkages[6] have been observed in virtually all poly(pyrrole) films, however, and are a matter of concern as they can disrupt the linear nature of the polymer and result in a lowered conductivity. The extra one-fourth to one-third electron equivalents come from the doping of the polymer via the generation of polaron and bipolaron charge carriers, Figure 3.2. These delocalized, cationic charge carriers can be reversibly generated on and removed from the polymer chains to make both conducting and insulating films, respectively.

The oxidation potential of 1-*H*-pyrrole monomer is ca. +0.6 V vs. a saturated calomel electrode (SCE) reference. Above this faradaic onset potential, polymer begins to form in solution and grows to a high enough molecular weight until it becomes insoluble and precipitates on the electrode surface. Electrochemical currents indicating reduction of oxidized monomer are not seen because coupling of activated pyrroles proceeds rapidly resulting in a species which is electroinactive in that potential region.[1] This is typically referred to as an EC mechanism[7] and has been verified in this case[8] using extremely fast scan rates to reduce the radical cation prior to irreversible chemical coupling. Anodic and cathodic waves representing reversible doping and de-doping of

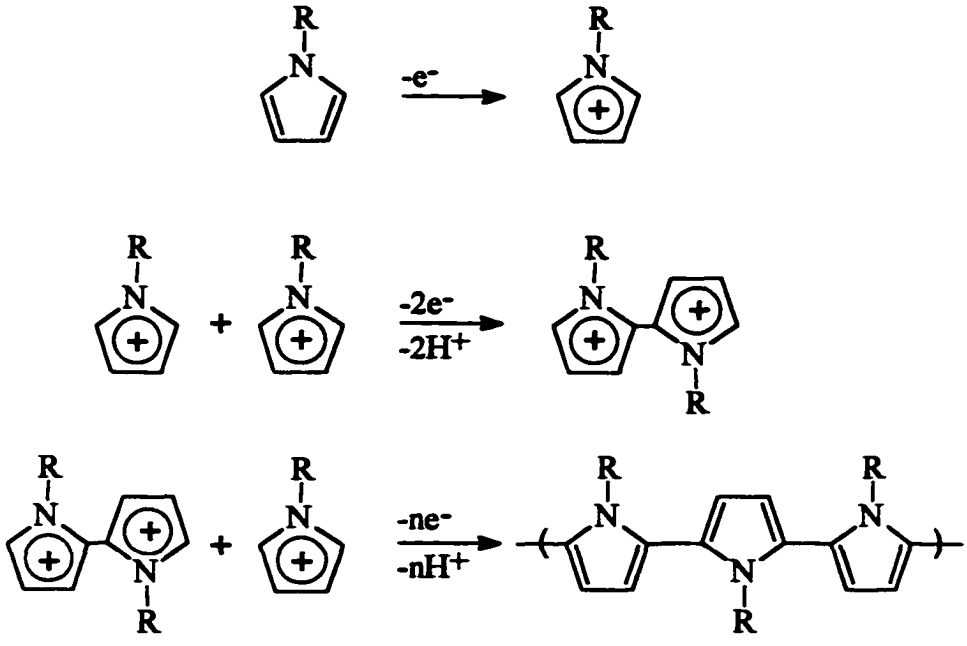

Figure 3.1 **Mechanism for electroxidative formation of poly(pyrrole) from solution-phase pyrrole monomer.**

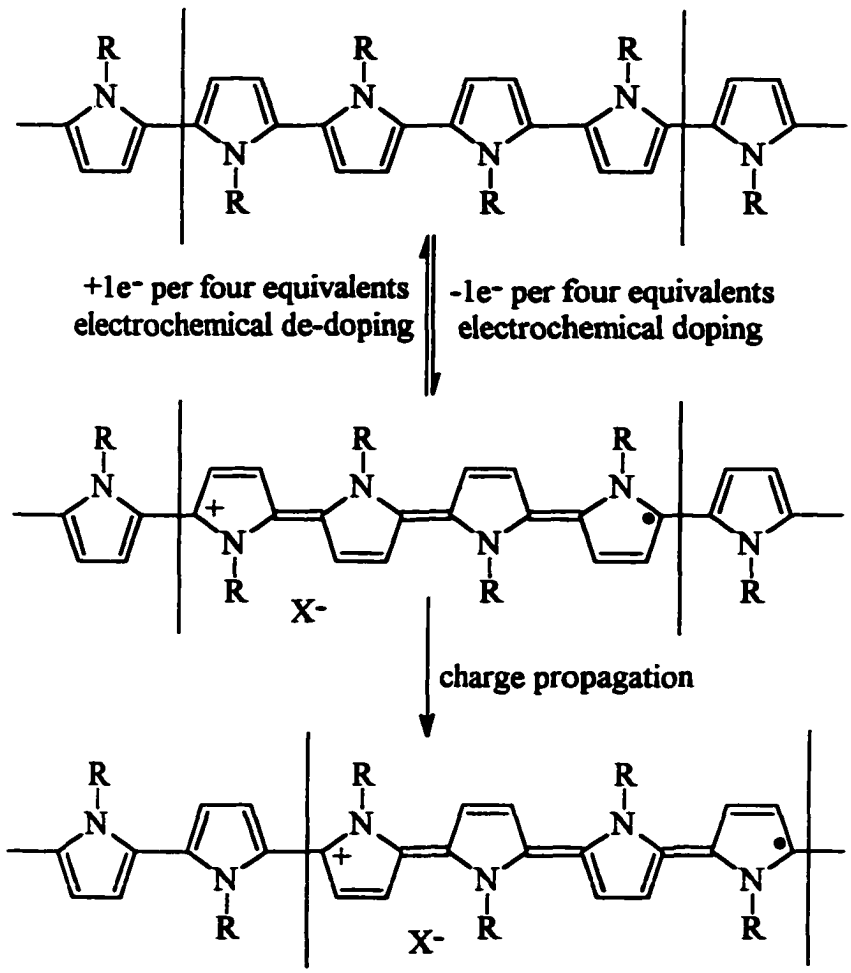

Figure 3.2 **Mechanism for polaronic charge propagation in poly(pyrrole)-based conducting polymers.**

the deposited polymer can be seen at more negative potentials. The current in this region increases as a function of increasing scan number due to the continual deposition of conducting polymer onto the electrode surface. The potential for polymer doping and de-doping (also referred to as charging and discharging) is centered at approximately -0.2 V vs. SCE.[9]

The solvent and electrolyte used during electrochemical oxidation of pyrrole monomer affect the properties of the resulting polymer films. Poly(pyrrole) films have been formed in both aqueous and non-aqueous solvents with fairly good results. It is generally found, however, that aqueous solvents result in films with good mechanical flexibility but lower conductivity.[1] This probably results from a higher number of chain-terminating defects formed when nucleophiles such as H_2O react with the growing polymer chains. Non-aqueous solvent/electrolyte combinations have been shown to result in the formation of films with high conductivities and good physical properties[10] and are also extensively used because they are compatible with inert atmosphere protocols. The choice of counteranion has also been shown to affect the observable morphology of the resulting polymer film. The dependence of polymer morphology on anion is thought to be due to sterics because the anion must enter and exit the film upon doping and de-doping to maintain charge neutrality.

3.2 Experimental

3.2.1 Chemicals

Acetonitrile (Burdick and Jackson) and propylene carbonate (Aldrich) were received under N_2 and stored/used under Ar. Tetra-*n*-butyl ammonium perchlorate

(TBAP) was synthesized as described in the literature,[11] thrice recrystallized from ethyl acetate (Aldrich), and dried overnight at 60 °C in a vacuum oven (VWR Scientific) before use. Perchloric acid (Curtin-Matheson), sulfuric acid (Mallinckrodt), neutral alumina (Aldrich), and hydrogen peroxide (EM Sciences) were all reagent grade or better and used as received. Absolute ethanol (Aaper), electrometric grade tetra-*n*-butyl ammonium tetrafluoroborate (SAchem), *n*-hexanethiol (Aldrich), and ferrocene (Aldrich) were used as received. Silver, gold, and platinum metals (Nevada Refining Systems Inc.) were all 99.99% pure. The $(C_5H_5)Fe(C_5H_4(CH_2)_8SH)$, abbreviated as FcC_8SH, was a kind gift from Professor Larry Curtin (Youngstown State University). High purity water (18 MΩ cm) was provided by a Nanopure purification system (Barnstead) using a distilled water feed and a pre-filter reverse osmosis system.

3.2.2 Electrochemistry

Cyclic voltammetry in standard three-electrode mode was conducted with either a PAR 273A (Princeton Applied Research) potentiostat or a Pine AFRDE5 bipotentiostat (Pine Inc.) and output on a Yokogawa 3025 X-Y recorder. Voltammetry was performed in 0.1 M solutions of TBAP in either acetonitrile (MeCN) or propylene carbonate (PC). A glass electrochemical cell with medium porosity ceramic frits (Ace Glass Inc.) separating the working and reference electrodes was used. All electrochemical experiments were carried out using a Ag/Ag^+ pseudoreference electrode whose potential was periodically checked vs. the Fc/Fc^+ couple. All potentials are given vs. the Ag/Ag^+ pseudoreference electrode unless noted otherwise. Electrochemical experiments were performed in a N_2-purged (Braun, model MB 150M) or Ar-purged glovebox (Vacuum Atmospheres Inc., model

HE-493). Standard convention was followed for the display of current-potential curves (voltage and current increase positively going left and up, respectively).

3.2.3 Fabrication of Au Electrodes

Au electrodes were fabricated by sealing Au wires in borosilicate glass tubes using a H_2/O_2 flame. A Cu wire connection was first made with the Au wire using silver solder (Highland Hardware). The electrodes were initially polished using 240 and then 600 grit sandpaper until all visible air bubbles between the Au wire and the glass were removed. The roughly-polished electrodes were further polished with successively smaller (15 to 0.25 μm) diamond pastes (Buehler) spread on a nylon pad. These electrodes were given a final finish with a slurry of 50 nm alumina particles (Buehler) in 18 MΩ cm water. The electrodes were cleaned after every polishing step by a five minute sonication (Branson 1200) in 18 MΩ cm water. Finally, the electrodes were electrochemically polished by repetitive cycling between +1.4 V and -1.0 V in 1 M $HClO_4$ until voltammetry indicative of clean AuO_x was obtained. A photograph of a typical Au electrode fabricated in this manner is shown in Figure 3.3.

3.2.4 Alkanethiol Monolayer Formation

Monolayers were typically formed by immersion of a freshly electropolished Au electrode into a 1 x 10^{-3} M solution of a given thiol in absolute ethanol (EtOH). Immersion times varied from a minimum of two hours to a maximum of several weeks but typically were three hours. Bain et al.[12] have shown conclusively that film formation is essentially complete after two hours of immersion.

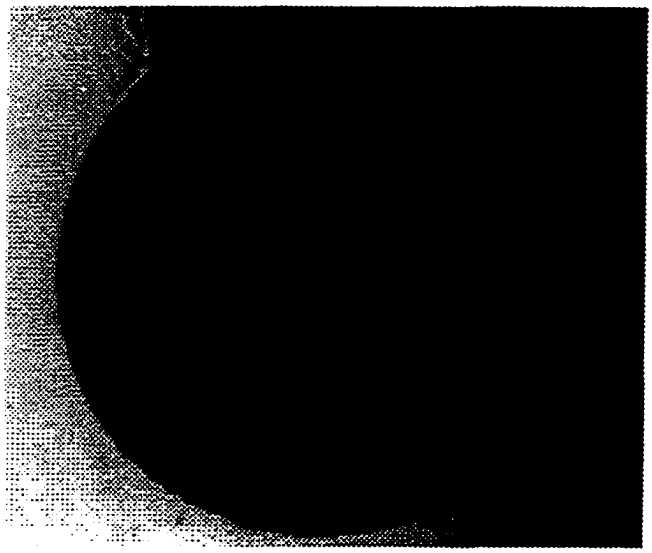

Figure 3.3 **Photograph of a polished Au electrode sealed in glass. The electrode diameter is 2.8 x 10^{-1} cm.**

3.2.5 Wetting Analysis

Wetting analysis was performed with 18 MΩ cm H_2O using the sessile (free-standing) drop method and one minute equilibration times. All contact angles were measured on a VCA2000 Video Contact Angle System (AST Inc.) and are the average of at least three drops on each of three different substrates.

3.3 Results and Discussion

The first electrochemical assessment of a pyrrole-containing monomer was performed with a bare Au electrode placed in a 50 mM solution of PyC_5SH in 0.1 M TBAP/acetonitrile. Oxidation of solution-phase monomer to form a relatively thick polymer film on an electrode was an important experiment designed to determine if *N*-alkylation of the pyrrole ring would prohibit the formation of a conducting organic polymer. The electrode was cycled between 0 and +1.4 V repetitively as shown in

Figure 3.4. A peak beginning at ca. +1.2 V as well as a set of waves centered at ca. +1.0 V was noted and attributed to monomer oxidation and polymer charging/discharging respectively. Repetitive cycling of the electrode between these potentials resulted in an increase in current in the polymer charging/discharging region, and the growth of a thin, black film on the electrode surface. The potentials at which current flows for the oxidation of the monomer and the oxidation/reduction of the polymer are in good agreement with literature values for the two processes.[9] Poly(*N*-butyl)pyrrole monomer oxidation occurs at +1.32 V and polymer charging/discharging is centered around +0.74 V vs. saturated calomel electrode (SCE). This behavior is very indicative of a film of conducting polymer forming on the electrode. Essentially, the increase in current with time comes from the addition of more electrically conducting material to the surface of the electrode as the potential for oxidation of solution-phase monomer is reached on the next anodic excursion.[7]

The success of this experiment confirmed literature reports of polymer formation from solution-phase *n*-methyl[13] and other *n*-alkyl[9] pyrroles substituted at the 1-position. This information was crucial considering the difference in the relative amount of freedom a solution-phase species would have with respect to a surface-confined species. If the solution-phase species, possessing a greater amount of freedom, was unable to couple together upon oxidation, it would be unlikely that the more constrained surface species would be able to couple. This conclusion is based on the fact that the positions through which polymerization typically occur (α and α') must be relatively close to each other - an assumption that might not prove true for the surface-confined monomers. Our observations confirm that the *N*-alkylated pyrroles

are still capable of polymerization despite the difference in their structure in relation to unsubstituted pyrrole monomer.

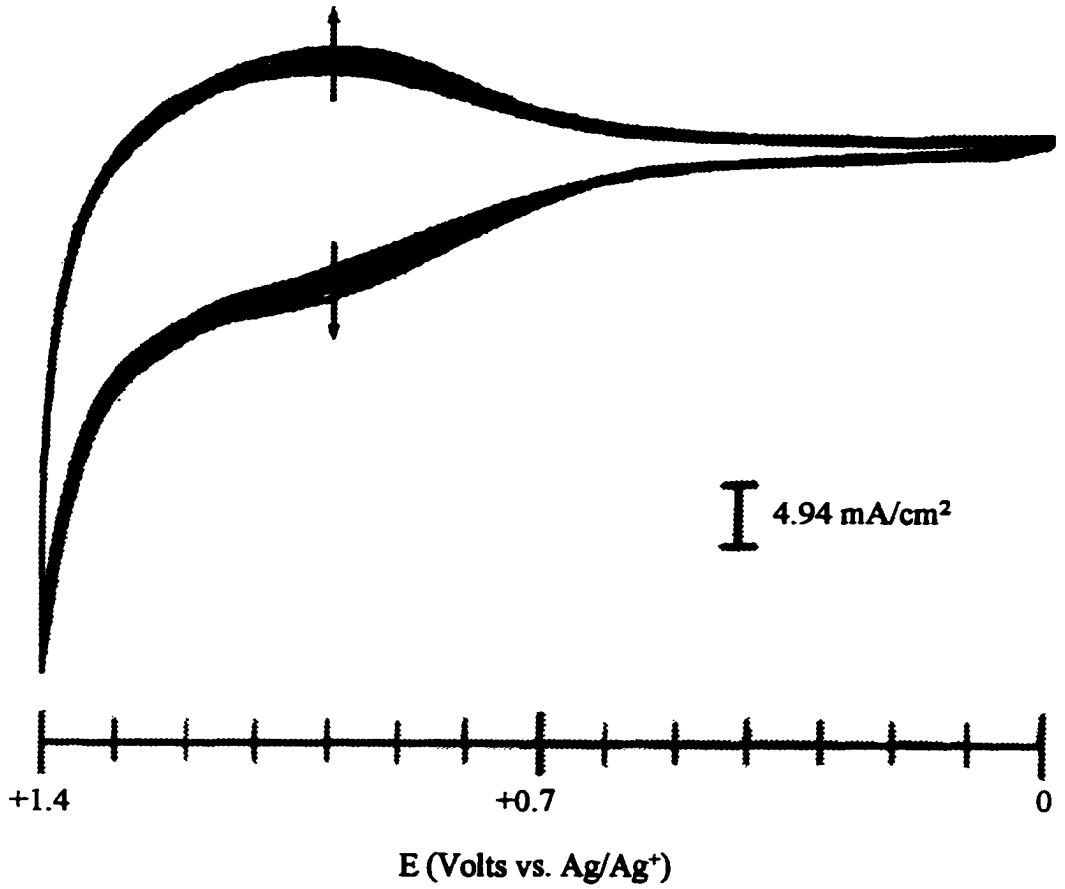

Figure 3.4 **Electropolymerization of 5 x 10^{-2} M PyC_5SH monomer in Bu_4NClO_4/MeCN solution at a clean Au electrode. Arrows indicate increasing current with scan number. A_{elec} = 4.05 x 10^{-3} cm^2 and ν = 100 mV/sec.**

After proving that solution-phase polymerization was feasible, the next step was to confine the various monomers to clean Au electrode surfaces and repeat the voltammetric experiment. An Au electrode was soaked in a 1 x 10^{-3} M $PyC_{10}SH$

solution for ca. two hours, emmersed from the dosing solution and then rinsed with pure ethanol to remove any physisorbed thiol from the surface. The sample was then dried in a stream of dry N_2 or Ar and placed in an electrochemical cell with clean electrolyte solution.

After immersion in 0.1 M Bu_4NClO_4/MeCN electrolyte, a potential scan identical to that performed on the bulk monomer was executed. Figure 3.5B shows a typical voltammogram resulting from such an excursion in which the same general monomer oxidation behavior is noted. In this instance, however, irreversible monomer oxidation occurred at ca. +1.1 V and was complete after the first scan yielding virtually no current in that region for successive scans. The lack of current in this area after the initial scan suggests that extensive if not complete oxidation of the pyrrole units in the film has occurred. A careful inspection of the region encompassing +0.2 V to +0.85 V shows a small amount of current flowing that could be attributable to polymer doping and dedoping. Evidence that this increase in current does not arise from electrochemical desorption of material from the electrode surface is demonstrated by the observation that no change in the blocking capability of the monolayer to solution-phase redox probes occurs after electrochemical cycling. Indeed, electrochemical cycling for hours in clean electrolyte solution indicated little or no loss of the material from the surface. Analogous behavior was noted for all the various chain-length thiols. The behavior of a bare Au electrode to the same electrochemical cycling is shown in Figure 3.5A, clearly displaying the absence of oxidative features resembling those discussed above.

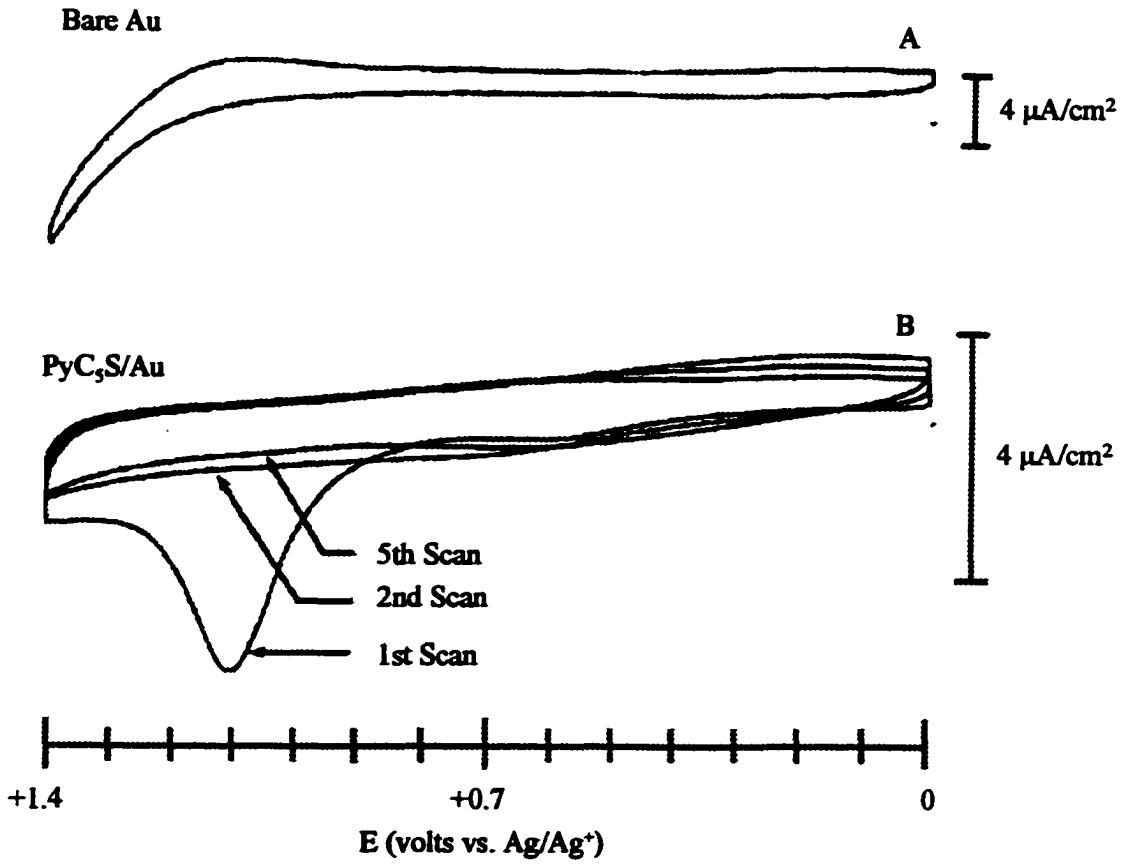

Figure 3.5 **Cyclic voltammetry in 0.1 M Bu_4NClO_4/MeCN electrolyte at a (A) bare Au electrode and (B) PyC_5SH-modified Au electrode. $A_{elec} = 6.2 \times 10^{-2}$ cm² and $\nu = 100$ mV/sec.**

A voltammogram of PyC_6S/Au in 0.1 M Bu_4NClO_4/PC is shown in Figure 3.6 and displays the same behavior for monomer oxidation as the PyC_5S/Au monolayer in 0.1 M Bu_4NClO_4/MeCN. Part C of the figure, however, shows an expanded view of the region from 0 to +0.8 V vs SCE after the initial potential excursion in 3.6B. This potential region clearly exhibits a "whale head" waveshape, which has been shown

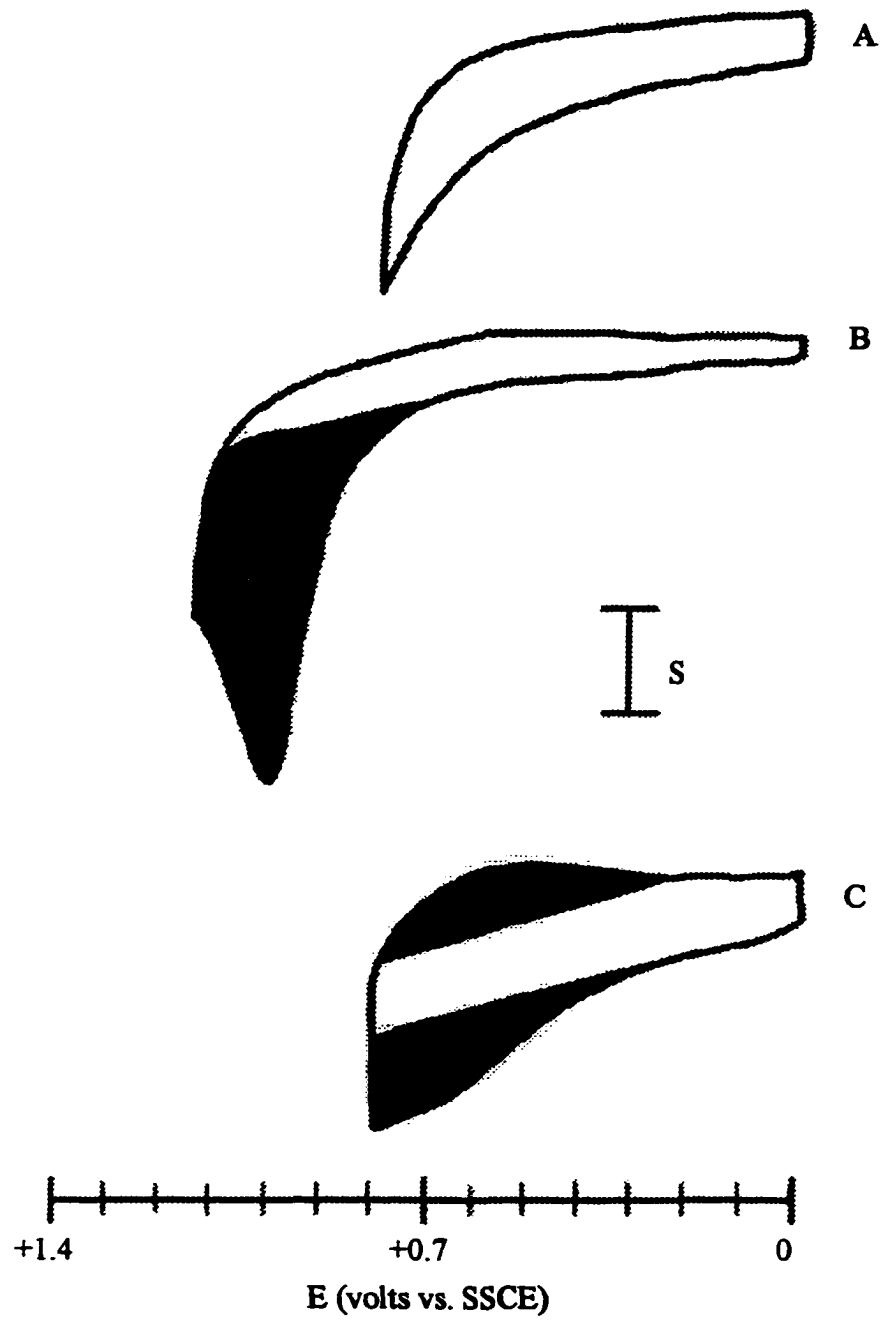

Figure 3.6 **Cyclic voltammetry in 0.1 M Bu_4NClO_4/PC electrolyte at (A) PyC_6SH-modified Au electrode scanned between 0 and +0.75 V vs. SSCE (B) PyC_6SH-modified Au electrode scanned between 0 and +1.1 V vs. SSCE and (C) PyC_6SH-modified Au electrode scanned between 0 and +0.75 V vs. SSCE after the potential excursion in B. S= 10 nA in A and C; S = 25 nA in B and ν =100 mV/sec for all three scans.**

convincingly in the literature to be indicative of the doping and dedoping of pyrrole-based polymers.[14] The broadness of the wave, which results from the diffusion-limited movement of counteranions in and out of the film, is also an indication of pyrrole-based polymer formation. The large positive potentials at which these polymer doping/de-doping processes are occurring is indicative of substitution on the pyrrole ring[9] strongly supporting the proposal that pyrrole monomer units are linking together in the surface-confined film to form polymer or oligomer chains. A recent report by Collard and Sayre drew identical conclusions for a very similar experiment involving the oxidation of 3-(mercaptoalkyl)pyrroles self-assembled onto Au surfaces. Identical behavior was noted for our surface-confined pyrroles in MeCN-based electrolyte solutions but it was necessary to dry the solutions more extensively with 3 Å molecular sieves or dry alumina before polymer formation could be seen.

The formation of such a polymerized SAM film had not previously been reported in the literature. Thus, this is the first successful attempt to form a surface-confined polymer film from a self-assembled monolayer of monomer on a Au substrate. The same general behavior was noted for all the different alkyl chain length pyrroles. As proof that the current flowing in the polymer charging/discharging region was due to a surface-confined species and not some pyrrole-containing contaminant, the current was measured at different scan rates and found to increase linearly. This well-known behavior, seen in Figure 3.7, is observed for redox species confined to the immediate proximity of the electrode surface[7] and results from lack of redox-center diffusion to the surface in order to undergo electron transfer. Additionally, wetting studies with a sessile H_20 drop on a PyC_6S/Au surface indicated an initial contact angle of $58 \pm 4°$

which fell to 49 ± 2° upon monomer oxidation. This observation is consistent with the formation of a monolayer containing charged sites.

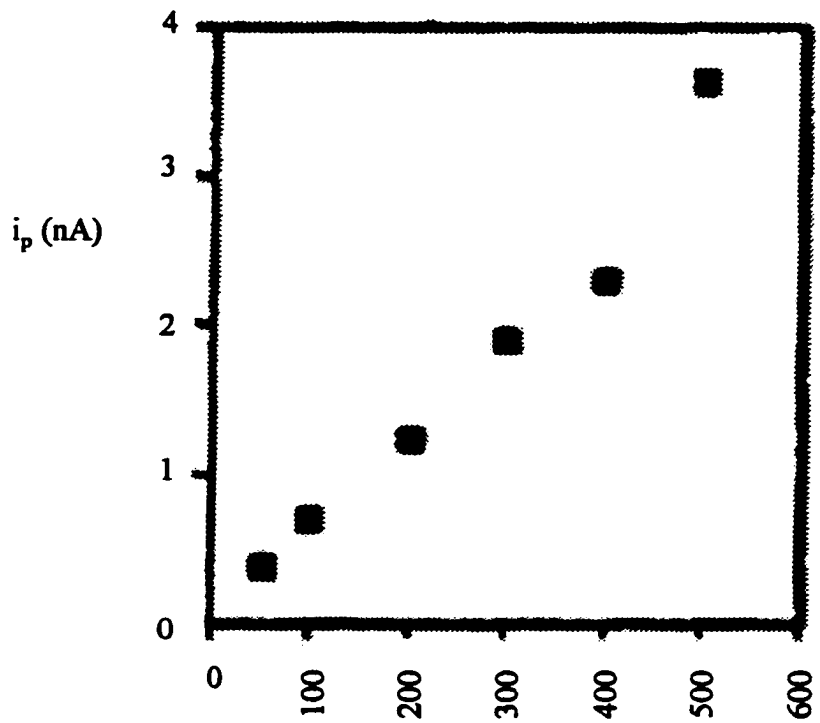

Figure 3.7 **Plot of peak current for monomer oxidation vs. scan rate for a PyC_6SH-modified Au electrode in 0.1 M Bu_4NClO_4/PC electrolyte. The correlation coefficient was 0.98.**

Further confirmation of the conversion of monomer units to polymer or oligomer chains was achieved by analysis of the integrated current under the monomer oxidation and polymer doping/dedoping wave, represented by the shaded regions in Figure 3.6B and 3.6C, respectively. As discussed in section 3.1, the electron stoichiometry for both reactions is already known from previous studies.[1] A comparison of the integrated currents (the charge, Q) associated with the two peaks

should therefore allow a determination of the extent of polymerization of the monomer film since we have already shown that complete oxidation of the monomer occurs after one potential excursion. A charge of 75 μC cm^{-2} for monomer oxidation and 9.6 μC cm^{-2} for the polymer charging (or discharging) waves is observed after subtraction of the appropriate double-layer charging current (background). An 8:1 charge ratio for the two processes is found and is exactly the electron stoichiometry ratio for *N*-alkyl pyrrole conversion to poly(*N*-alkylpyrrole). Extended immersion of Au electrodes in the pyrrole thiol dosing solution did not change the integrated currents, indicating that they are representative of monolayer coverage for the redox sites. Thus we can say that extensive conversion of the monomer units in the film to polymer or oligomer occurs upon electrochemical oxidation of the monolayer.

Surface coverages, Γ, for the various *N*-alkylpyrroles were obtained from the charge under the monomer oxidation wave using equation 3.1. In Equation 3.1, Q is the charge (C), n is the number of electrons, F is Faraday's constant (96487 C/eq.), A is the electrode area (cm^2), and Γ is the maximum surface coverage (mol cm^{-2}). The

Equation 3.1 $Q = nFA\Gamma$

geometric electrode area was corrected for surface roughness by a literature electrochemical method.[15] Briefly, the electrolytic charge necessary to convert a close-packed monolayer of adsorbed iodine atoms on Au to aqueous IO_3^- was measured and corrected for background current from the formation of AuO_x. This charge can be converted to an electrode area using the known values of the electron stoichiometry for

oxidation and the maximum surface coverage of iodine on Au. The surface coverage for a PyC_6S/Au monolayer determined by this method was calculated to be 4.0 ± 0.4 x 10^{-10} mol cm^{-2} after five separate measurements. This value, which is a little more than half that for a close-packed, methyl-terminated alkanethiol SAM (7.6 x 10^{-10} mol cm^{-2}),[16] is reasonable considering the large size of the pyrrole tailgroup in relation to the van der Waals radius of the alkane chain. Previous reports have shown large terminal groups, such as ferrocene, to have a similar effect on monolayer packing. Chidsey et al. reported a maximum surface coverage value for $FcCO_2(CH_2)_{11}S$/Au of ca. 5.5 x 10^{-10} mol cm^{-2}.[17] Surface coverage values were verified by reductive desorption of the monolayers in aqueous NaOH solutions.[16]

From Figure 3.6 it can be argued that the correct assessment of the charging, or background, current is a fairly subjective process. This is in fact true and is difficult to correct for non-ideal experimental conditions. In order to verify that the currents observed during the initial positive potential scan arose from electrochemical oxidation of pyrrole-based monomer, it was necessary to subject a surface-confined electroinactive thiol of similar length to the same conditions. The currents observed for an electroinactive species should be due only to double-layer charging (assuming no desorption) and thus lower in magnitude than those currents comprised of both double-layer charging and electrochemical oxidation of pyrrole-based monomer.

To such ends a monolayer of *n*-hexanethiol was formed on a Au electrode by immersion for ca. 2 hours in a 1 x 10^{-3} M solution of the thiol in ethanol, followed by emmersion, rinsing with pure EtOH, and drying in an inert gas stream. A set of potential excursions identical to that performed in Figure 3.5 were carried out on the

hexanethiol-modified electrode and are displayed in Figure 3.8. It is clear that no voltammetric features resembling those in Figure 3.6A and 3.6B are present in this control experiment. A small amount of current present at the anodic potential limit is noted due to oxidative desorption of the short-chain thiol.[18] This hypothesis is supported by the increase in the double-layer charging current near 0 V indicating the loss of a portion of the passivating organic layer.

As further proof that the observed electrochemical currents represented monomer coupling to form poly(*N*-alkylpyrrole), a potent nucleophile was added to the electrolyte solution prior to oxidation of the monomer monolayer. Addition of pyridine to solutions of pyrrole has been found to effectively inhibit the electrochemical production of poly(pyrrole) through a variety of different mechanisms.[19] A PyC_5SH-modified Au electrode immersed in a 0.1 M TBAP/MeCN electrolyte solution containing 30 mM pyridine was found to undergo monomer oxidation quite readily. No faradaic current, however, was evident in the region thought to represent poly(*N*-alkylpyrrole) charging and discharging. We attribute this behavior to coupling of the monomer cation radicals with solution-phase pyridine resulting in little or no coupling to form polymer. Analogous results were obtained upon addition of ca. 1% H_2O to dry electrolyte solution.

It was interesting to find that potent nucleophiles effectively quenched polymer formation while having little or no effect on oxidation of the monomer. Dilution of pyrrole-based monomers with electroinactive species was attempted next to see what effect replacing active sites with electroinactive diluents would have on the electrochemistry of the monolayers. It is reasonable to assume that at some mole

fraction of diluent, the pyrrole units would be unable to couple together to form long enough polymer strands to be detected electrochemically.

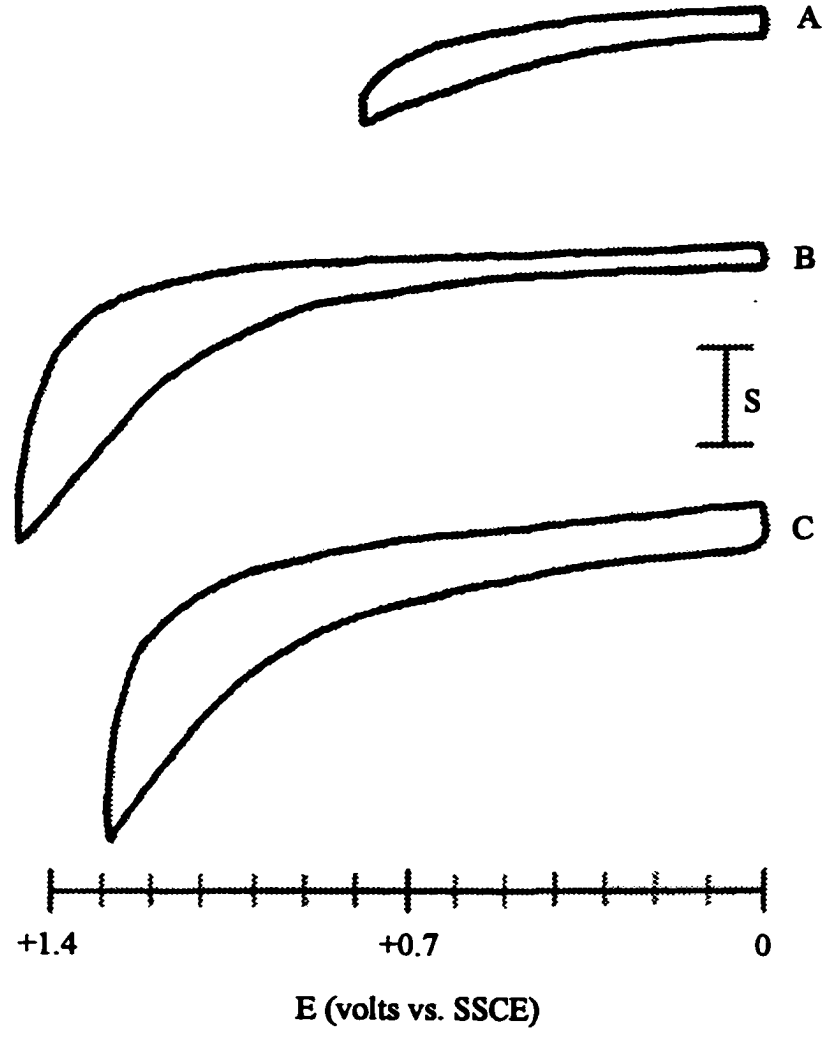

Figure 3.8 **Voltammograms of *n*-hexanethiol monolayers on Au in 0.1 M Bu_4NClO_4 electrolyte successively scanned from (A) 0 to +0.8 V vs. SSCE (B) 0 to +1.5 V vs. SSCE and (C) 0 to +1.3 V vs. SSCE. $A_{elec} = 4.05 \times 10^{-3}$ cm^2 and $\nu = 100$ mV/sec. S = 5 μA cm^{-2} in A and C; S = 13 μA cm^{-2} in B.**

Mixed monolayers were prepared from solutions containing various mole fractions of PyC_6SH ($X_{pyrrole}$) and *n*-hexanethiol. Figure 3.9 shows voltammograms of Au electrodes soaked in solutions containing $X_{pyrrole}$ = 0.75 (A and C) and $X_{pyrrole}$ = 0.25 (B and D). Monomer oxidation excursions are shown in 3.9A and B, polymer doping\de-doping excursions in 3.9C and D. The most obvious thing to note from the two voltammograms is the presence of a prominent monomer oxidation wave in both instances. Apparently, even extreme dilution of the monomer with *n*-hexanethiol does not appreciably affect the waveshape and peak potential of the monomer oxidation wave. Equally important is the difference in the polymer charging/discharging regions for the two electrodes modified in solutions containing different $X_{pyrrole}$. For the monolayer derived from $X_{pyrrole}$ = 0.75, the polymer charging/discharging region looks virtually unchanged from that of a monolayer formed from a pure ($X_{pyrrole}$ = 1.0) pyrrole-containing solution. The potential region for the monolayer formed from the solution with $X_{pyrrole}$ = 0.25, however, is absent of polymer features indicating that polymer formation was kept below a minimum detectable amount by the presence of the electroinactive molecules on the surface.

Surface coverage calculations performed on the mixed monolayer surfaces are also very revealing. The integrated currents for monolayers formed from solutions containing PyC_6SH at $X_{pyrrole}$ = 0.75 and 0.25 give calculated surface coverages equivalent to $X_{pyrrole}$ = 0.9 and 0.4, respectively. That is, the mole fraction of pyrrole thiols on the surface was found to exceed their solution mole fraction in both cases. Further analysis indicated this to be true for all the various dilutions, as shown in Figure 3.10. At this point it is speculated that some interaction among pyrrole rings on the

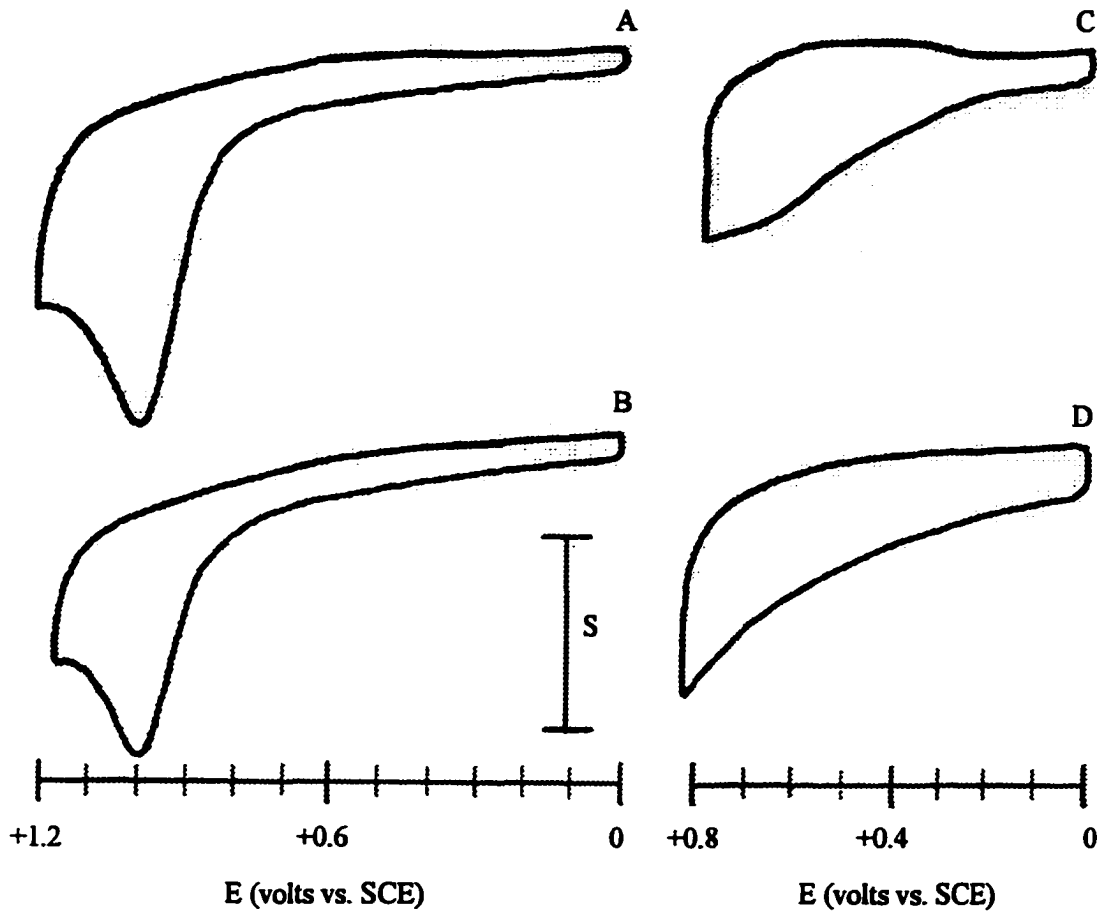

Figure 3.9 **Voltammograms in 0.1 M TBAP/MeCN electrolyte of monolayers on Au formed from mixtures of PyC_6SH and *n*-hexanethiol in EtOH (total thiol concentration of 1×10^{-3} M). Monolayer formed from (A) $X_{pyrrole} = 0.75$ scanned from 0 to +1.2 V (B) $X_{pyrrole} = 0.25$ scanned from 0 to +1.15 V (C) $X_{pyrrole} = 0.75$ scanned from 0 to +0.75 V after the potential excursion in A and (D) $X_{pyrrole} = 0.25$ scanned from 0 to +0.8 V after the potential excursion in B. S = 100 nA in A and B; S = 40 nA in C and D; $\nu = 100$ mV/sec for all scans.**

surface could be occurring that lowers their energy of adsorption and results in their preferential adsorption. In any event, the mixed monolayer studies further support the idea of a linking of pyrrole units within the surface-confined film.

All the experiments described thus far argue very strongly for the formation of a surface-confined monolayer film that undergoes electroxidative linking to form polymer or oligomer chains. Examination of the robustness of the monolayers was performed to further support this argument. Loss of organosulfur monolayers in general,[18] and the pyrrole-terminated monolayers in particular, from the electrode surface can be initiated by scanning to greater than +1.5 V or repetitive scanning between 0 and +1.2 V in incompletely dried electrolytes evidenced by an increase in the double-layer charging current near 0 V. Loss of organic monolayers from their substrates is an important issue concerning their use in the manufacture of sensors and other devices that require reproducible measurements using the same surface. In light of this, the stability of the pyrrole monolayers was investigated before and after electrochemical oxidation.

Literature reports have shown that surface-confined thiols can be removed and replaced by solution-phase thiol competitors to varying degrees.[20,21] For simple alkanethiol monolayers, these "exchange" experiments established that longer chain thiol competitors in solution removed and replaced bound thiols more quickly than short chain thiols.

Exchange experiments were performed on a $PyC_{10}S/Au$ sample with an 8-carbon ferrocenyl octanethiol (FcC_8SH) dissolved in absolute ethanol. The ferrocene-terminated thiol was chosen to reasonably mimic the presence of a large group containing pi-electrons at the chain terminus - analogous to the pyrrole-terminated alkanethiols. The experiment was performed as follows. First, an unoxidized monolayer of $PyC_{10}S/Au$ was exposed for 135 minutes to 2.5×10^{-4} M FcC_8SH in

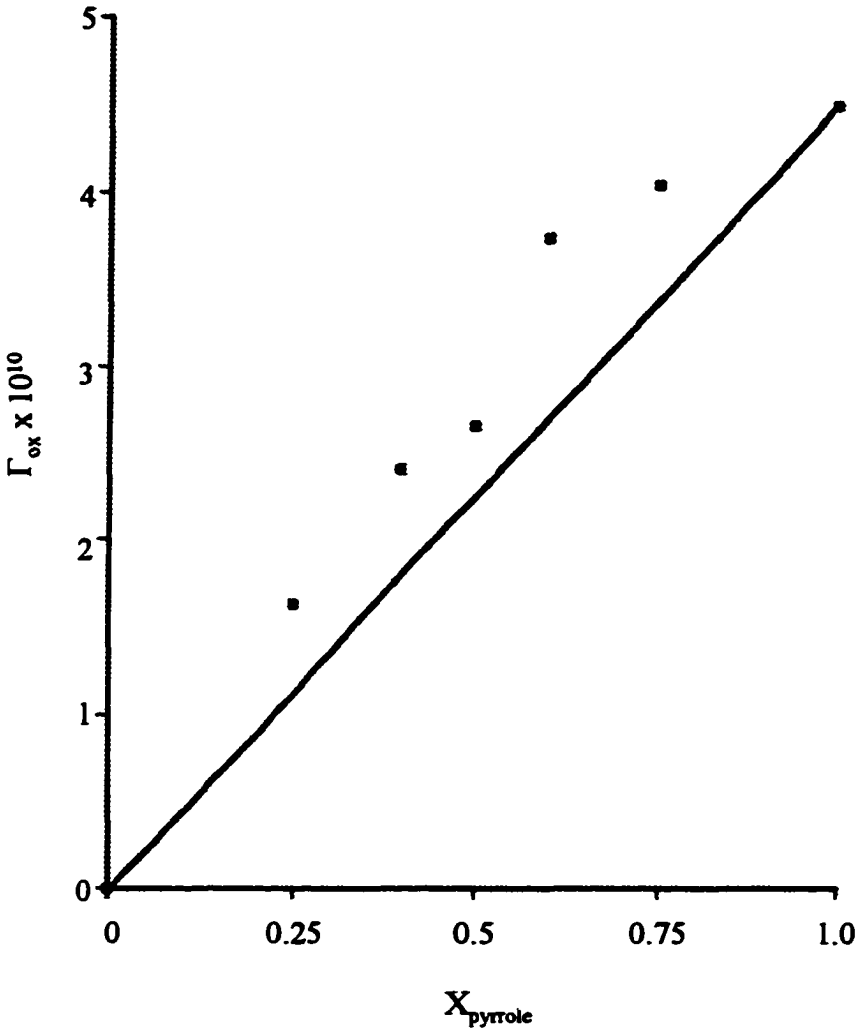

Figure 3.10 **Plot of surface coverage of PyC_6SH on Au surface vs. $X_{pyrrole}$ in solution. The solid line represents the ideal case where the fractional surface coverage of PyC_6SH equals $X_{pyrrole}$ in solution.**

ethanol, emmersed, rinsed, dried and oxidized by scanning to +1.0 V in clean 0.1 M TBAP/MeCN electrolyte, past the potential for both ferrocene and monomer oxidation. In another experiment, a monomer monolayer was treated in the same way with the

exception that one full monomer oxidation excursion to +1.15 V was performed immediately prior to the 135 minute exposure to FcC_8SH in ethanol.

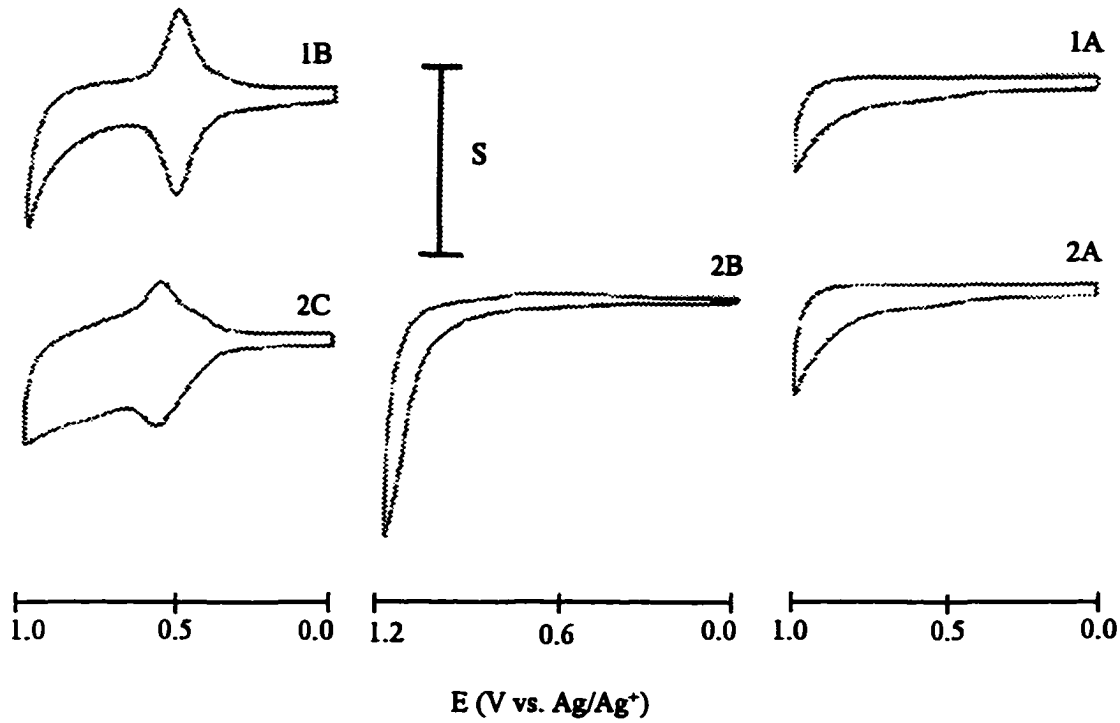

Figure 3.11 **Voltammetry in 0.1 M TBAP/MeCN of $PyC_{10}SH$-modified Au electrode (1A and 2A) scanned from 0 to +1.0 V (1B) scanned from 0 to +1.0 V after the potential excursion in 1A and exposure to 2.5×10^{-4} M FcC_8SH in EtOH for 135 minutes (2B) scanned from 0 to +1.15 V after potential excursion in 2A (2C) after potential excursion in 2A and 2B plus 135 minute exposure to 2.5×10^{-4} M FcC_8SH and then scanned from 0 to +1.0 V. S = 25.4 nA in 1A, 1B, 2A, and 2C; S = 63.5 nA in 2B and ν = 100 mV/sec for all scans.**

The voltammograms resulting from the two experiments are shown in Figure 3.11. As can be seen, the presence of the ferrocene redox wave is prominent in the voltammogram of the monolayer formed from exposure of unoxidized $PyC_{10}SH$ monomer to FcC_8SH indicating considerable exchange of the pyrrolyl alkanethiol for

ferrocenyl alkanethiol. The story is very different for the monolayer oxidized to form poly(*N*-mercaptoalkylpyrrole), Figure 3.11(2C) - the presence of ferrocene exchange can still be observed for this sample but it is much smaller and a substantial polymer charging/discharging wave is still present indicating that a considerable amount of the pyrrole-containing species is still adsorbed on the surface. These results point to a substantial increase in the stability of a $PyC_{10}S$/Au monolayer vs. strongly competitive adsorbates *after* oxidation of the monomer sites in the film. The stability of the electrochemically oxidized monolayer to only mildly competitive adsorbates (e.g. hydrophobic solvent molecules or short-chain hydrocarbons) should therefore be substantially greater.

The electrochemical data point directly toward a linking of the pyrrole units in the monolayer together to form a "knit" oligomer or polymer system. One possible model for this knit system is shown in Figure 3.12. This model is similar to one proposed for a Langmuir-Blodgett (L-B) film of an amphiphilic poly(thiophene).[22] The increased stability demonstrated in the exchange experiments is explained in terms of the formation of multiple attachment points to the surface. Any attempt to remove a given pyrrole thiol monomer would then necessitate an energetically unfavorable breakage of multiple Au-S bonds.

3.4 Conclusions

Electrochemical data consistent with the conversion of monomer to polymer *in a surface-confined monolayer* has been presented. In the next chapter, an experimental method more sensitive to changes in monolayer structure during and after oxidation will be discussed in support of this proposed polymeric monolayer. Spectroscopic

evaluation of the various surface-confined *N*-alkylpyrroles and the 2,5-disubstituted *N*-alkylpyrrole as electrochemical oxidation occurs will be discussed in detail.

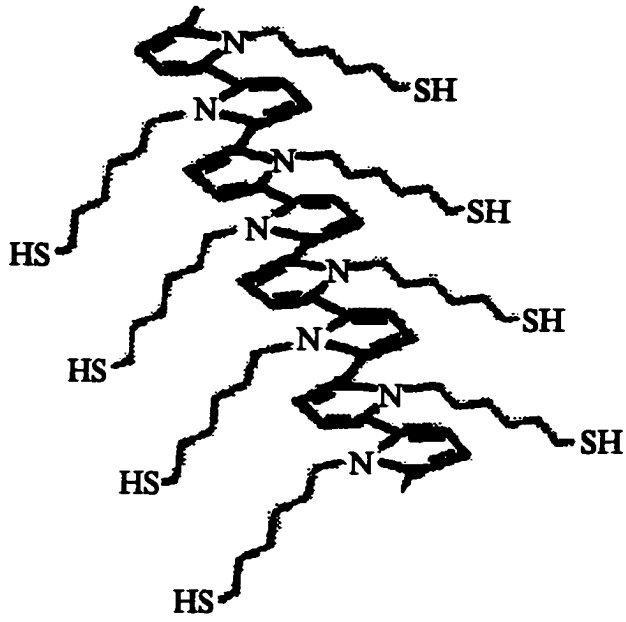

Figure 3.12 **Proposed structure of surface-confined poly(*N*-alkyl)pyrrole.**

3.5 References

1) Skotheim, T. A. *Handbook of Conducting Polymers*; Marcel Dekker: New York, 1986; Vol. 1.

2) Diaz, A. F.; Crowley, J. I.; Bargon, J.; Gardini, G. P.; Torrance, J. B. *J. Electroanal. Chem.* **1981**, *121*, 355.

3) Pfluger, P.; Street, G. B. *J. Chem. Phys.* **1984**, *80*, 544.

4) Nazzal, A.; Street, G. B. *J. Chem. Soc. Chem. Commun.* **1983**, *83*, 1983.

5) Diaz, A. F.; Castillo, J. I.; Logan, J. A.; Lee, W.-Y. *J. Electroanal. Chem.* **1981**, *129*, 115.

6) Clarke, T. C.; Scott, J. C.; Street, G. B. *IBM J. Res. Dev.* **1983**, *27*, 313.

7) Bard, A. J.; Faulkner, L. R. *Electrochemical Methods*; Wiley: New York, 1980.

8) Andrieux, C. P.; Audebert, P.; Hapiot, P.; Savéant, J.-M. *J. Am. Chem. Soc.* **1990**, *112*, 2439.

9) Diaz, A. F.; Castillo, J.; Kanazawa, K. K.; Logan, J. A.; Salmon, M.; Fajardo, O. *J. Electroanal. Chem.* **1982**, *133*, 233.

10) Diaz, A. F.; Kanazawa, K. K. *J. Chem. Soc., Chem. Commun.* **1979**, 635.

11) Sawyer, D. T.; Roberts, J. L. *Experimental Electrochemistry for Chemists*; Wiley: New York, 1984.

12) Bain, C. D.; Troughton, E. B.; Tao, Y.-T.; Evall, J.; Whitesides, G. M.; Nuzzo, R. G. *J. Am. Chem. Soc.* **1989**, *111*, 321.

13) Asavapiriyanont, S.; Chandler, G. K.; Gunawardena, G. A.; Pletcher, D. *J. Electroanal. Chem.* **1984**, *177*, 245.

14) Asavapiriyanont, S.; Chandler, G. K.; Gunawardena, G. A.; Pletcher, D. *J. Electroanal. Chem.* **1984**, *177*, 229.

15) Rodriguez, J. F.; Mebrahtu, T.; Soriaga, M. P. *J. Electroanal. Chem.* **1987**, *233*, 283.

16) Walczak, M. M.; Popenoe, D. D.; Deinhammer, R. S.; Lamp, B. D.; Chung, C.; Porter, M. D. *Langmuir* **1991**, *7*, 2687.

17) Chidsey, C. E. D.; Bertozzi, C. R.; Putvinski, T. M.; Mujsce, A. M. *J. Am. Chem. Soc.* **1990**, *112*, 4301.

18) Finklea, H. O.; Avery, S.; Lynch, M.; Furtsch, T. *Langmuir* **1987**, *3*, 409.

19) Morse, N. J.; Rosseinsky, D. R.; Mortimer, R. J.; Walton, D. J. *J. Electroanal. Chem.* **1988**, *255*, 119.

20) Bain, C. D.; Whitesides, G. M. *J. Am. Chem. Soc.* **1988**, *110*, 6560.

21) Bain, C. D.; Whitesides, G. M. *J. Am. Chem. Soc.* **1988**, *110*, 3665.

22) Sagisaka, S.; Ando, M.; Iyoda, T.; Shimidzu, T. *Thin Solid Films* **1993**, *230*, 65.

Chapter 4

Spectroscopic Analysis of Pyrrole-Containing Monolayers

4.1 Introduction to Infrared Methods for the Analysis of Thin Films on Reflective Substrates

Infrared spectroscopy (IR) has long been a powerful tool in the structural elucidation of organic molecules. Bulk samples are the primary targets of most infrared analyses but often it is necessary to detect very small amounts of materials. Attenuated Total Reflectance Infrared Spectroscopy (ATR-IR) and Infrared Reflection-Absorption Spectroscopy (IRRAS) are two examples of methods that have the capability to garner useful information from very small amounts of material.

ATR-IR involves[1] the use of a crystal, called an internal reflection element (IRE), with a high index of refraction surrounded by a rarer medium. When the angle of the light entering the IRE is below a critical angle, θ_c, the light undergoes total reflection from the internal faces of the IRE, travels down the length of the IRE, and exits through the opposite end. It has been shown that a small amount of the light reflected from the crystal/surrounding medium interface penetrates into the surrounding medium. The decrease in light intensity, or the magnitude of the electric field, is exponential with increasing penetration distance. This penetrating light is often referred to as an evanescent wave. When an analyte comprises the surrounding medium, absorption of some of the light can occur, thereby attenuating the intensity of the beam exiting the crystal. This absorption event is really no different from that in a transmission experiment. Thus, ATR-IR spectra are very similar to traditional transmission spectra.

ATR-IR is very useful for analyses involving small amounts of sample because the penetration depth of the evanescent wave is dependent on the incident angle of the light with respect to the entrance face of the crystal. Steep entrance angles restrict the infrared beam to very shallow penetration depths making it capable of probing very thin layers in contact with the ATR crystal. This IR technique has been widely applied to monolayer systems, such as Langmuir-Blodgett (L-B) films,[1] in the past.

IRRAS is another technique that has been successfully applied to the infrared analysis of extremely thin organic layers. Francis and Ellison[2] used both theory and experiment to demonstrate that thin absorbing layers could be analyzed by reflecting an infrared beam from the surface of a reflective metal using a 72° angle from the surface normal. Greenler[3] went on to show that the angle of incidence should actually be higher so as to achieve maximum sensitivity for infrared transitions of monolayer films. The angle of incidence needed to achieve maximum signal was found to be dependent on the metal used. Higher incidence angles could yield significant signal enhancements over the signal from a transmission infrared experiment on a film of comparable thickness.

The behavior of polarized light reflecting from a mirrored surface is responsible for the significant gain in absorption intensity of thin films at high incidence angles (grazing angles). For all angles of incidence, light that is polarized perpendicular to the plane of incidence, *s*-polarized light, will undergo a 180° phase shift. Light that is polarized parallel to the incident plane, *p*-polarized light, undergoes a phase shift that is a function of the angle of incidence. Phase shifts near 90° are typical for *p*-polarized light reflecting from a plane mirror at steep angles of incidence. A cartoon, depicting

these two scenarios for oppositely polarized light, is shown in Figure 4.1. It can clearly be seen from the figure that *s*-polarized light undergoes destructive interference at the interface for all angles of incidence, while a standing wave normal to the reflecting surface is generated for *p*-polarized light as a result of constructive interference. This standing wave can interact with vibrational modes that have components normal to the plane of the substrate. Such a result gives rise to the surface selection rules for reflection-absorption (RA) spectra. These selection rules preclude the observation of *any* significant absorption from components of infrared vibrational modes that are parallel to the surface.

ATR-IR and IRRAS can both be used to obtain structural and orientational information about ultrathin films. ATR-IR has been used to study L-B films, which are often prepared on substrates that are suitably transparent to light in the infrared region of the spectrum. ATR-IR can also be utilized to study self-assembled monolayer (SAM) films on ATR crystals pre-coated with a thin metal film. Use of this ATR-IR method for the characterization of monolayers has not been widespread due to complications arising from the intense reflectivity of metals in the infrared.

IRRAS is an ideal technique for studying the characteristics of ultrathin films of various types formed on metallic substrates due to the requisite use of a reflecting surface. For this reason, IRRAS was chosen as the most suitable technique for the ex-situ investigation of our surface-confined monomer and polymer films. The goals of this spectroscopy chapter are to confirm the structural changes that must occur in the surface-confined layer to achieve polymerization by monitoring the changes in the

orientation of the pyrrole ring and alkane chain after electrochemical polymerization has been carried out.

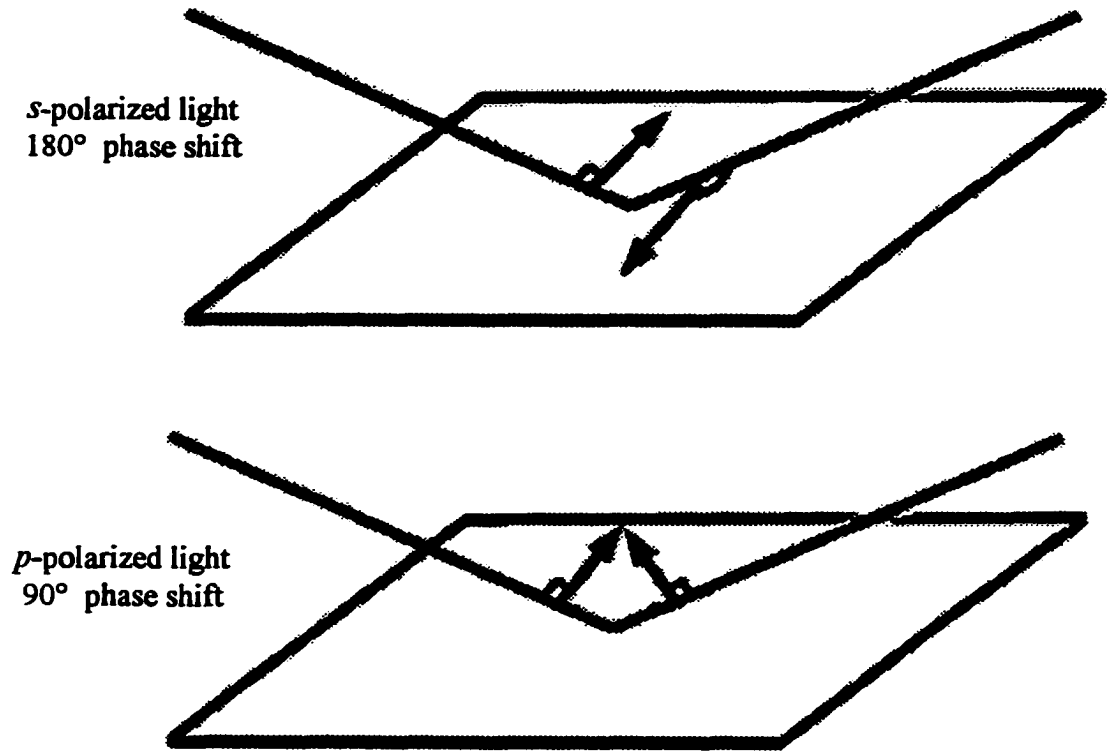

Figure 4.1 **Cartoon depicting the phase shift of the electric field vectors for light reflected from a plane mirror. The plane of incidence is normal to the reflecting substrate.**

4.2 History of Analysis of Various SAMs on Metal Substrates Using IRRAS

Allara and Swalen pioneered the use of IRRAS for the characterization of monolayers. Their studies involved examining oriented L-B films of cadmium arachidate on silver surfaces.[4] IRRAS was used by Nuzzo and Allara to confirm the formation of SAMs on Au prepared from cyclic disulfides.[5] They were able to determine the orientation of the terminal rings from an analysis of the infrared band

intensities. Experiments were also conducted by Allara and Nuzzo on the adsorption of *n*-alkanoic acids on aluminum oxide substrates.[6] In this latter study, analysis of the C-H stretching region allowed a quantitative determination of the orientation of the alkane chain with respect to the surface.

Monolayers on Au prepared from the self assembly of alkanethiols of various chain lengths were studied by Porter et al.[7] In addition to the conclusion that the alkane chains in the monolayer were tilted 20°-35° from the surface normal, information concerning the order of the films was obtained. Earlier reports by Snyder et al.[8,9] indicated that the frequency for asymmetric and symmetric C-H stretching modes ($\upsilon_{C\text{-}H}$ modes) in bulk paraffin compounds increased as the length of the alkane chain decreased due to decreases in van der Waals attractions between molecules. This same observation was reported in the work by Porter for *n*-alkanethiol monolayers. SAMs formed from *n*-alkanethiols with more than ten carbons (or methylene units) were shown to exhibit crystalline-like packing. IRRAS has also been used to examine a variety of ω-functionalized alkanethiol SAMs and compare their structures to those of their methyl-terminated counterparts.

Chidsey and Loiacono[10] examined ferrocene-terminated alkanethiols while Sinniah et al.[11] measured orientations for ω-hydroxyalkanethiol monolayers containing internal ether functionalities. There are several reports of the analysis of various pyrrole- and poly(pyrrole)-containing films in the literature using IRRAS. Iyoda et al.[12] examined L-B films formed from a mixture of octadecane and octadecyl 4-methylpyrrole-3-carboxylate. In this study, disappearance of the symmetric

out-of-plane C-H deformation (ω_{C-H}) band at 780 cm^{-1} of the 3,4-disubstituted monomer was stated to be indicative of the polymerization of the monomer units in the film, although no spectra were shown to support this claim. Yang et al.[13] reported the RA spectrum in the C-H stretching region for poly(3-hexadecyl)pyrrole layers formed on Pt substrates using L-B techniques. The orientation of the alkane chains with respect to the surface was found to change upon going from monolayer to multilayer assemblies. Cheung et al.[14] reported that the pyrrole rings of poly(pyrrole) chains formed on Pt using L-B techniques were preferentially oriented parallel to the plane of the Pt substrate. These polymer films were obtained using mixtures containing a high excess of pyrrole monomer in the presence of a polar, 3-substituted pyrrole derivative to aid in the formation of close-packed layers. Rikukawa and Rubner[15] obtained similar results for the ordering of poly(pyrrole) chains upon chemical oxidation of L-B films containing a mixture of pyrrole, 3-octadecanoyl pyrrole and poly(3-hexylthiophene).

Several important points should be noted about the studies performed on the conducting polymers and their precursors described above. First, all the films were prepared using L-B methods, complicating the interpretation of the resulting spectra due to the need to use mixtures of monomers and substituted monomers to achieve good film formation. Second, none of these reports display the pyrrole ring-stretching region of these L-B films before polymerization. *This probably stems from the fact that stable films could only be formed on oxidizing sub-phases that could promote oxidative linking of the surface-confined pyrrole units.* Third, none of these reports show the ring-stretching region for a *single* layer of conducting polymer deposited using these techniques; this region has been shown for films containing a minimum of

five sequentially deposited layers. Fourth, in all the spectra that exist for L-B films of poly(pyrrole)-containing multilayers, a ω_{C-H} band located in the 700-800 cm^{-1} range is not present. Thus, infrared spectroscopic evidence for poly(pyrrole) formation in L-B films is scant at best. The purpose of this chapter is to spectroscopically confirm the electrochemical evidence for formation of a single molecular layer of conducting polymer from its surface-confined monomer precursor.

4.3 Experimental

4.3.1 Spectroscopic Analysis

All infrared spectra were collected on a Nicolet 740 FTIR system with wide and narrow band detectors sensitive to wavenumbers down to 550 cm^{-1} and 780 cm^{-1}, respectively. A custom-made poly(ethylene) shroud continuously purged with house nitrogen (liquid nitrogen boil-off) protected the analyzing chamber from water and CO_2 contamination. The optical bench was purged with house nitrogen passed through a home-made water and CO_2 scrubbing system. Reflection spectra were collected using a versatile reflection accessory with retro-mirror attachment (VRA-RMA, Harrick Scientific) using incidence angles of 86° with respect to the substrate normal. Spectra were typically recorded using 1024 co-added scans at 2 cm^{-1} resolution with Happ-Genzel apodization. Purge correction to remove residual water vapor bands from the infrared RA spectra were typically used. Baseline correction of spectra was performed using the Nicolet SX software. Purge times between spectral collection were roughly 20 minutes.

X-ray photoelectron analysis (XPS) was performed on a Kratos XPS spectrometer employing a monochromatic $Al_{k\alpha}$ source at 1486.6 eV. The anode voltage was 12 kV and the anode current was nominally 20 mA.

4.3.2 Fabrication of Au Substrates

Thin Au films as substrates for SAM formation were prepared by vapor deposition of Au from a resistively-heated tungsten boat in a cryogenically-pumped evaporator (Edwards Auto306). Glass microscope slides (Curtin-Matheson, CMS no. 358-762) were used as the support for Au films. Prior to their placement in the vacuum system, the microscope slides were cleaned in a 1:4 mixture of 30% hydrogen peroxide (EM Sciences) and concentrated, analytical grade sulfuric acid (Mallinckrodt), (pirahna solution), heated to 70 °C. *Caution: this is a strongly oxidizing solution which should be kept away from any organic materials and handled with extreme caution.* The glass slides were soaked in the hot pirahna solution for 30 minutes and then allowed to cool for ca. 15 minutes. At this time, they were rinsed with copious amounts of 18 MΩ cm water (Barnstead) and absolute ethanol (Aaper), and blown dry with dry nitrogen. Au films ca. 150 nm in thickness were deposited onto the glass slides after a 5 nm adhesion promoting layer of chromium was vapor deposited. Au films were produced using pellets of 99.99% purity metal (Nevada Refining Systems) while chromium was deposited from a resistively-heated, Cr-coated tungsten wire (Kurt Lesker).

4.3.3 Monolayer Formation

All monolayer formation was carried out in an inert atmosphere box (Vacuum Atmospheres). Substrates for SAM formation were brought into the box under

Ar-purged absolute ethanol in sealed vials. The Au substrates were rinsed with pure ethanol and allowed to soak in the assembling solution for varying amounts of time with the minimum being two hours. Fully-formed SAMs that had to be reintroduced to the inert atmosphere box were sealed in Ar-flushed glass vials.

4.4 Results and Discussion

4.4.1 Pristine *N*-Substituted Pyrrole-Terminated Monolayers

A representative infrared RA spectrum in the lower energy region of a $PyC_{10}SH$ monolayer on Au is shown in Figure 4.2. The IR spectrum exhibits several sharp bands that can all be assigned to various motions of the pyrrole ring. One of the most important bands in this region of the spectrum is the in-phase (symmetric) C-H out-of-plane deformation centered at ca. 722 cm^{-1} (ω_{C-H}). This is an intense transition in the spectra of heterocyclic compounds due to the large dipole moment change associated with the vibration.[16] It should also be noted that the direction of the transition dipole moment for this vibration is perpendicular to the plane of the aromatic ring.[17] Several other bands are observed at 1089 cm^{-1}, 1285 cm^{-1}, and 1502 cm^{-1}, representing the in-plane C-H deformation (δ_{C-H}), aliphatic C-N stretching (υ_{C-N}), and C=C ring stretching ($\upsilon_{C=C}$) modes, respectively. All of these modes have transition dipole moment directions that are contained within the plane of the aromatic ring and are thus orthogonal to the ω_{C-H} mode at 722 cm^{-1}.[17] A complete band assignment can be found in Table 4.1 for the *N*-substituted pyrrole analogues used in this work. These assignments were made based on previous analyses performed on the isotropic spectra of pyrrole and substituted pyrroles.[17,18]

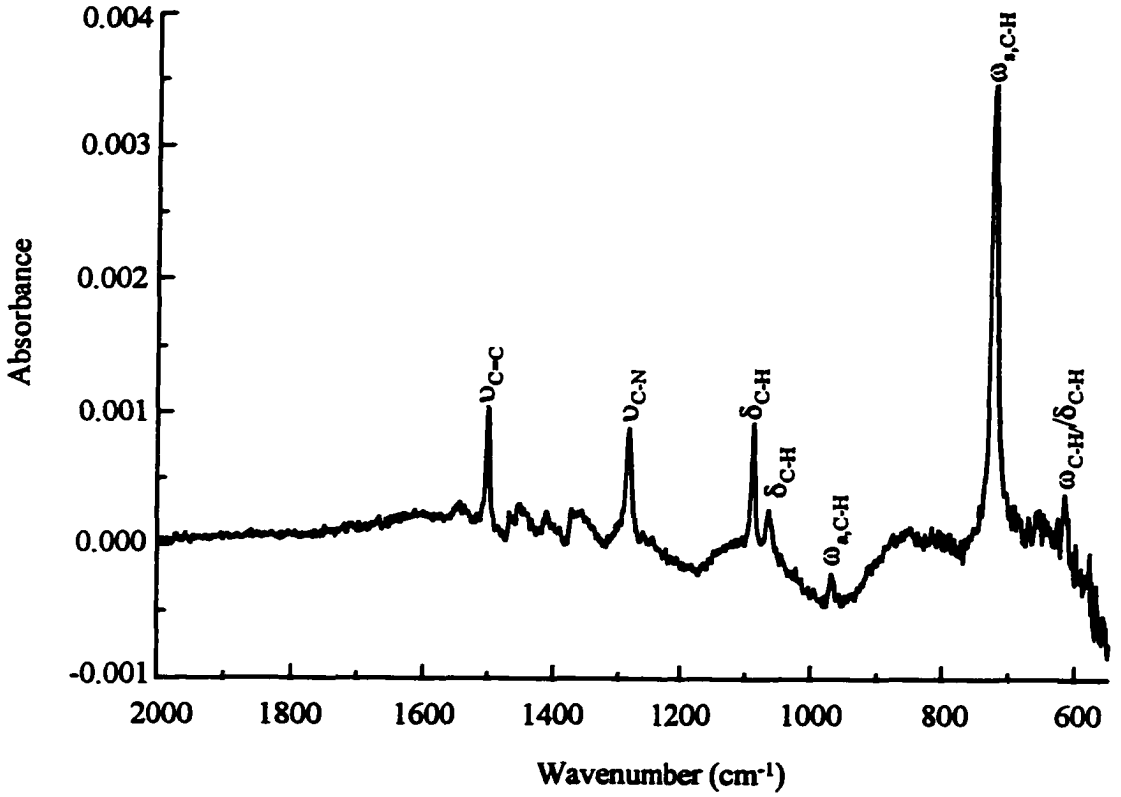

Figure 4.2 **Low energy RA spectrum of a pristine $PyC_{16}SH$ monolayer on Au.**

Table 4.1 **Band assignments in the lower frequency region for *N*-substituted pyrrole-derived SAMs.**

Mode of vibration	Wavenumber (cm^{-1})	Direction of transition dipole moment
C=C, C-C stretch	1500	in plane of aromatic ring
aliphatic C-H deformation (δ_{CH2})	1465	perpendicular to alkane chain axis
aliphatic C-N stretch (υ_{C-N})	1282	in plane of aromatic ring
aromatic in-plane C-H deformation (δ_{C-H})	1089	in plane of aromatic ring
aromatic in-plane C-H deformation (δ_{C-H})	1065	in plane of aromatic ring
asymmetric out-of-plane C-H deformation ($\omega_{a,C-H}$)	969	perpendicular to plane of aromatic ring
symmetric out-of-plane C-H deformation ($\omega_{s,C-H}$)	722	perpendicular to plane of aromatic ring
aromatic out-of-plane C-H or in-plane aromatic C-H deformation ($\omega_{C-H}/\delta_{C-H}$)	616	perpendicular to or in the plane of aromatic ring, respectively

In order to begin to understand how the pyrrole ring is oriented with respect to the surface of the anchoring substrate, it is first necessary to obtain the isotropic spectrum of PyC_xSH. Comparison of the intensities of the bands for the surface-reflection spectrum and transmission spectrum should allow for a qualitative view of how the pyrrole ring is oriented with respect to the surface normal. The transmission spectrum in the low energy region for pure $PyC_{10}SH$ in a 10 μm liquid cell is shown in Figure 4.3. Several interesting observations are immediately apparent upon a comparison of the isotropic and reflectance spectra. First, all the bands that are present in the reflectance spectrum are present in the transmission spectrum. Second, the relative absorbance ratios among the four bands mentioned above ($\upsilon_{C=C}$, υ_{C-N}, δ_{C-H}, ω_{C-H}) are not different when comparing the transmission spectrum to the reflectance spectrum. This is very strong evidence that the pyrrole rings on the surface are isotropic. That is to say that the pyrrole rings appear, on average, to have no preferred orientation with respect to the surface. This is very interesting due to the fact that we had earlier postulated that the pyrrole groups on the surface would probably need some measure of "floppiness" in order to undergo the dynamics needed to couple to each other. This disorder is also present for monolayers of PyC_6SH on Au, as evidenced by a comparison of the infrared RA spectra and isotropic spectra in the low energy region. Both the isotropic and reflection spectra display the same bands with the same band ratios. This indicates that the PyC_6SH- and $PyC_{10}SH$-modified Au surfaces exhibit roughly the same amount of disorder at the chain terminus despite the potential for increased van der Waals attraction between alkane chains in the monolayer formed from the longer alkane chain component. Another way to assess the amount of

disorder present in each of the assemblies is to examine the symmetric and asymmetric C-H stretching modes (υ_{C-H}) for the alkane methylene groups.

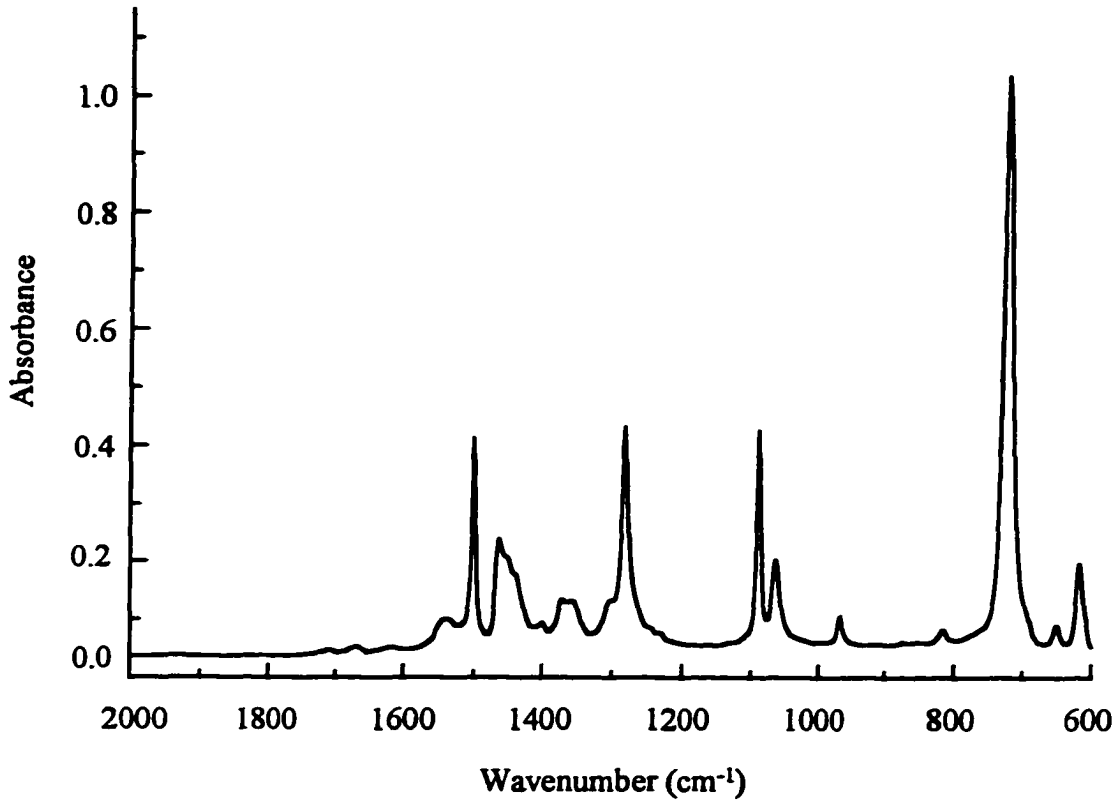

Figure 4.3 **Low energy transmission IR spectrum of neat $PyC_{16}SH$ in 10 μm liquid cell.**

Snyder[8,9] and Porter[7] have shown that the frequency at which the band maximum occurs for the methyl and methylene stretches of bulk *n*-alkanes and *n*-alkanethiol monolayers on Au can be used as a qualitative indicator of the amount of order present amongst the alkane chains (vide supra). Short chain alkane compounds that exhibit little order (liquids) tend to have much higher C-H methylene stretching frequencies than their long-chain counterparts. This is a result of the significant van der Waals interactions that exist between the longer chains. Porter et al. found

experimentally that *n*-alkanethiol monolayers with an alkane chain of nine carbons or more began to exhibit semi-crystalline order. As discussed in Chapter 2, pyrrole-terminated alkanethiols were synthesized with several different chain lengths in an attempt to investigate the effect that the order of the alkane chain would have on the surface-confined polymerization reaction. Unfortunately, it was found that the monolayers formed from the different chain length monomers used in this study were *all* quite disordered.

Comparisons of the peak frequencies of the $\upsilon(CH_2)$ modes for the $PyC_{10}S$/Au and PyC_6S/Au monolayers can be made with those experimental results in mind. It was found that the $PyC_{10}S$/Au monolayers exhibited slightly more order than the PyC_6S/Au monolayers but both were quite disordered in comparison to *n*-octadecanethiol monolayers on Au. The high energy region of a typical infrared spectrum of a $PyC_{10}SH$ monolayer on Au is shown in Figure 4.4. A statistical analysis of the frequency values yielded an average peak frequency for the asymmetric methylene stretch of 2930 ± 2 cm^{-1} in the case of PyC_6SH monolayers on Au and 2928 ± 1 cm^{-1} for $PyC_{10}SH$ monolayers on Au. Similar analysis of the symmetric methylene stretch gave 2860 ± 2 cm^{-1} and 2856 cm^{-1} for PyC_6SH and $PyC_{10}SH$ monolayers on Au, respectively. This lack of order in both of the pyrrole monolayers is not all that surprising considering the large van der Waals radius of the tailgroup with respect to the alkane chain. The small amount of difference between the frequency of a given methylene stretch for the two monolayers was not, however, anticipated. The observed lack of order is consistent with the isotropic nature of the pyrrole ring vibrations discussed above for all the chain

lengths studied and also supports the electrochemical data suggesting no decrease in polymerization efficiency with increasing alkane chain length.

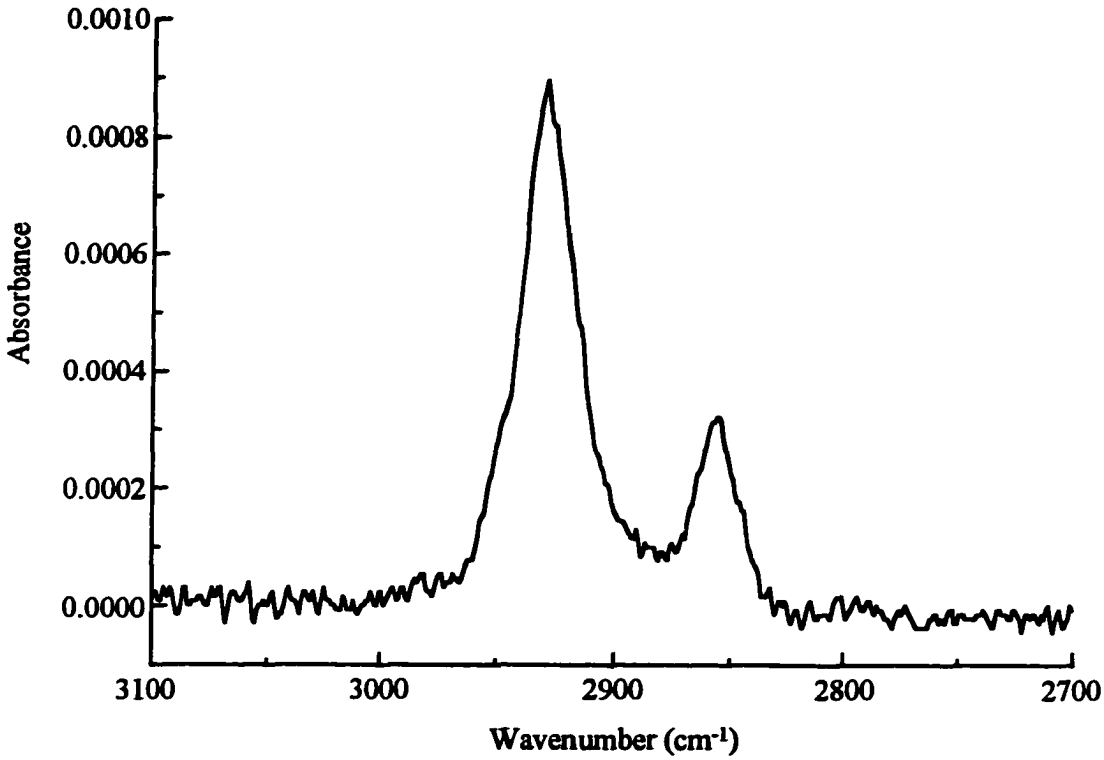

Figure 4.4 **High energy RA spectrum of pristine $PyC_{10}SH$ monolayer on Au.**

4.4.2 Electrochemically Oxidized *N*-Substituted Pyrrole Monolayers

A $PyC_{10}S$/Au monolayer was first oxidized electrochemically under Ar to +0.950 V vs. Ag/Ag^{+}, just below the potential for onset of monomer oxidation. The infrared RA spectrum in the low energy region for the monolayer after the potential excursion is shown in Figure 4.5. For this small amount of monolayer oxidation, a very small decrease in the peak absorbances for the $\upsilon_{C=C}$, υ_{C-N}, δ_{C-H}, and ω_{C-H} has occurred. Even more interesting are the results obtained when a potential excursion for the same

monolayer is extended to +1.15 V vs. Ag/Ag^+, a potential slightly above that needed for onset of monomer oxidation. The resulting spectrum is shown in Figure 4.6 where it can be seen that all four bands (υ_{C-C}, υ_{C-N}, δ_{C-H}, ω_{C-H}) have undergone significant decreases in peak intensity. The salient point to note here, however, is that *all of the bands are decreasing by approximately the same amount*, giving valuable insight into the reason behind loss of absorbance in the film. Electrochemical excursions to +1.2 V result in complete oxidation of the film (no monomer oxidation wave evident on second anodic scan, see Chapter 3) with the corresponding loss of all infrared intensity for the four ring modes discussed above.

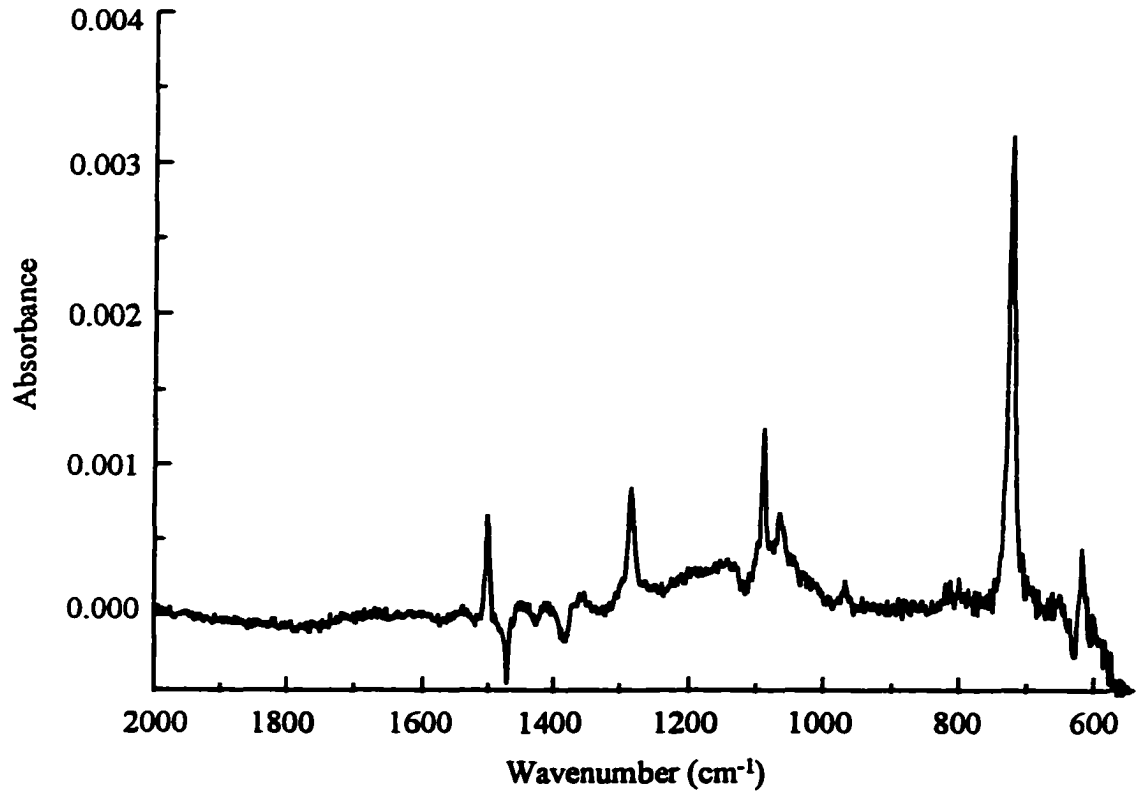

Figure 4.5 **Low energy RA spectrum of $PyC_{16}SH$ monolayer on Au electrochemically oxidized to +0.950 V in one cycle.**

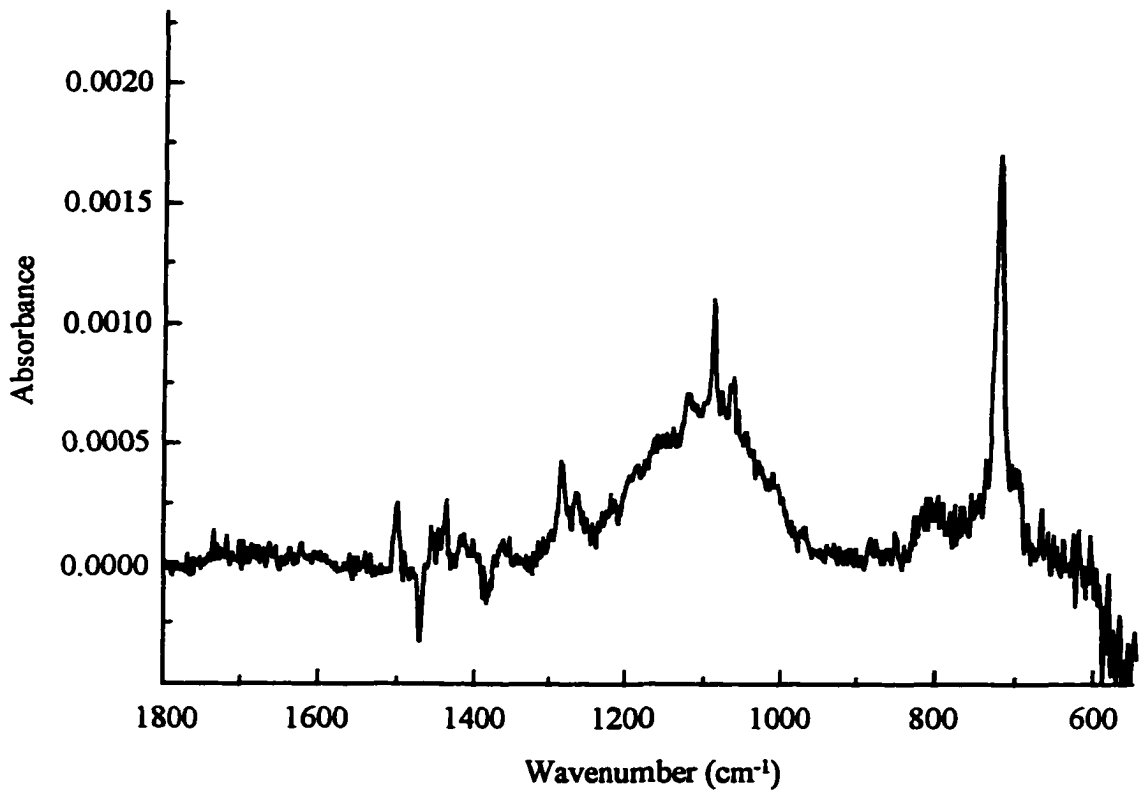

Figure 4.6 **Low energy RA spectrum of $PyC_{10}SH$ monolayer on Au electrochemically oxidized to +1.15 V.**

If the molecules on the surface were to experience a potential (as a result of a potential excursion) that changed the orientation of the modes with respect to the surface without changing the strength of the transition dipole moments associated with those modes, an entirely different situation would be expected. The intensity changes of the bands orthogonal to each other would be inversely related to each other as the orientation of the ring changed. Thus, it would be expected that the in-plane modes would decrease while the out-of-plane modes increased or vice versa. The absence of this type of behavior is good evidence that the band intensity changes are not a function of orientation, but rather a result of chemical changes in the groups responsible for the observed vibrations.

The decrease in the intensity of the absorbance bands associated with the pyrrole ring as a result of chemical changes in the monolayer was not unexpected, but the lack of any *new* bands appearing in the reflectance spectrum was surprising. Polymerization of the surface-confined pyrroles through the α and α' carbons leaves two adjacent hydrogens on the pyrrole ring in the β and β' positions. The $\omega_{C\text{-}H}$ band for these two remaining C-H groups would be expected to appear as a blue-shifted band of decreased intensity with respect to the original $\omega_{C\text{-}H}$ band. Such a blue-shift and intensity decrease has been demonstrated in the *bulk spectra* of a series of pyrrole oligomers.[19] This band is not apparent in the reflectance spectra of partially or fully oxidized monolayers of $PyC_{10}SH$ on Au under the voltammetric conditions used here to produce electrochemically observable polymer. The loss in intensity for the ring modes of the monolayers described here is also puzzling due to the fact that substitution at the

α and α' carbons (due to polymerization) *should* cause a blue-shift in their frequency along with some intensity changes. For a fully oxidized $PyC_{10}SH$ monolayer on Au, no detectable intensity remains for those modes.

One possible explanation for the loss in intensity from all the pyrrole ring modes is the pyrrole tailgroup or perhaps the entire (mercaptoalkyl)pyrrole could be desorbing from the surface under the potential conditions employed here. No evidence to support this idea is observed upon close inspection of the electrochemical data or electron spectroscopic data (vide infra). A possible explanation for the total loss in intensity of the ω_{C-H} band at 722 cm^{-1} with no new observable bands is that all the C-H groups on the pyrrole ring have been substituted, thus leaving no C-H groups present to give rise to an absorption in this region. This possibility was tested by exposing an electrochemically oxidized $PyC_{10}SH$ monolayer on Au to air for 11.7 hours. The spectrum resulting from this experiment is shown in Figure 4.7. Upon comparing this spectrum to that before exposure (Figure 4.6), it can be seen that there are several notable changes. All of the ring modes and the ω_{C-H} deformation mode have completely disappeared and several new bands have appeared. The most notable of these bands is the large band centered at ca. 1718 cm^{-1}. This band is in the expected frequency range for a carbonyl absorption and has been shown in the literature,[20] to be indicative of a carbonyl group attached to a pyrrole ring. The formation of the carbonyl group on the pyrrole ring requires that at least one of the ring carbon atoms must still have a hydrogen bonded to it. PyC_xSH monolayers on Au that are electrochemically overoxidized (E > +1.6 V) in organic solvents containing trace H_2O exhibit identical C=O absorption bands. This is good evidence that some substantial

number of hydrogens do indeed still exist on the pyrrole rings in the monolayer even though they do not show up with measurable intensity in the ω_{C-H} deformation region. Additional exposure of the same monolayer to air results in the formation of more intense and well-defined C=O and C-O bands, Figure 4.8.

As additional proof of the continued presence of the pyrrole ring on the surface after electrochemical oxidation, X-ray photoelectron spectroscopy (XPS) was used to analyze the $PyC_{10}SH$ monolayers before and after electrochemical oxidation. The N_{1s} and S_{2p} signals were both monitored and integrated before and after electrochemical oxidation. The integrated areas were found to remain unchanged, Figure 4.9.

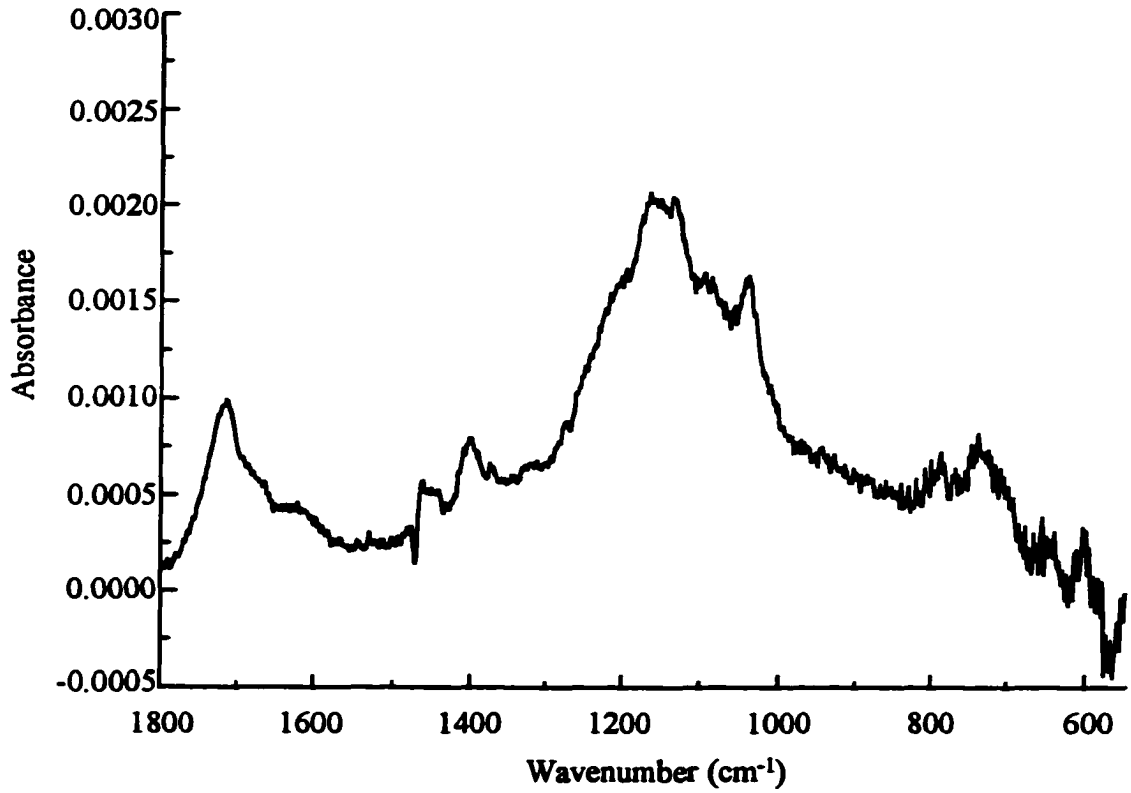

Figure 4.7 **Low energy RA spectrum of a $PyC_{10}SH$ monolayer on Au exposed to ambient atmosphere for 11.7 hours after electrochemical oxidation to +1.15 V.**

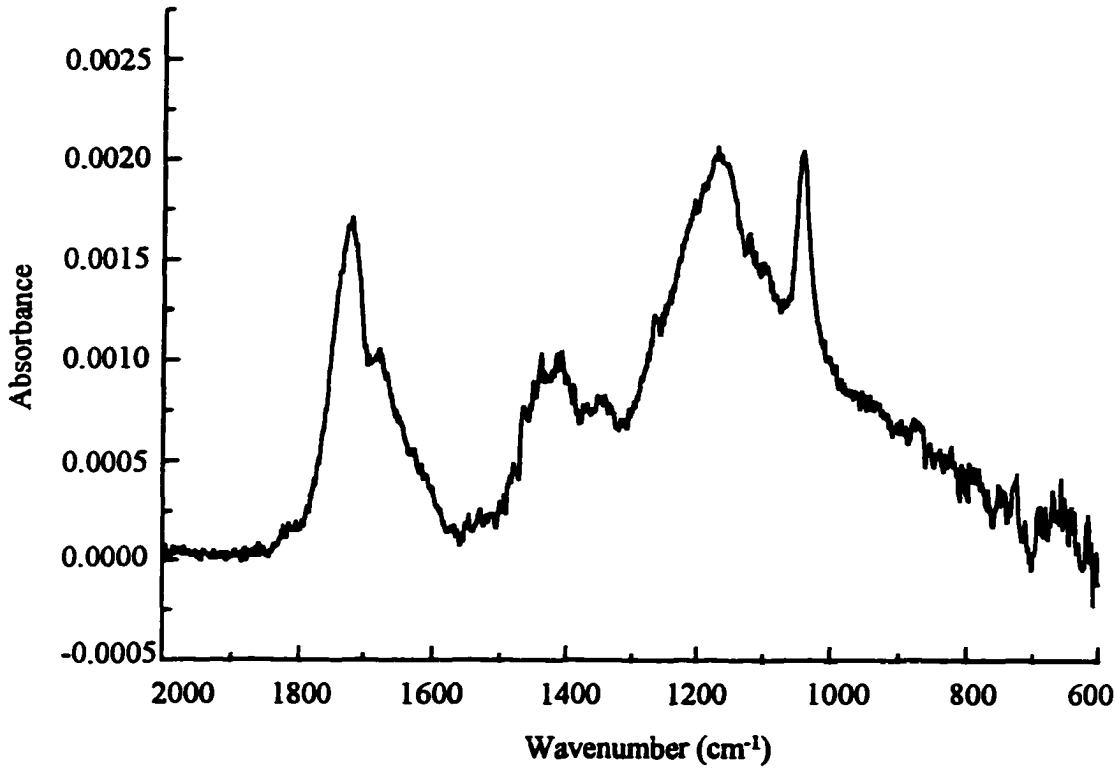

Figure 4.8 **Low energy RA spectrum of $PyC_{16}SH$ monolayer on Au from figure 4.7 exposed to ambient for a total of 83 hours.**

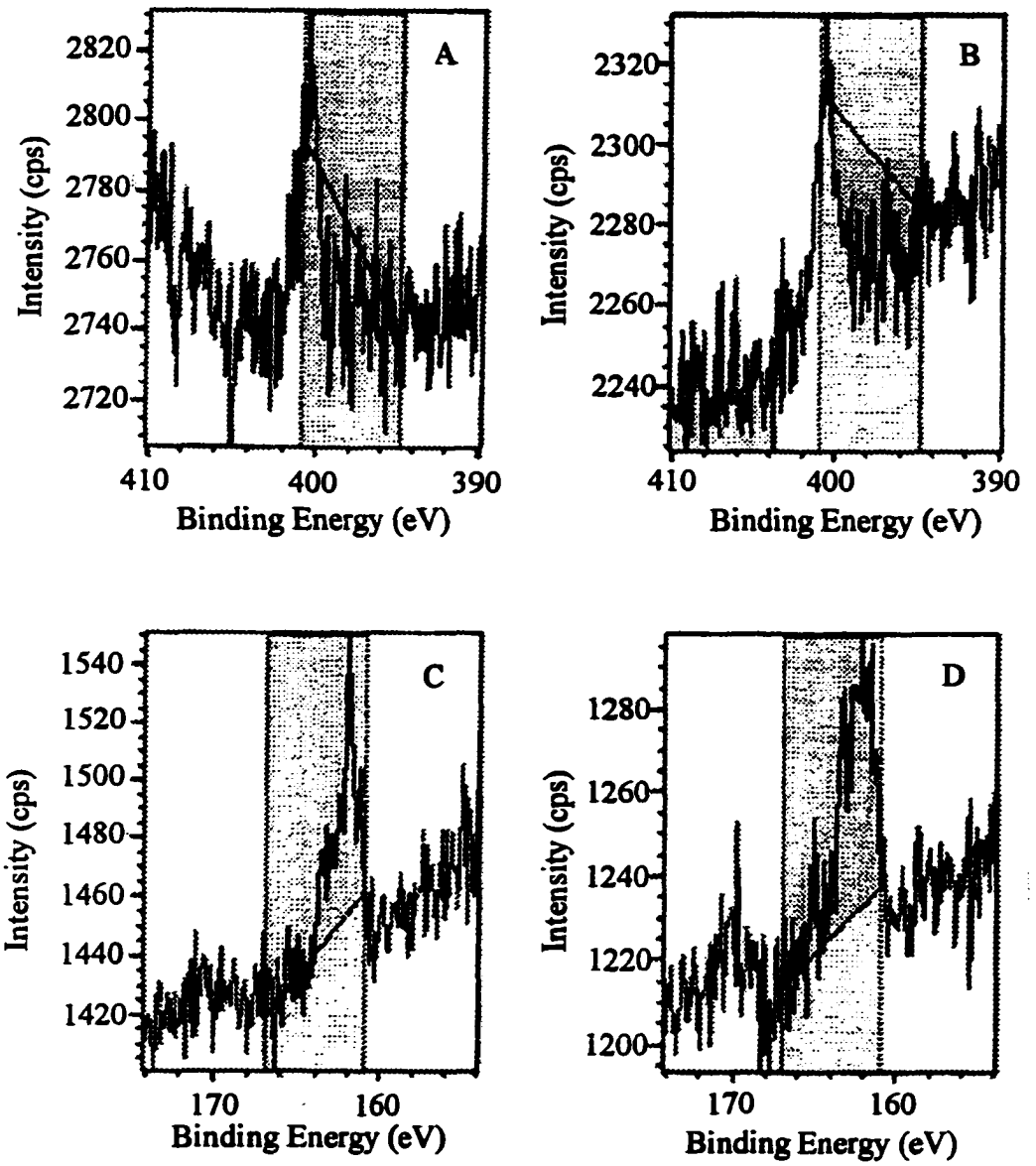

Figure 4.9 **High-resolution X-ray photoelectron spectra of (A) pristine $PyC_{10}SH$ monolayer on Au in N_{1s} region (B) $PyC_{10}SH$ monolayer on Au electrochemically oxidized to +1.2 V and emmersed at 0 V in N_{1s} region (C) pristine $PyC_{10}SH$ monolayer on Au in S_{2p} region (D) $PyC_{10}SH$ monolayer on Au electrochemically oxidized to +1.2 V and emmersed at 0 V in S_{2p} region.**

This data points to the lack of removal of any portion of the monolayer during electrochemical oxidation. This lack of monolayer loss was explored further by examining the peak intensity for the C-H methylene stretches after monolayer oxidation, Figure 4.10. It can clearly be seen that very little change in the intensity of this band occurs as a result of monolayer oxidation. All of these experiments demonstrate that *the monolayer is not being removed from the surface during electrochemical oxidation and that aromatic C-H groups are still present in the monolayer*, although they do not give rise to measurable absorption in the expected spectral region(s).

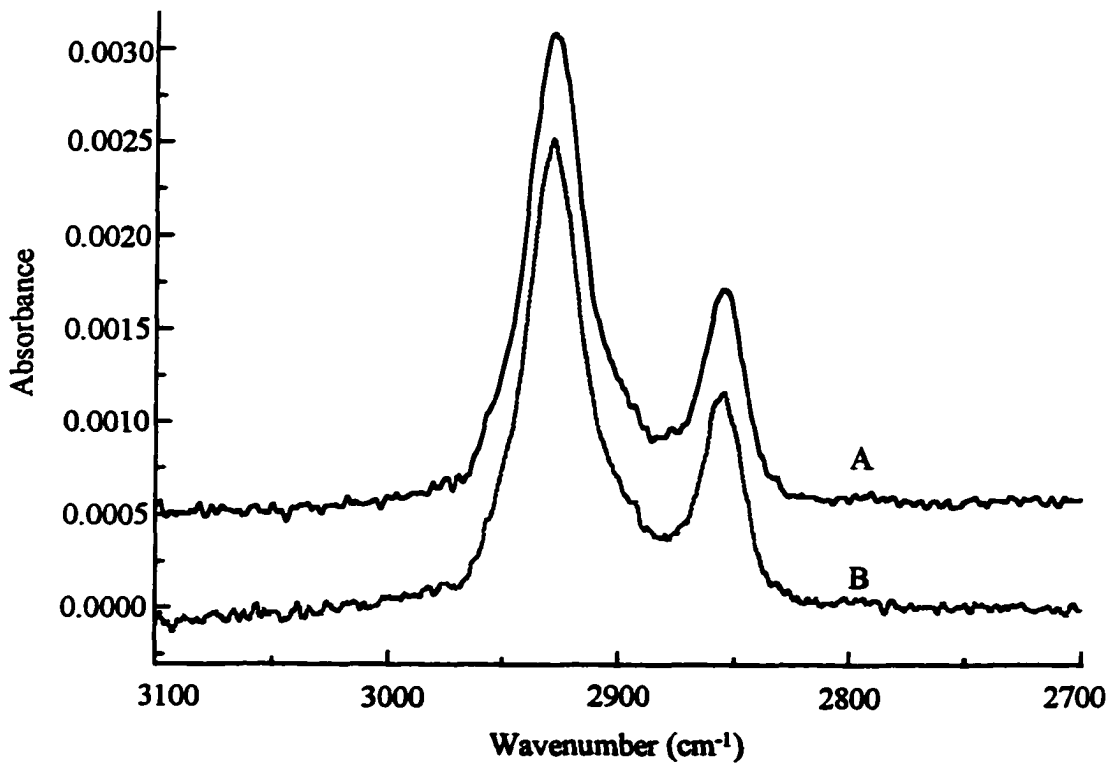

Figure 4.10 **High energy RA spectra of (A) pristine $PyC_{16}SH$ monolayer on Au and (B) $PyC_{16}SH$ monolayer on Au electrochemically oxidized to +1.2 V. The y-axis is arbitrary.**

The cause of the changes in the bands associated with the various ring modes upon electrochemical oxidation are not entirely understood either. Intensities of the ring modes decrease upon oxidation, and disappear completely upon total electrochemical oxidation of the monolayer. It can be argued from the XPS data that C-N groups must still exist in the monolayer after electrochemical oxidation, so the origin of the loss of all intensity for these vibrations is unclear. The only logical explanation for the loss of these bands excluding radical shifts in peak frequencies is a decrease in absorption intensity below a detectable level. A decreased infrared absorption cross-section for these modes in the monolayer could cause the decreases in observed intensities. Due to the fact that the number of pyrrole units on the surface is extremely small, such a proposed decrease in IR absorption cross-section could render the aromatic units undetectable with our instrumentation.

4.5 Pristine and Oxidized Dimethyl-Substituted Pyrrole-Terminated Monolayers

The origin of the differences expected in this monomer compared to the *N*-substituted pyrrole-terminated monomer lies in its reduced ability to couple with its neighbors due to the fact that only the beta groups of the ring are available for polymerization. Polymerization through the beta sites is possible and is seen to some extent in all poly(pyrrole) films. By forcing the polymerization to go through the beta sites, however, it is expected that no significantly long chains of pyrrole would be able to form due to the steric hindrance of the methyl groups present in the alpha positions. The only way that long polymer chains could form would be for the rings to contort significantly out of plane with respect to each other. If this were to occur, the

conductivity of the resulting polymer would be drastically reduced[21] and the effect on the corresponding ring modes could be studied.

A pyrrole monomer with methyl groups in the α and α' positions capable of self assembly on Au was synthesized to explore the behavior of a self-assembled monolayer with "blocked" α and α' ring sites. Such α, α'-blocked pyrroles have been shown to be incapable of forming highly conjugated polymers by coupling through the β and β' positions of the ring (vide supra). A spectrum of the pristine 2,5-PyC_6SH monolayer on Au is shown in Figure 4.11 and a complete band assignment can be found in Table 4.2. The spectrum appears very different from that of the *N*-substituted pyrrole-containing monolayers. The presence of the ω_{C-H} band is noted at 751 cm^{-1} (compared to 722 cm^{-1} for PyC_xSH on Au) and is of lower intensity than that observed for PyC_xSH on Au. This is expected from dipole strength considerations as a result of fewer consecutive C-H groups on the ring. Both the C=C and the C-N vibrations are blue-shifted and an extremely large ring-stretching mode is present at 1411 cm^{-1}, both of which are indicative of a 2,5-disubstituted pyrrole monomer.[18]

The reflectance spectrum was compared to a spectrum of the bulk liquid in a 13.4 μm transmission cell, shown in Figure 4.12. The relative changes in band intensity ratios are more significant when comparing the surface-confined spectrum to that of the bulk species for the 2,5-PyC_6SH vs. the *N*-substituted monomers. For example, the ratio of the peak intensities of the ω_{C-H} mode and either the C=C stretch at 1519 cm^{-1} or the ring stretch at 1410 cm^{-1} (both in the plane of the ring) is 1:2.2 in

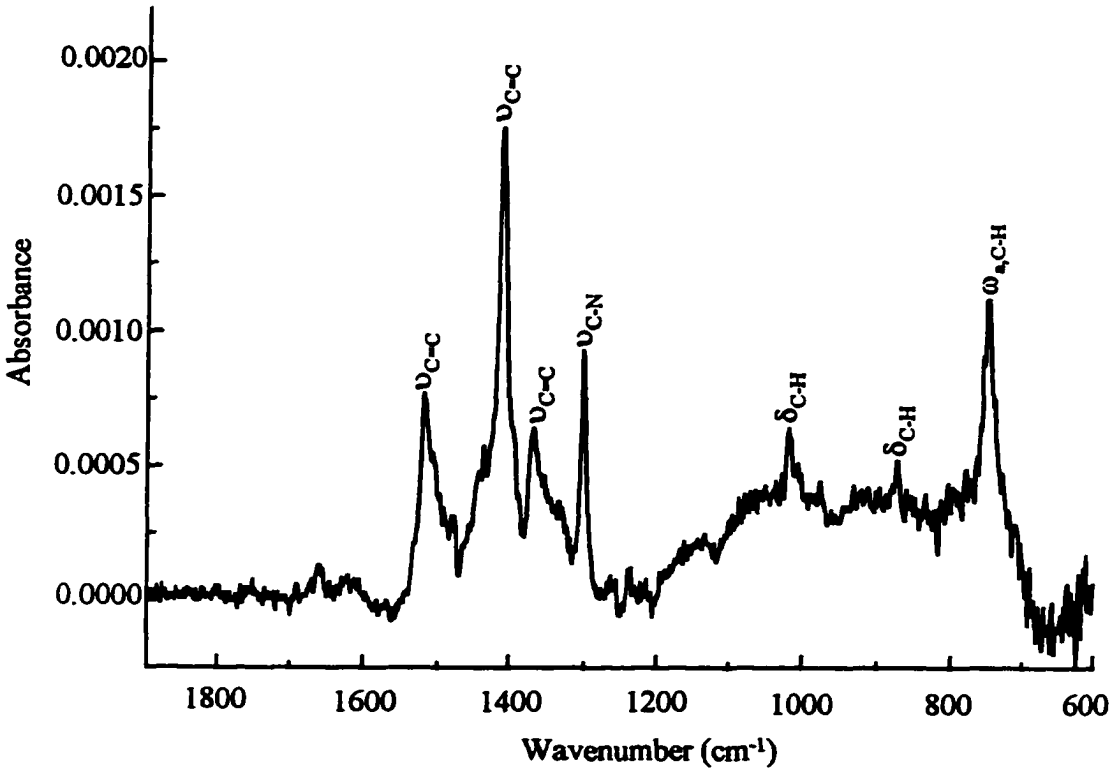

Figure 4.11 **Low energy RA spectrum of a pristine 2,5-PyC$_6$SH monolayer on Au.**

Table 4.2 **Band assignments in the lower frequency region for 2,5-PyC_6SH SAM on Au surface.**

Mode of vibration	Wavenumber (cm^{-1})	Direction of transition dipole moment
C=C, C-C stretch	1519	in plane of aromatic ring
ν_5 ring-stretch	1410	in plane of aromatic ring
C=C, C-C stretch	1364	in plane of aromatic ring
aliphatic C-N stretch ($\upsilon_{C\text{-}N}$)	1302	in plane of aromatic ring
aromatic in-plane C-H deformation ($\delta_{C\text{-}H}$)	1019	in plane of aromatic ring
aromatic in-plane C-H deformation ($\delta_{C\text{-}H}$)	874	in plane of aromatic ring
symmetric out-of-plane C-H deformation ($\omega_{s,C\text{-}H}$)	751	perpendicular to plane of aromatic ring

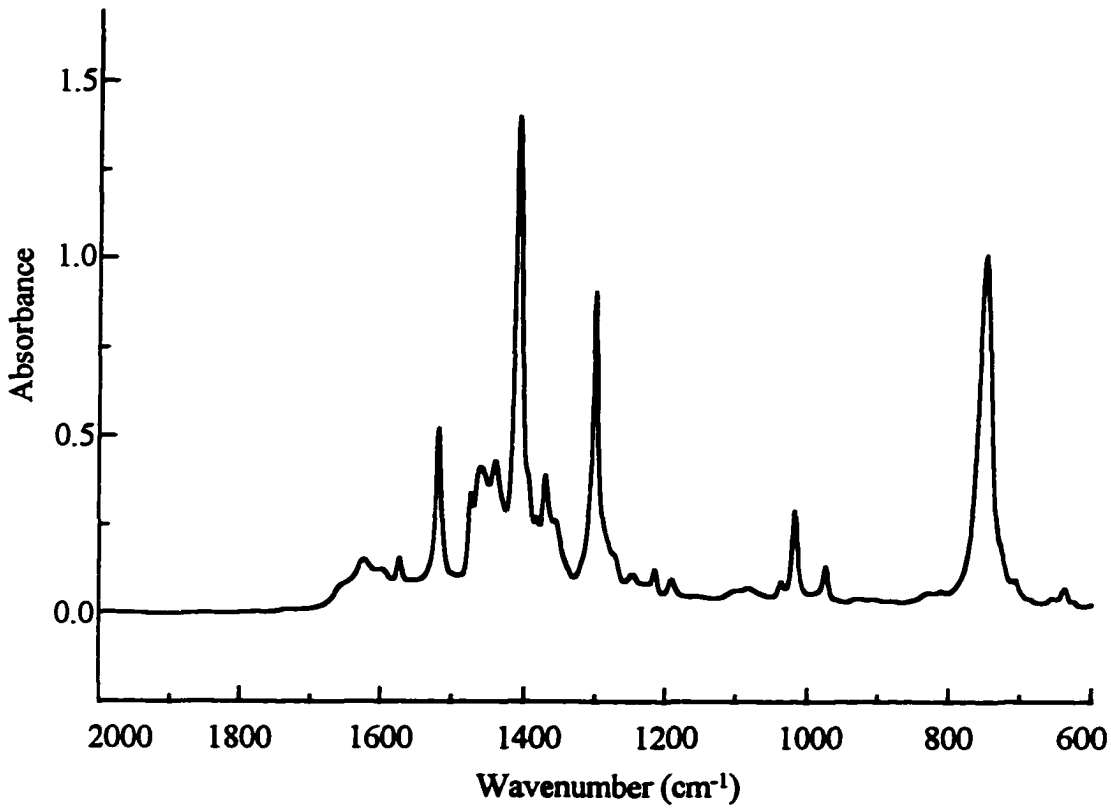

Figure 4.12 **Low energy transmission IR spectrum of neat 2,5-PyC_6SH in a 13.4 μm liquid cell**

the transmission spectrum and 1:1.2 in the reflectance spectra. This decrease in the band ratio is indicative of a monolayer where the plane of the aromatic ring is more closely aligned with the substrate normal. The preferred ring orientation in the 2,5-PyC_6SH monolayer compared to the isotropic ring orientation for the *N*-substituted pyrrole-terminated monolayers is not understood at this time.

An electrochemically oxidized 2,5-PyC_6SH monolayer on Au is shown in Figure 4.13. Several things are worthy of comment. First, the band associated with the ω_{C-H} out-of-plane deformation has apparently vanished, although an uneven absorption in this region makes this assessment questionable. Second, the ring modes have diminished in intensity by about half but the same relative peak intensity ratios with respect to each other remain roughly the same. This is similar to the behavior seen before with the *N*-substituted pyrroles except with the 2,5-PyC_6SH, the ring modes do not completely "disappear" even after complete oxidation of the monolayer. To confirm the presence of aromatic C-H bonds in the oxidized film, the electrochemically oxidized monolayer was exposed to ambient atmosphere. A large C=O band centered at ca. 1664 cm^{-1} was noted, Figure 4.14. This band indicates that not all of the hydrogens were eliminated during electrochemical oxidation and therefore, complete polymerization of the monolayer could not have occurred. Also, a trace of the ring modes are present at 1406 cm^{-1} and 1372 cm^{-1}. Due to the fact that we are using this blocked monomer to investigate changes in infrared band intensities for shorter polymer segments, it was deemed useful to examine the difference (if any) between doped and de-doped oligomer chains.

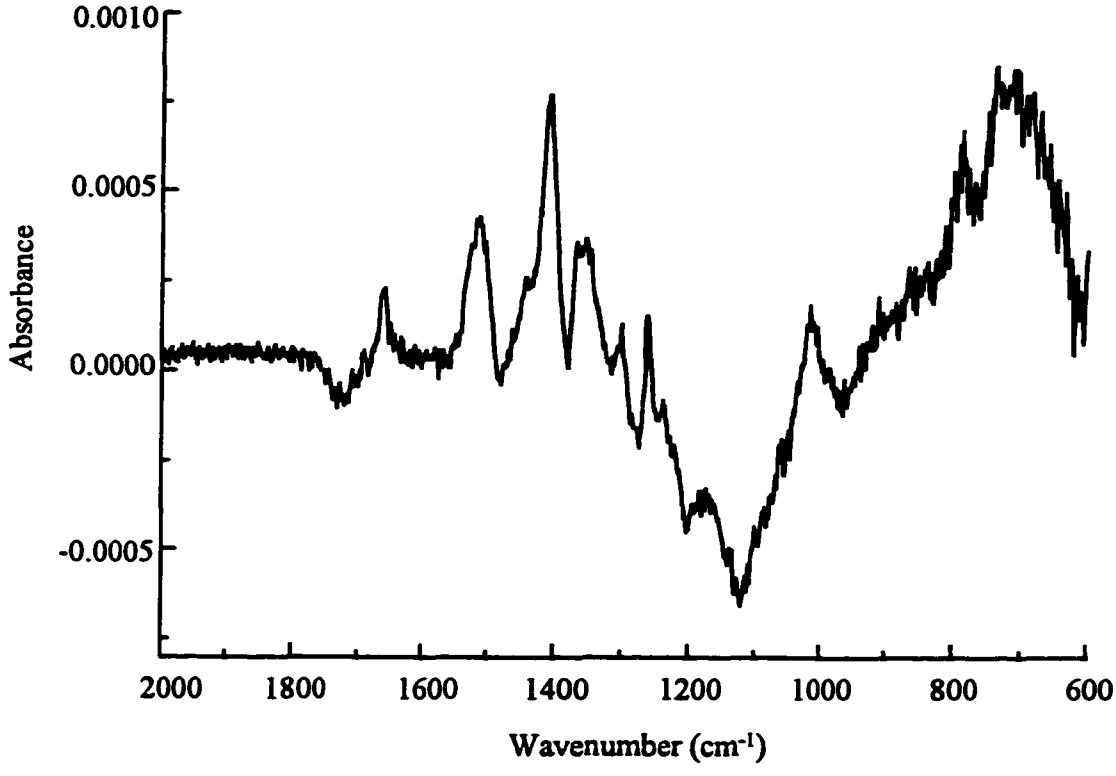

Figure 4.13 **Low energy RA spectrum of a 2,5-PyC_6SH monolayer on Au electrochemically oxidized to +1.3 V and emmersed at -0.1 V.**

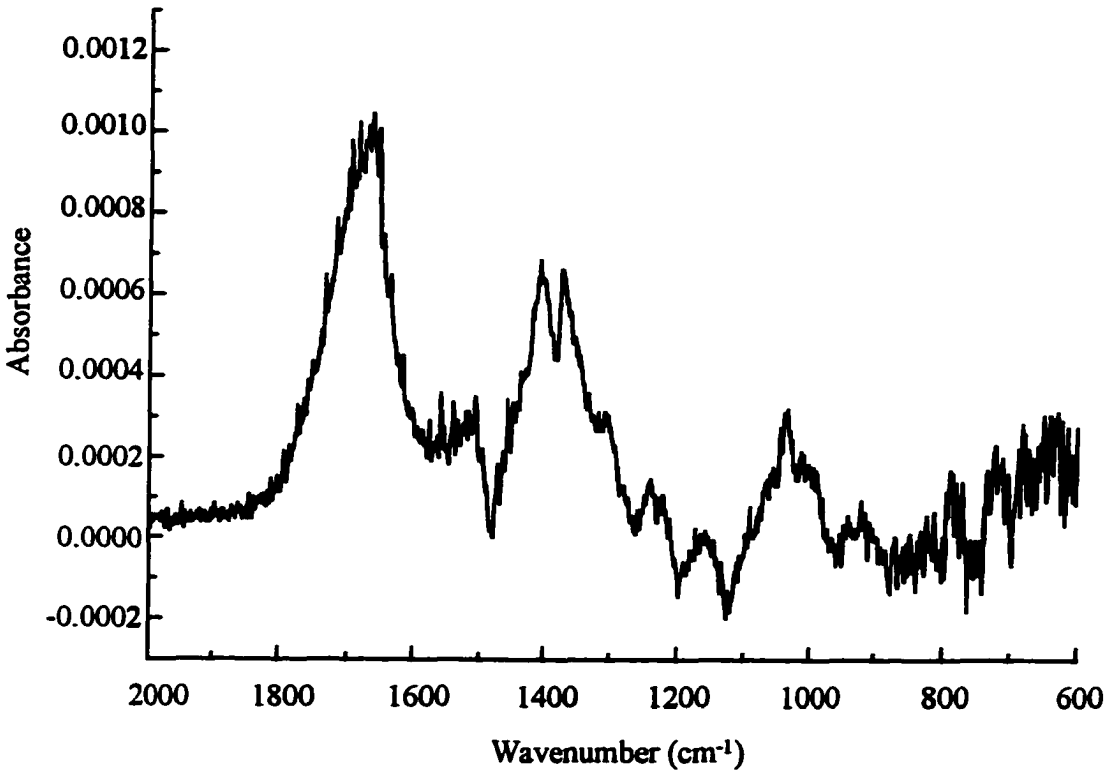

Figure 4.14 **Low energy RA spectrum of a 2,5-PyC$_6$SH monolayer on Au electrochemically oxidized to +1.3 V, emmersed at -0.1 V, and then subsequently exposed to ambient atmosphere for 2 hours.**

It is known, for example, that the ring modes are much more intense for bulk poly(pyrrole) in the conducting vs. the insulating state as seen by ex-situ and in-situ infrared experiments.[22] The significant increases in infrared absorption for doped vs. undoped (or de-doped) poly(pyrrole) chains is explained in terms of a charge delocalization effect. While not completely understood, the observation that film-trapped counteranions with intense infrared transitions could not be detected by infrared lends credence to this postulation. This can be understood by assuming that coupled pyrrole rings have lower infrared absorption cross-section values than monomeric rings but that the cross-section for absorption is somewhat a function of the doping level of the polymer backbone. The monolayers discussed thus far were all fully oxidized and then removed at -0.1 V where any resulting oligomer or polymer would be fully reduced to eliminate any effects that having a conducting chain with delocalized charges could have.

A monolayer that was treated identically to that in Figure 4.14 except that it was emmersed under positive potential, which should result in conducting oligomer or polymer chains, is shown in Figure 4.15. The pyrrole ring region looks very similar to that in Figure 4.13, but the situation has changed for the $\omega_{C\text{-}H}$ out-of-plane deformation region. A small amount of signal is now present at 795 cm^{-1}. This band is in the spectral region expected for the blue-shifted $\omega_{C\text{-}H}$ out-of-plane deformation of a substituted ring. The fact that it does indeed show up may have to do with the lowered conductivity of the polymer chains because the chain length of any oligomer formed should be shorter. The lower amount of pi-electron delocalization should then have less of an affect on the IR absorption cross-section of the resulting ring modes.

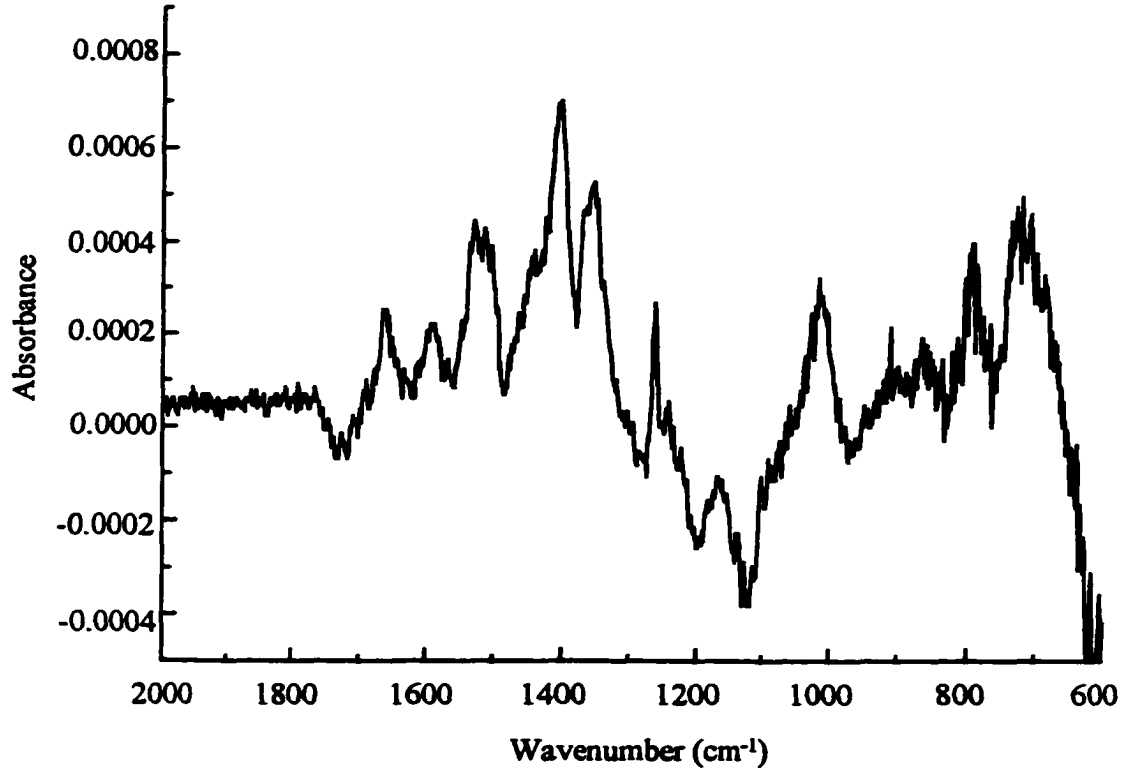

Figure 4.15 **Low energy RA spectrum of a 2,5-PyC$_6$SH monolayer on Au electrochemically oxidized to +1.3 V and emmersed at +1.2V.**

The increased absorption for a monolayer emmersed at oxidizing potentials might be a function of the oxidized nature of the pyrrole rings that have been coupled (vide supra).

This 2,5-PyC$_6$SH monolayer previously oxidized at +1.3 V and emmersed at +1.2 V was exposed to air for two hours in a manner similar to the undoped monolayer, Figure 4.16. The resulting spectrum exhibits the characteristic ring C=O mode as well as the expected corresponding loss of the ω_{C-H} deformation mode. The previously noted decrease in the ring modes is also apparent when comparing Figure 4.15 to Figure 4.16. The fact that ring modes still exist for both the undoped and doped monolayers after air exposure indicates that the nature of the

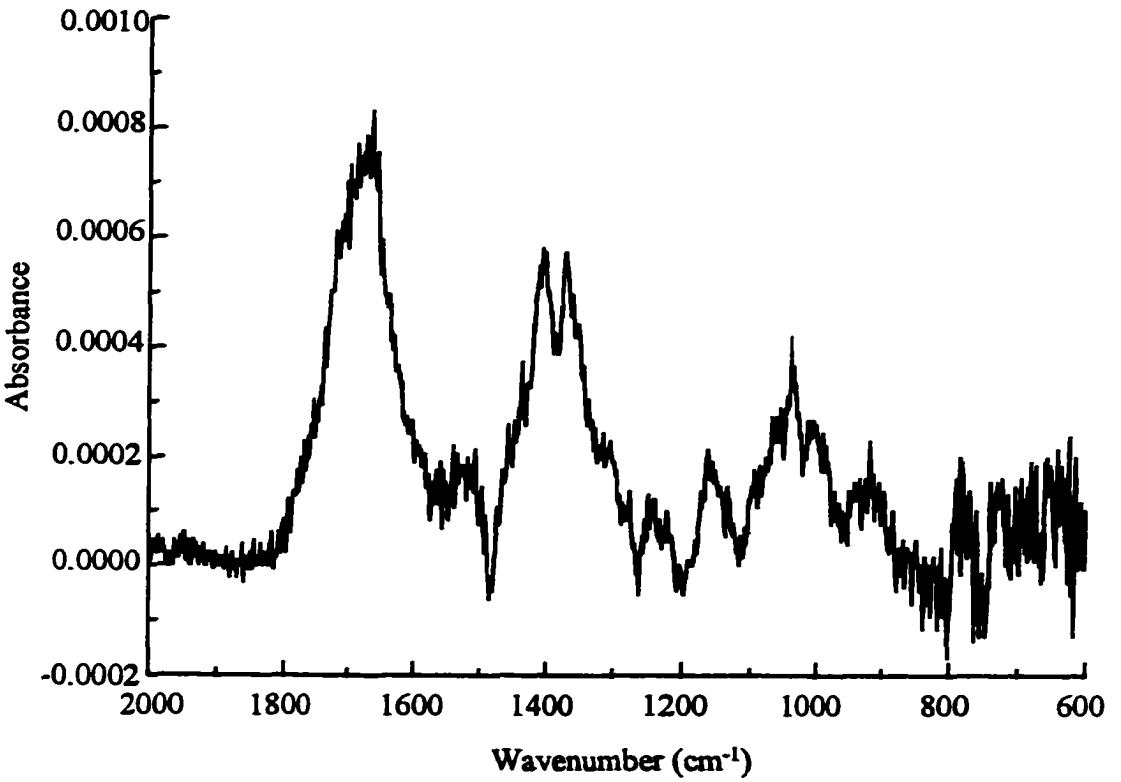

Figure 4.16 **Low energy RA spectrum of a 2,5-PyC$_6$SH monolayer on Au electrochemically oxidized to +1.3 V, emmersed at +1.2 V, and subsequently exposed to ambient atmosphere for 2 hours.**

oligomeric/polymeric 2,5-PyC_6SH is different from that derived from PyC_xSH on Au. The low polymerization efficiency exhibited by this monomer implies that the differences in the absorbances are due to a conductivity effect. This infrared data by itself does not allow us to rule out band intensity losses due to changes in ring orientation, however.

The reflectance spectra of three PyC_6SH monolayers on Au treated under different electrochemical conditions are shown in Figure 4.17. A large feature in the 1050-1200 cm^{-1} range exists due to imperfections in the Au layer coating the glass substrate. The first sample (Figure 4.17B) was oxidized to approximately +0.05 V past the potential for onset of oxidation of the monomer by scanning between 0 and +1.0 V for 10 cycles and then emmersed at reducing potentials. The second sample was treated similarly, except it was emmersed under oxidizing potentials where any oligomer or polymer formed would be doped (see figure legend). It can be seen that the ω_{C-H} out-of-plane deformation is still strong in the de-doped sample, Figure 4.17B, and there is a small decrease in the absorbance of the ring modes. The doped sample (emmersion at +0.87 V) shows a decrease in the ring modes as well. In addition, a broad band centered at 798 cm^{-1} is observed, indicating that coupling of the monomer units together to form polymer has occurred for some fraction of the surface. All three samples were subsequently exposed to air for two hours and the peak heights for the C=O bands were found to decrease as follows: pristine > oxidized, emmersed at negative potential > oxidized, emmersed at positive potential. This is consistent with the observation for bulk poly(pyrrole) that the doped polymer is much more stable to oxidation than the de-doped polymer.

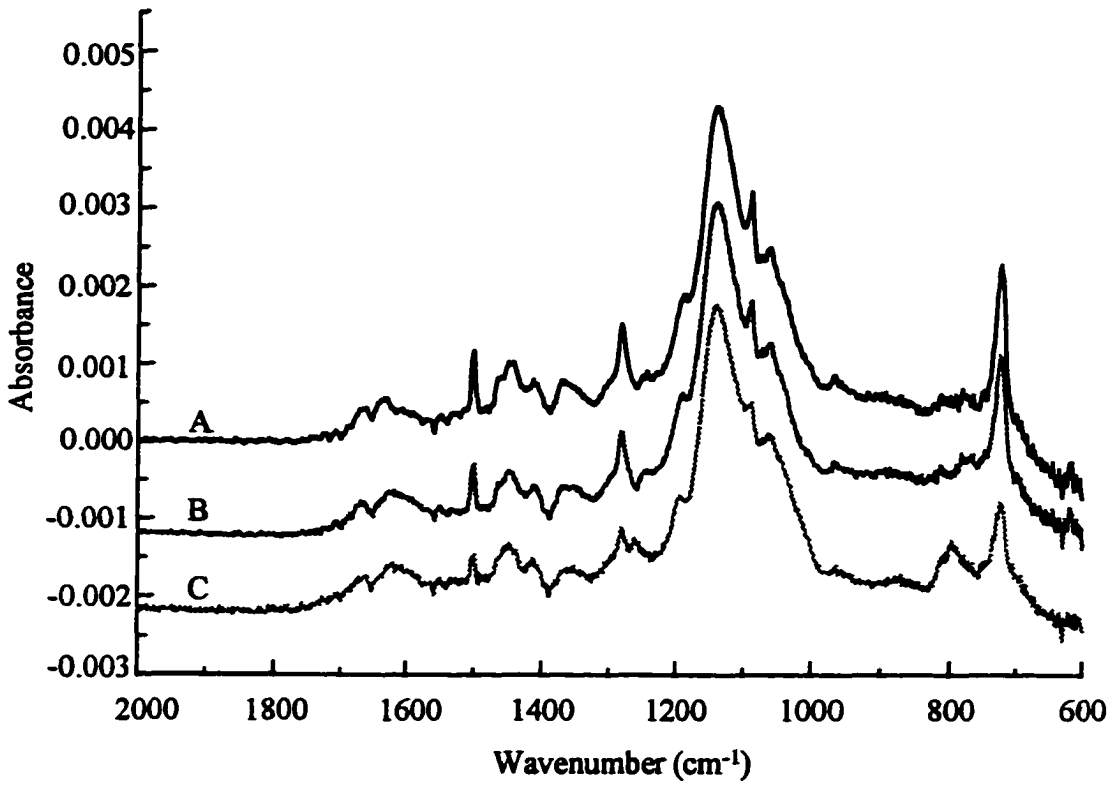

Figure 4.17 **Low energy RA spectra of (A) pristine PyC_6SH monolayer on Au (B) PyC_6SH monolayer on Au electrochemically oxidized 10x to +1.0 V and emmersed at -0.15 V (C) PyC_6SH monolayer on Au electrochemically oxidized 10x to +1.0 V and emmersed at +0.87 V. The y-axis is arbitrary.**

The experiment above was designed to limit the conductivity of the pyrrole chains and try to repeat the results found for the 2,5-disubstituted pyrrole monolayers (which we know do not form long chains). This could occur because only small amounts of polymer were formed when the potential was reversed just past the oxidation potential. A more controlled way of limiting the length of poly(pyrrole) chains is by coadsorbing the monomer with an electroinactive thiol. This would essentially place a non-reactive group in the way of pyrroles desiring to couple together and limit their maximum chain length. It was thought that curtailing the chain length,

and thus the proposed decrease in infrared absorption cross-section, would allow the remaining aromatic C-H bands of the oligomeric pyrrole species to be seen.

A PyC_6SH monolayer on Au was exposed to a 1 mM solution of $C_{18}D_{37}SH$ in ethanol for four hours to allow replacement of a controlled amount of the PyC_6SH with the electroinactive perdeuterated alkanethiol component. The electrochemically oxidized monolayer is shown in Figure 4.18. It can be immediately recognized that a strong, broad C-H deformation is present in the monolayer at ca. 795 cm^{-1} seeming to indicate that the formation of short chain oligomers does allow infrared spectroscopic confirmation of polymerization in the monolayer. The presence of the $C_{18}D_{37}SH$ in the monolayer was confirmed by the C-D stretching vibrations present at 2200 cm^{-1} and 2095 cm^{-1}.

4.6 Chemically Oxidized *N*-Substituted Pyrrole Monolayers

To ensure that the effects seen thus far are due to chemical changes in the monolayer and not due simply to the large electric field generated at the electrode surface, chemical oxidation of the monolayers was performed. A monolayer of $PyC_{10}S/Au$ was exposed to a saturated solution of "magic blue," tris(4-bromophenyl)aminium hexachloroantimonate(V), in acetonitrile for 30 min. This molecule has an effective oxidation potential above that of the surface-confined pyrrole and thus should also effect the formation of a surface-confined polymer. The spectrum of chemically oxidized $PyC_{10}SH$ on Au is shown in Figure 4.19A. It is clear that all of the bands associated with the pyrrole ring have disappeared in exactly the same manner as a completely electrochemically oxidized pyrrole-terminated monolayer.

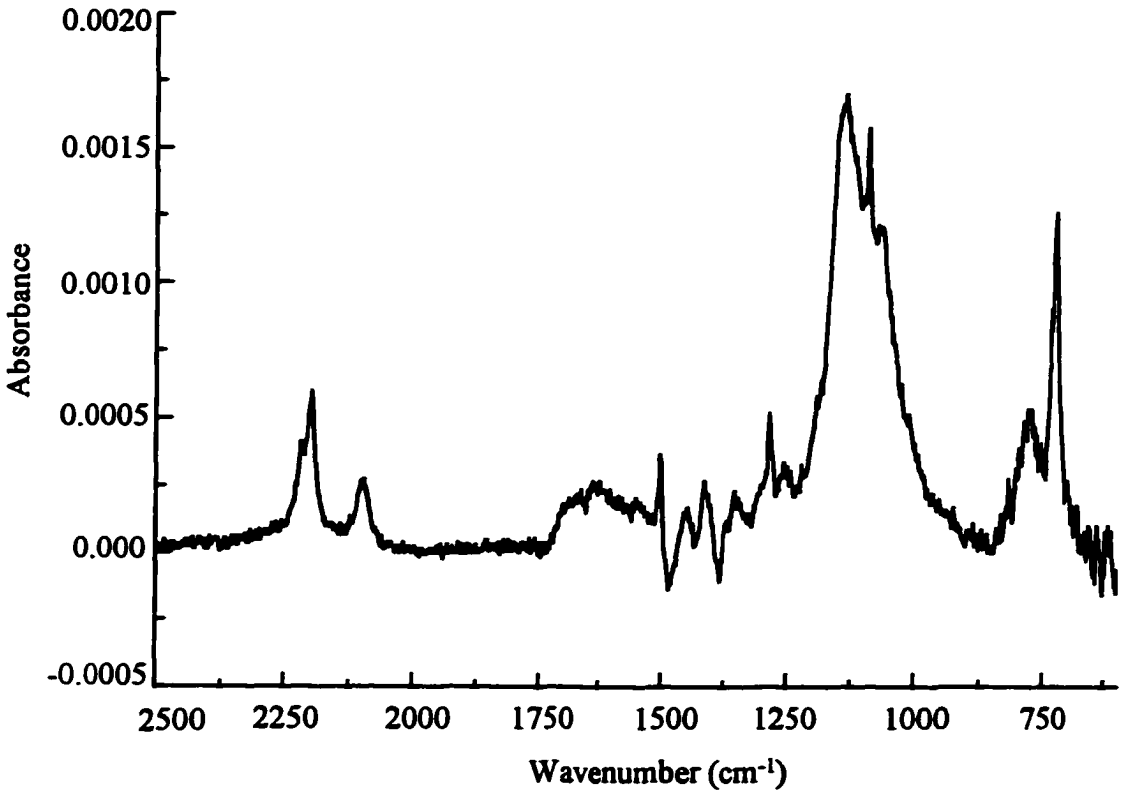

Figure 4.18 **Low energy RA spectrum of PyC_6SH monolayer on Au exposed to 1 mM $C_{18}D_{37}SH$ in EtOH for 4 hours and electrochemically oxidized to +1.2 V in clean 0.1 M TBAP/MeCN electrolyte.**

Thus, it can be said that an analogous compound results from oxidation by a completely different route. The chemically oxidized monolayer was also exposed to air for 2 hours to ensure that there were C-H groups remaining on the rings after oxidation, Figure 4.19B. The presence of the C=O band centered at ca. 1710 cm^{-1} clearly indicates the same type of behavior noted before. In addition, bands appear that are due to the presence of physisorbed oxidant. For example, the C=C stretching bands at ca. 1474 cm^{-1} are present in the films as well as a ω_{C-H} deformation band at 820 cm^{-1} which is indicative of the *para*-substituted benzene molecule present in the chemical oxidant.

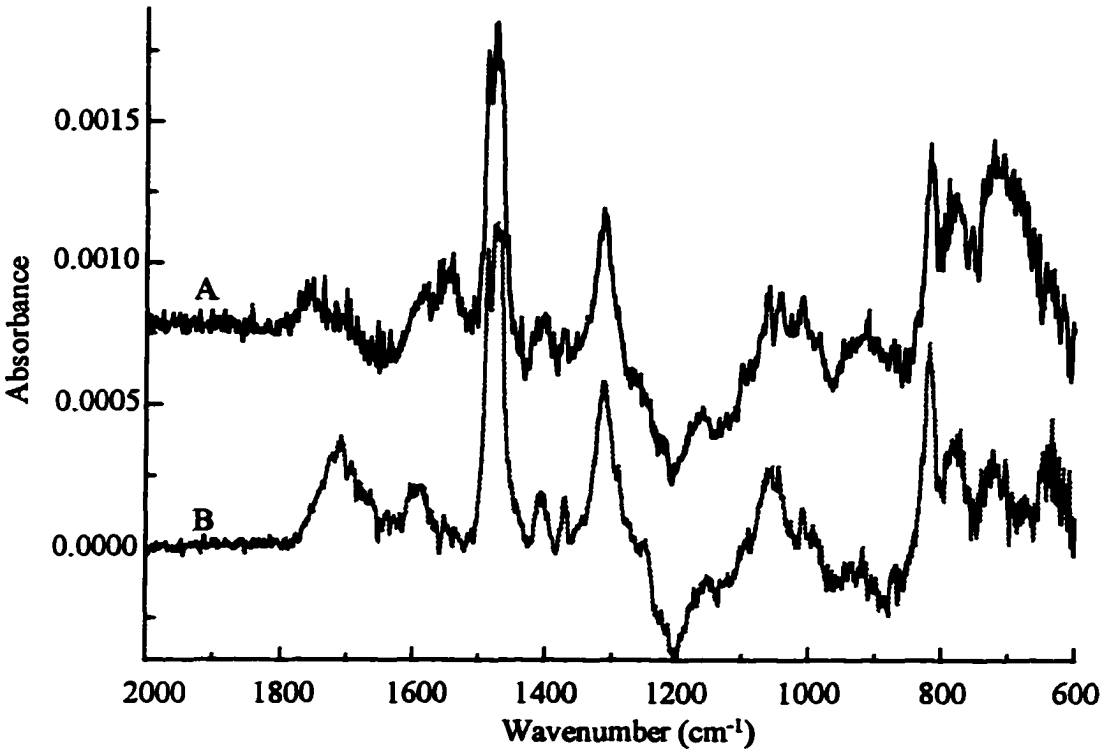

Figure 4.19 **Low energy RA spectra of $PyC_{10}SH$ monolayer (A) exposed to "magic blue" for 30 minutes and (B) subsequently exposed to ambient atmosphere for two hours. The y-axis is arbitrary.**

4.7 Conclusions

The IR analysis of the various pyrrole-terminated monolayer films is very consistent with the formation of a surface-confined, pyrrole-derived polymer layer. The disappearance of the ω_{C-H} band in the lower frequency region is not entirely understood, but correlates with the electrochemical data and is consistent with the single literature reference that analyzed that region of the spectrum[12] for L-B films of pyrrole derivatives. In addition, the spectroscopy that has been presented effectively discounts the theory that the electrochemical currents we have observed are due to a desorption mechanism of some kind.

Structural characteristics of the monolayer, however, were unable to be ascertained from the spectroscopic analysis presented in this chapter. The most logical explanation at this point for the lack of any bands in the spectra of the oxidized compounds argues that the infrared absorption cross-section of the resulting polymer is lower than that of the surface-confined monomer. The appearance of a small ω_{C-H} band shifted to higher frequencies for the 2,5-disubstituted pyrrole and the more-isolated PyC_6SH monolayers exposed to electroinactive diluent is attributed to the increased intensity of ring modes for oxidized polymer layers compared to their unoxidized counterparts. Chapter 6 will discuss some of the possible ways to achieve an understanding of the structural changes in the monolayer through a modification of these spectroscopic methods.

4.8 References

1) Ulman, A. *An Introduction to Ultrathin Organic Films from Langmuir-Blodgett to Self-Assembly*; Academic: San Diego, 1991.

2) Francis, S. A.; Ellison, A. H. *J. Opt. Sci. Am.* **1959**, *49*, 131.

3) Greenler, R. G. *J. Chem. Phys.* **1965**, *44*, 310.

4) Allara, D. L.; Swalen, J. D. *J. Phys. Chem.* **1982**, *86*, 2700-2704.

5) Nuzzo, R. G.; Allara, D. L. *J. Am. Chem. Soc.* **1983**, *105*, 4481.

6) Allara, D. L.; Nuzzo, R. G. *Langmuir* **1985**, *1*, 52.

7) Porter, M. D.; Bright, T. B.; Allara, D. L.; Chidsey, C. E. D. *J. Am. Chem. Soc.* **1987**, *109*, 3559.

8) Snyder, R. G.; Strauss, H.; Ellinger, C. A. *J. Phys. Chem.* **1982**, *86*, 5145.

9) Snyder, R. G.; Maroncelli, M.; Strauss, H. L.; Hallmark, V. M. *J. Phys. Chem.* **1986**, *90*, 5623.

10) Chidsey, C. E. D.; Loiacono, D. M. *Langmuir* **1990**, *6*, 682.

11) Sinniah, K.; Cheng, J.; Terrettaz, S.; Reutt-Robey, J. E.; Miller, C. J. *J. Phys. Chem.* **1995**, *99*, 14500.

12) Iyoda, T.; Ando, M.; Kaneko, T.; Ohtani, A.; Shimidzu, T.; Honda, K. *Tetrahedron Lett.* **1986**, *27*, 5633.

13) Yang, X. Q.; Chen, J.; Hale, P. D.; Inagaki, T.; Skotheim, T. A.; Okamoto, Y.; Samuelson, L.; Tripathy, S.; Hong, K.; Rubner, M. F.; denBoer, M. L. *Synth. Met.* **1989**, *28*, C251.

14) Cheung, J. H.; Rosner, R. B.; Watanabe, I.; Rubner, M. F. *Mol. Cryst. Liq. Cryst.* **1990**, *190*, 133.

15) Rikukawa, M.; Rubner, M. F. *J. Mater. Sci., Pure Appl. Chem.* **1994**, *A31*, 793.

16) Colthup, N. B.; Daly, L. H.; Wiberley, S. E. *Introduction to Infrared and Raman Spectroscopy*; 3rd ed.; Academic Press: Boston, 1990.

17) Jones, R. A.; Bean, G. P. *The Chemistry of Pyrroles*; Academic Press: New York, 1977; Vol. 34.

18) Jones, R. A. *Aust. J. Chem.* **1966**, *19*, 289.

19) Zerbi, G.; Veronelli, M.; Martina, S.; Schlüter, A.-D.; Wegner, G. *J. Chem. Phys.* **1994**, *100*, 978.

20) Novák, P.; Rasch, B.; Vielstich, W. *J. Electrochem. Soc.* **1991**, *138*, 3300.

21) Skotheim, T. A. *Handbook of Conducting Polymers*; Marcel Dekker: New York, 1986; Vol. 1.

22) Lei, J.; Liang, W.; Martin, C. R. *Synth. Met.* **1992**, *48*, 301.

Chapter 5

Microscopic Analysis of Pyrrole-Containing Monolayer Films

Microscopic methods are some of the most powerful experimental tools at the disposal of the surface scientist. It is the goal of this chapter to describe in detail microscopic investigations that we have performed on various pyrrole-containing monolayers on Au surfaces. The highly investigated *n*-alkanethiol SAMs, which are known to form ordered, reproducible structures on Au surfaces, will provide a reference point for conclusions derived from microscopic data acquired on our monomer-containing monolayers.

5.1 Theory of Scanning Tunneling Microscopy

The most recent and powerful microscopic technique developed for the analysis of surfaces is scanning tunneling microscopy (STM). STM was developed by Binnig and Rohrer[1] in the early 1980s and was lauded as a breakthrough accomplishment due to its ability to differentiate structural characteristics of surfaces at the molecular level. STM developed from fundamental studies conducted in the late 1960s[2] and early 1970s[3] on the tunneling of electrons between two conductors separated by a thin dielectric gap. The use of piezoelectric materials - ceramics that undergo changes in length in one dimension in response to an applied voltage - to control the motion of one of the conductors (the tip) with high precision, led to successful demonstration of atomic imaging with the STM.

The extremely high resolution of STM, better than 0.1 nm in the Z direction (perpendicular to surface) and 1 nm in the X and Y directions (parallel to surface),

respectively, can be understood by examining the physical principles responsible for the magnitude of the tunneling current that flows between two narrowly separated conductors. The magnitude of the tunneling current can be represented as a simple proportionality dependent upon the distance that separates the two conductors and the bias applied across them, Equation 5.1. In this equation, *I* represents the tunneling

Equation 5.1 $I \propto e^{-2\kappa d}$

current (nA), κ is a variable dependent on the bias across the two electrodes, and *d* is the separation distance (nm). The exponential dependence of the tunneling current on the separation distance gives the tunneling microscope spatial resolution in the Z direction (perpendicular to surface) in the sub-nanometer range. For real-time generation of three-dimensional images, the tunneling tip is rastered over the surface by applying voltages to orthogonal piezoelectric elements aligned in the X and Y directions. A topographical "map" of the surface can be generated by measuring the change in tunneling current as a function of X and Y position.

5.2 STM Analysis of Various Surfaces

A variety of different samples can be imaged using STM due to the fact that the experiment can be carried out under vacuum, under ambient conditions, and under liquids (with some modification of the probe tip). Large biological samples whose structures are sensitive to changing environments can thus be analyzed under "native" conditions. STM is applicable to the study of small molecules physisorbed on surfaces as well because high vacuum is not required - a condition that can often alter or

damage the physisorbed layer. STM has been utilized extensively in the study of many types of chemisorbed species on smooth surfaces as well - a fact that this thesis will attempt to exploit for the in-depth analysis of our monomer-containing monolayers.

The local atomic structure of *n*-alkanethiol absorbates on Au(111) surfaces was predicted to be $(\sqrt{3} \times \sqrt{3})R30°$ from helium[4] and transmission electron[5] diffraction measurements. Widrig et al.[6] were able to confirm these predictions by measuring the lattice spacing of ethanethiolate and *n*-octadecanethiolate monolayers on Au(111) by resolving the sulfur atoms in the adlattice. This was the first molecular-level view of an alkanethiol SAM. Poirier was later able to exploit the real-time capability of STM to monitor the self assembly of *n*-alkanethiols on Au(111) as a function of time.[7] In addition to simple *n*-alkanethiols, ω-functionalized alkanethiols on Au(111) were studied by Kim et al.[8] who found that no apparent deviations from $(\sqrt{3} \times \sqrt{3})R30°$ structure were found even for SAMs containing bulky chain-terminating functionalities.

We have attempted to image pyrrole-terminated monolayers on Au(111) with molecular-level resolution to record changes in packing structure upon electrochemical conversion of a monomer monolayer to a layer of conducting polymer. Determination of orientation changes of pyrrole rings in these constrained films during conducting polymer formation was another goal of these experiments. It was proposed that upon successful completion of monomer and polymer characterization goals, a more technologically-oriented set of experiments would be undertaken. It was our intention to use the STM as a lithographic tool to polymerize surface-confined monomer under the moving tip giving rise to polymer features with dimensions on the order of nanometers. A cartoon displaying the electrochemical polymerization of terminal

pyrrole units by a tip scanning directly above a pyrrole-based monolayer is shown in Figure 5.1. In this depiction, polymerization occurs when the bias voltage applied between the tip and the substrate (E_{bias}) is greater than the voltage needed to initiate oxidation of the pyrrole units in the film ($E_{faradaic}$).

This ambitious project has roots in efforts by previous researchers to use the STM as a lithographic tool for the creation of small features. Slightly less sophisticated approaches to depositing metal and polymer structures than the one proposed here have been successful in the past. These approaches have generally used high voltage pulses to induce emission of electrons from the tunneling tip while scanning over a material capable of undergoing chemical changes upon exposure to an electron beam. Poly(methyl methacrylate),[9] glutaraldehyde,[10] and hydroxy-propylcellulose[11] are just a few examples of different molecules that have been investigated for the formation of small polymeric features.

There are two main differences between the work cited above and the method proposed here. First, the monomer-containing molecule in our method is confined to the conducting surface prior to any manipulation by the STM tip. Important effects on polymer feature size through the minimization of "diffusional broadening" have already been discussed (see Chapter 1). Second, the transformation from monomer to polymer for the pyrrole-based films is predicted to occur not because of an emission of electrons from the tip but rather due to an electrochemical redox reaction between the pyrrole groups and redox-mediating species present in the adsorbed water layer that is ubiquitous on surfaces examined under ambient conditions.[12] Thus, the tip in this proposal would be used as a sort of nanofaradaic reaction initiator.

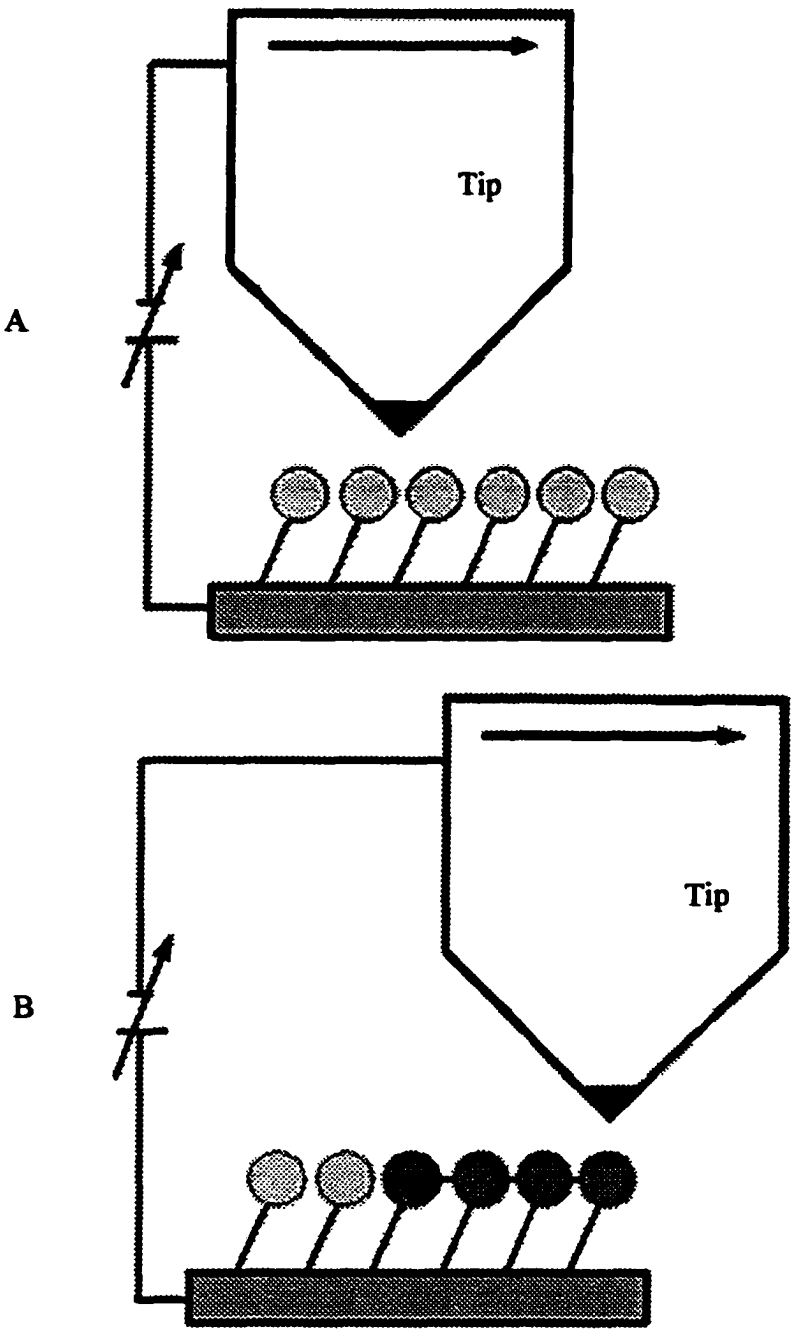

Figure 5.1 **Cartoon of a STM tip scanning from left to right over a surface-confined monomer (A) with $E_{bias} < E_{faradaic}$ and (B) with $E_{bias} > E_{faradaic}$.**

The difference between previous reports and the proposed experiments described here is important as our method represents an attempt to initiate *controlled* chemical reactions in extremely small volumes. That is, the reactions (degree of reaction) here are limited by the amount of faradaic charge deposited in the area scanned by the tip.

5.3 Experimental

5.3.1 Scanning Probe Microscopy

Scanning probe microscopy (SPM) is a term encompassing a range of different surface sensitive techniques - STM being the most well-recognized of these. Two different types of SPM techniques will be used in this report: STM and lateral force microscopy (LFM).

5.3.1.1 STM

STM experiments were performed with a Nanoscope III scanning probe microscope (Digital Instruments) equipped with 0.8 μm x 0.8 μm and 13 μm x 13 μm piezoelectric scanners. The entire scanning head was isolated from low- and mid-frequency vibrations by suspension from a homemade vibration isolation stand with a resonant frequency close to 1 Hz. All images shown here were collected in air on freshly-prepared SAMs on Au (111) surfaces and have not been filtered. The tunneling conditions used to collect each image are detailed in each figure caption.

5.3.1.2 LFM

LFM was performed on the same Nanoscope III scanning probe microscope as above fitted with a Multimode Microscope Head. Pyramidal cantilevers with ca. 40 nm tip diameter fabricated from Si_3N_4 were used as received. Tip motion was monitored

using a four quadrant photodiode detector whose sensitivity to lateral torsions of the cantilever were calibrated via a literature method.[13]

5.3.2 Fabrication of Au(111) Substrates

Au(111) films were prepared by thermal evaporation of Au (see Chapter 3) on mica sheets (V-2 grade, Asheville-Schoonmaker) freshly cleaved in air. Evaporation of ca. 150 nm of Au onto the mica followed by annealing at 350 °C in air for four hours resulted in Au films with large, flat crystallites (ca. 300 nm). Literature reports have shown this and similar procedures to result in the formation of predominantly Au(111) films suitable for SPM experiments.[14]

5.4 Results and Discussion

STM analysis was first performed on simple *n*-alkanethiol monolayers adsorbed onto Au(111) electrodes in order to verify the ability of our system to replicate literature results. An STM image displaying an *n*-octadecanethiol monolayer scanned in air is shown in Figure 5.2. The observed holes covering the surface at periodic distances from each other have origins that have been the subject of some controversy in the literature but are agreed to be an unmistakable indicator of successful organothiol monolayer formation.[15,16] Alkanethiol monolayer formation was confirmed by first imaging SAMs at lower spatial resolutions due to the relative ease in obtaining such images in comparison to images resolving molecular features.

STM imaging of a PyC_6SH-modified Au(111) substrate yielded the image shown in Figure 5.3 for comparison. It can immediately be seen that this surface does not display the same features seen on the $C_{18}H_{37}SH$-modified Au(111) substrate. Images of this monolayer and monolayers derived from all the pyrrole alkanethiol

analogues contain evidence of Au crystallites beneath the outer, "fuzzy," coating. The nature of the difference present in the images of the two types of monolayers is not completely clear but is probably due in large part to one of two scenarios. Either the pyrrole-terminated surface has oxidized to form a somewhat fibrillar polymer or adsorption of contaminants onto the surface from the air has occurred and interferes with our ability to obtain a clear image.

To test the first theory, pyrrole-based monolayers were analyzed immediately after deposition of the thiol and after exposure to ambient conditions for long periods of time (hours to days). In all cases the images were the same - a result that would not be expected if oxidized polymer were the origin of the fuzziness because infrared analysis indicated no significant oxidation of the pyrrole-terminated films for ambient exposure times less than about one hour. A more rigorous set of experiments was executed by building a lead-weighted aluminum vibration isolation apparatus that allowed the STM to be operated in an inert atmosphere box. Monolayers formed in Ar-purged absolute ethanol solutions and imaged under inert atmosphere showed no difference in the amount of "fuzziness" present on the surface of the resulting SAM.

Evidence that the observed features could arise from adventitious contaminants adsorbed onto the pyrrole-terminated monolayers came in the form of STM experiments designed to promote the physical interaction of the tunneling tip with the surface. It is well known that a STM tip can physically interact with a sample surface while scanning under moderate or even mild tunneling conditions.[17] A good example of such an interaction is shown in Figure 5.4 for a STM tip scanning over a "fuzzy" PyC_6S/Au monolayer on Au(111). Sequential scanning of the tip from top to

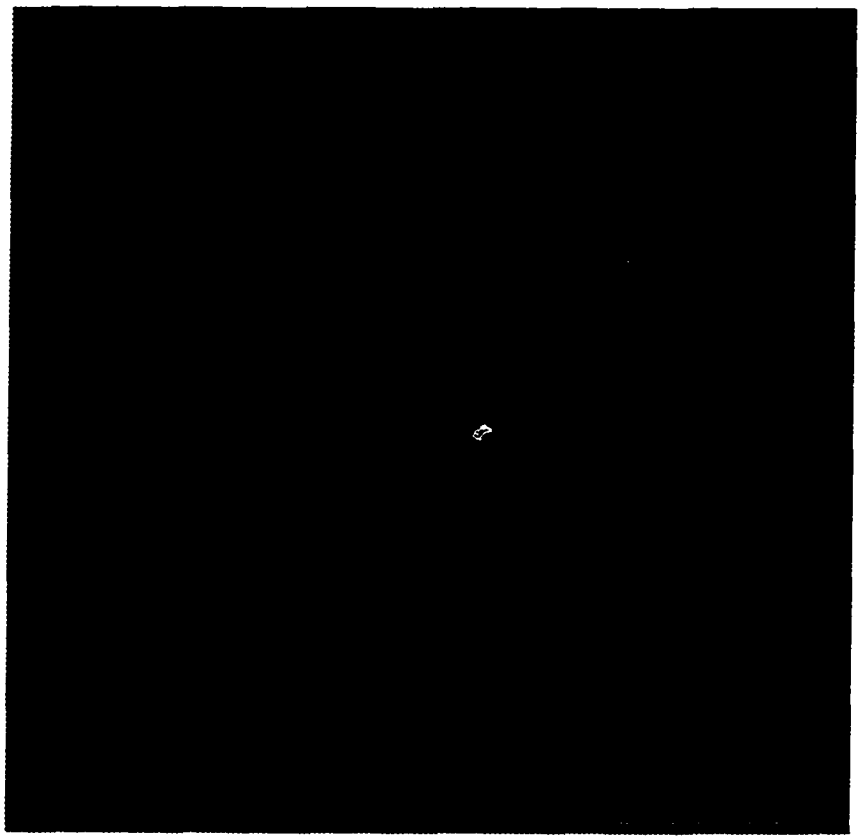

Figure 5.2 **$C_{18}H_{37}SH$ monolayer on Au(111) scanned in air with E_{bias} = 1.0 V, $i_{tunneling}$ = 1 nA, and scan rate = 3 Hz. The black bar in the lower right-hand corner represents 10 nm.**

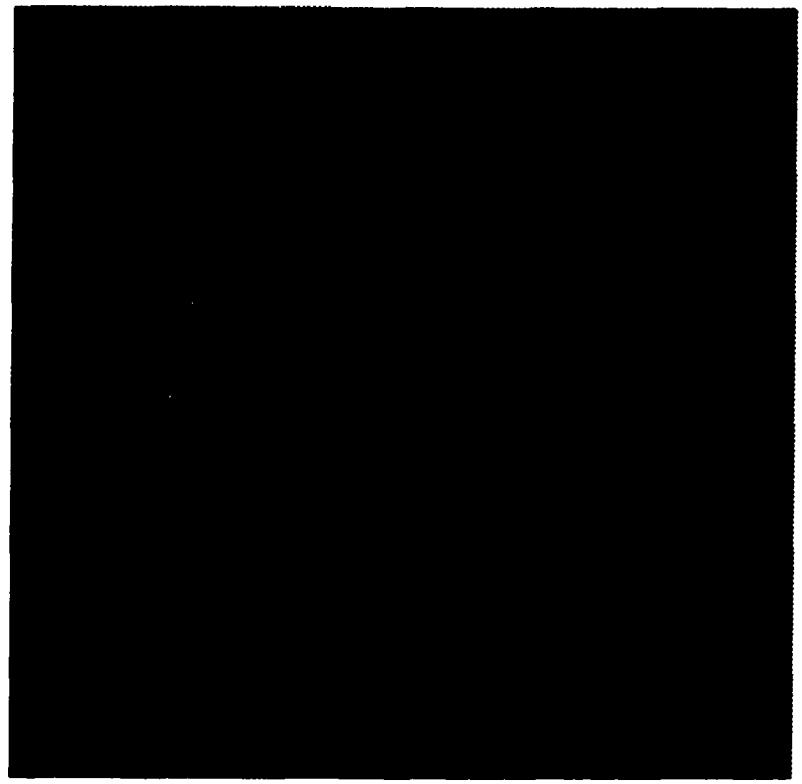

Figure 5.3 **PyC_6SH monolayer on Au(111) with E_{bias} = 1.25 V, $i_{tunneling}$ = 0.3 nA, Z-range = 20 nm and scan rate = 4.1 Hz. The scan size is 235 nm x 235 nm.**

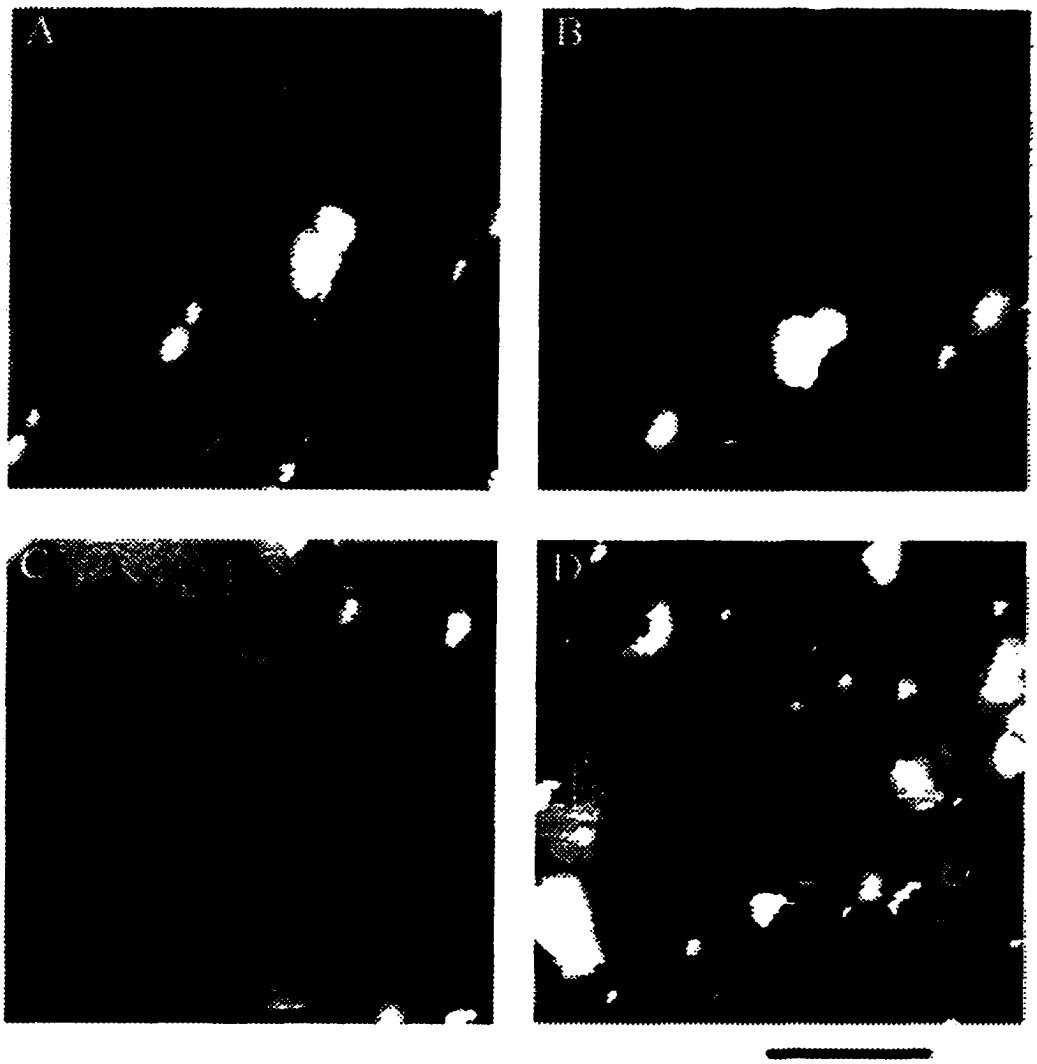

Figure 5.4 **PyC_6SH monolayer on Au(111) scanned in air sequentially in images A-D with E_{bias} = 505 mV, $i_{tunneling}$ = 0.5 nA, and scan rate = 1 Hz. The black bar in the lower right-hand corner represents 0.4 μm in A-C and 0.7 μm in D.**

bottom progressively displaced more of what we believe to be adsorbed material, thereby revealing a cleaner-appearing surface. Many attempts were made to obtain molecularly resolved images on the cleaner portions of samples treated in this manner but proved unsuccessful.

We have noted analogous contaminant behavior for other hydrophilic, high surface energy SAMs derived from organomercaptans on Au(111). Both carboxylic acid- and hydroxyl-terminated alkanethiol SAMs on Au(111) revealed "fuzzy" surface features when scanned under ambient or inert atmosphere conditions. This provides evidence that our inability to effectively image the pyrrole-terminated SAMs stems at least partly from their hydrophilic nature and is not strictly due to their relatively high reactivity toward water and oxygen.

Adsorption of adventitious contaminants onto the pyrrole-terminated monolayers is not terribly surprising. Water and small hydrophobic molecules are known to quickly adsorb onto high energy surfaces so as to lower the surface energy. This has been shown to drastically affect the ability of STM to resolve molecular features in monolayers containing hydrophilic terminal groups.[12] A very recent report by Hayes et al.[18] remarked on the inability to obtain molecular resolution on pure *p*-aminothiophenol monolayers on Au surfaces with a similar microscopic technique, lateral force microscopy, that had been used successfully to obtain molecularly-resolved images of *n*-alkanethiol monolayers on Au.

5.5 Lateral Force Microscopy

5.5.1 Theory

LFM is a microscopic method based on scanning a cantilever with a known force constant (perpendicular to the long axis of the cantilever) across a surface while monitoring the torsion of the cantilever as a function of X and Y position, Figure 5.5.

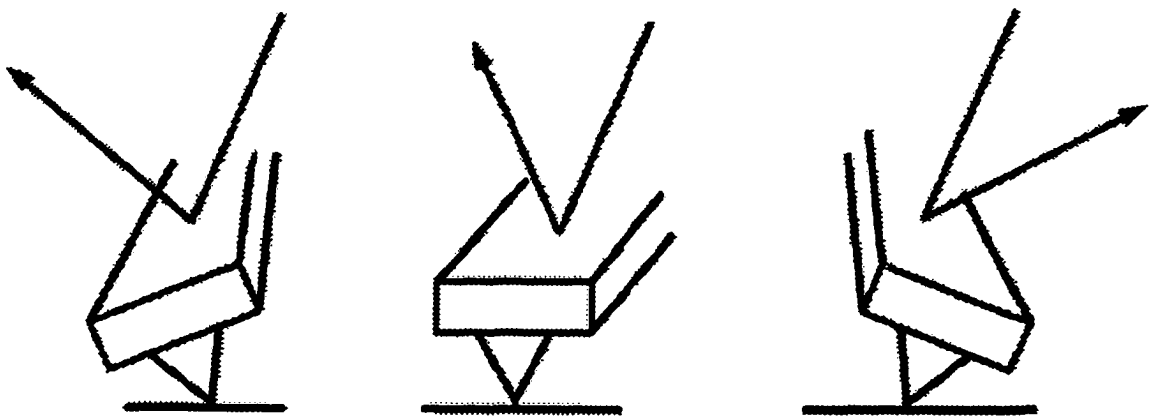

Figure 5.5 **Cartoon displaying the torsion of a lateral force cantilever scanning over a smooth surface and the resulting reflection of the laser beam.**

The torsion induced on the cantilever is measured by the changing position of a laser spot reflected from the top of the cantilever onto a four-quadrant photodiode. LFM was described by Meyer and Amer[19] who showed effectively that the magnitude of frictional forces between the tip and the underlying substrate determined the amount of cantilever twisting. Recently, Lieber et al.[20] went on to show that heterogeneous surfaces could be "mapped" by selectively modifying a probe tip with hydrophobic- or hydrophilic-terminated molecules. This technique, called chemical force microscopy (CFM), relies on changes in the interfacial energy between tip and sample (and thus

cantilever torsion) to chemically differentiate mixed monolayer surfaces. Green et al.[13] furthered the applicability of this technique to bilayer assemblies proving that CFM could operate at spatial resolutions in the *nanometer regime*.

5.5.2 LFM Applications to SAMs

We analyzed various surfaces with LFM in order to compare $PyC_{10}SH$-modified Au surfaces with other, more thoroughly studied monolayers. 11-hydroxy-undecanethiol (11-SOL) on Au was probed as a monolayer with a high surface free energy and $C_{18}SH$-modified Au surfaces served as very low surface free-energy controls. LFM results obtained from these two monolayers as well as a $PyC_{10}S$/Au monolayer are shown in Figure 5.6. Surfaces exhibiting high free-energies have been shown to undergo increases in friction more rapidly with increasing load as evinced by large positive values of the slope for a plot of normal force (load) vs. lateral force.[13] It can be seen then from Figure 5.6 that $PyC_{10}SH$-modified surfaces are intermediate in surface energy between the hydroxyl- and methyl-terminated monolayer surfaces. This is in agreement with contact angle measurements performed on the $PyC_{10}S$/Au monolayers (Chapter 3).

An interesting thing occurs when a probe tip is scanned across a pyrrole-terminated monolayer on Au at high load for ca. 30 seconds. Lateral force vs. normal force plots before and after such a protocol are present in Figure 5.6 as triangles and inverted triangles, respectively. Before scanning at high load, the interfacial energy of $PyC_{10}S$/Au and the probe tip is quite high (vide supra) while the interfacial energy drops significantly after high-load scanning.[13] Based on previous studies utilizing carboxylic acid-containing molecules, this decrease in interfacial energy is consistent

with the adsorption of hydrophobic molecules to the probe tip. Changes in interfacial energy due to removal of the monolayer by the tip would not be expected to give the same response. In support of this, it was found that pristine areas of the same $PyC_{10}S$/Au surface scanned with the modified probe tip exhibited a much lower interfacial energy than with a new tip.

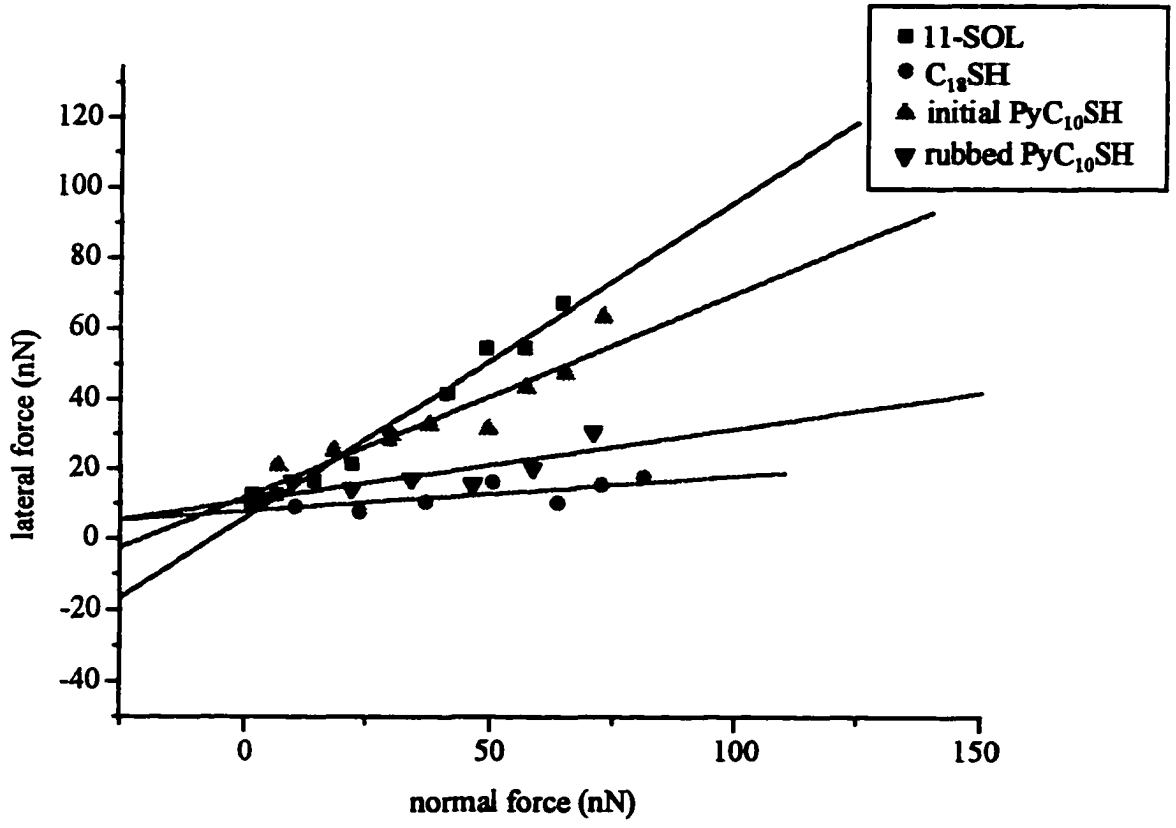

Figure 5.6 **Lateral force vs. normal force curves taken for several different monolayers on Au(111) with a Si_3N_4-tipped cantilever.**

Adsorption of contaminants onto the pyrrole-terminated monolayers defeated every attempt to gain a more in-depth understanding of the films through visualization

of their structure on the surface. Several different types of experiments were performed on the monolayer films to ensure that the inability to obtain molecularly-resolved images was not due to errors in analysis or preparation protocols.

Despite the drawbacks encountered in the analysis of the pyrrole-containing monolayer films, an attempt was made to form conductive features in the films using bias potentials above that for faradaic onset of the monomers (Figure 5.1). All of these attempts were unsuccessful although changes in tip stability due to increases in faradaic current were noted at much lower bias potentials (ca. 650 mV) for pyrrole-terminated monolayers than for *n*-alkanethiol monolayers (ca. 1600 mV). We believe the potential still exists for nanoscale electrochemical patterning of these surfaces to be feasible as will be discussed in Chapter 6.

5.6 Bulk Poly(pyrrole) on Modified Au Surfaces

The inability to form small conducting features in the pyrrole-terminated SAMs did not preclude their study for other possible technological applications. Enhanced adhesion of thick polymer films on conducting substrates is another area where monolayer films of this type could make a contribution. Thick poly(pyrrole) films in particular could benefit from a pretreatment of the Au surface that increases the substrate-polymer adhesion because the electrochemically-formed films are very easily removed from the electrode surface. Facile removal of the polymer is a positive attribute when free-standing films are desired, but can be very troublesome when attempting to construct a sensor or other device to be used under harsh conditions.

The use of pyrrole-terminated layer(s) to enhance the adhesion of deposited poly(pyrrole) films has been demonstrated previously with a pyrrole-terminated

alkoxysilane layer self-assembled onto an Si/SiO_2 surface.[21] A similar experiment describing an increase in adhesion for a poly(aniline) film deposited on a self-assembled monolayer of *p*-aminothiophenol on Au can also be found in the literature.[22] More efficient nucleation of solution-phase polymer onto the pre-adsorbed monomer sites on the surface was given as a possible explanation for the vast differences seen between the thick polymer films deposited on all of these modified and unmodified surfaces. Based on these observations, experiments were undertaken to determine if our pyrrole-terminated SAMs could effectively change the characteristics of thick poly(pyrrole) films deposited from solution.

5.6.1 Adhesion Testing

A very simple experiment was performed initially to determine if the pyrrole-terminated SAMs could increase the adhesion of poly(pyrrole) films to the electrode surface. A cartoon depicting the experimental procedure followed to directly compare the adhesion of poly(pyrrole) films on modified and unmodified Au surfaces is shown in Figure 5.7. Briefly, an Au film electrode (see Chapter 4) was painted[23] with neat PyC_6SH in the upper left-hand corner (Figure 5.7A) using a small camel's hair brush and rinsed copiously with ethanol after approximately 30 seconds of assembly time. This partially-modified electrode was immersed in 0.1 M TBAP/MeCN containing 50 mM pyrrole and then scanned above the faradaic onset potential of the bulk monomer so as to deposit poly(pyrrole) from solution. Poly(pyrrole) films ca. 1 μm thick were formed on the electrode (Figure 5.7B) as determined by the amount of charge passed during the oxidation reaction. The modified Au electrodes were emmersed from the electrolyte, rinsed thoroughly with pure MeCN and allowed to dry under an Ar

atmosphere. Testing of the adhesion of the poly(pyrrole) film was achieved by covering the entire surface of the electrode with adhesive tape and then quickly removing the tape. A photograph of an electrode after one removal of adhesive tape is shown in Figure 5.8. It can clearly be seen from the photograph that poly(pyrrole) remains only on the portion of the electrode that was modified with PyC_6SH prior to polymer deposition. Lateral streaks on the electrode surface are scratches in the Au formed by briskly rubbing the entire electrode with a paper towel in an unsuccessful attempt to remove the deposited poly(pyrrole) film. Poly(pyrrole) films formed in this manner had to be removed from electrode surfaces by sequential polishing with diamond pastes (see Chapter 3). This is strong evidence that our pyrrole-terminated SAMs increase the adhesion of thick poly(pyrrole) films to Au surfaces as poly(pyrrole) films deposited on bare Au or Au modified with *n*-hexanethiol monolayers were easily removed.

5.6.2 Scanning Electron Microscopy

Scanning Electron Microscopy (SEM) was employed to examine poly(pyrrole) films deposited on bare and PyC_6SH-modified Au surfaces in an attempt to correlate the increased adhesion of the films on the modified substrate to changes in the morphology of the resulting polymer. A SEM image of an approximately 1 μm-thick poly(pyrrole) film on a bare Au electrode is shown in Figure 5.9. The presence of nuclei 0.4 to 1 μm in diameter is noted over the entire surface of the film. A poly(pyrrole) film of comparable thickness deposited on a PyC_6SH-modified Au electrode is shown for comparison in Figure 5.10. The objects in the upper left-hand corner are artifacts present on all surfaces. This poly(pyrrole) film exhibits a very

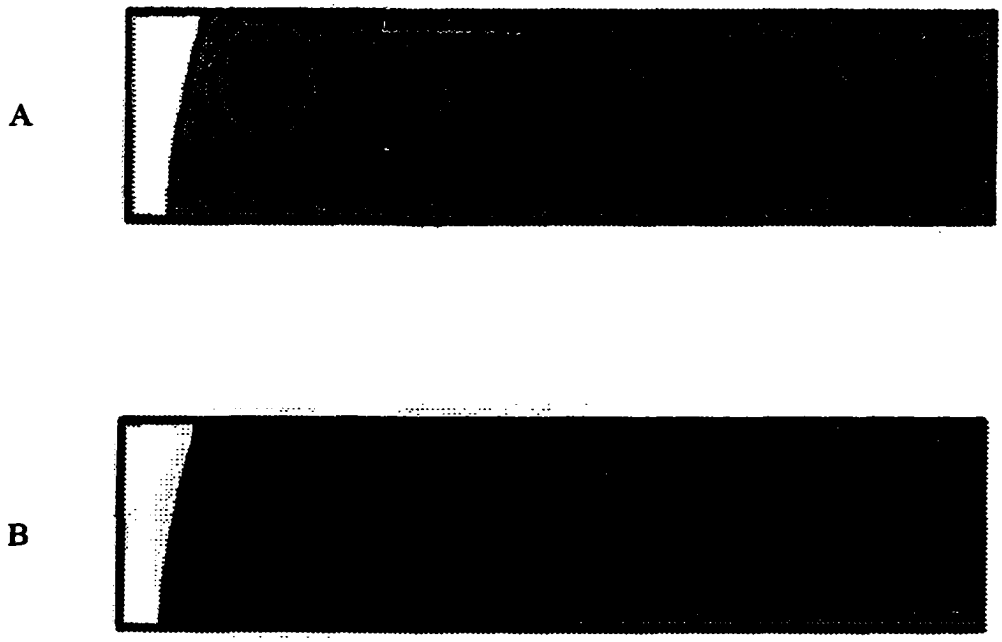

Figure 5.7 **Cartoon of Au electrode modification with (A) PyC_6SH in upper left-hand corner and then (B) 1 μm poly(pyrrole) film.**

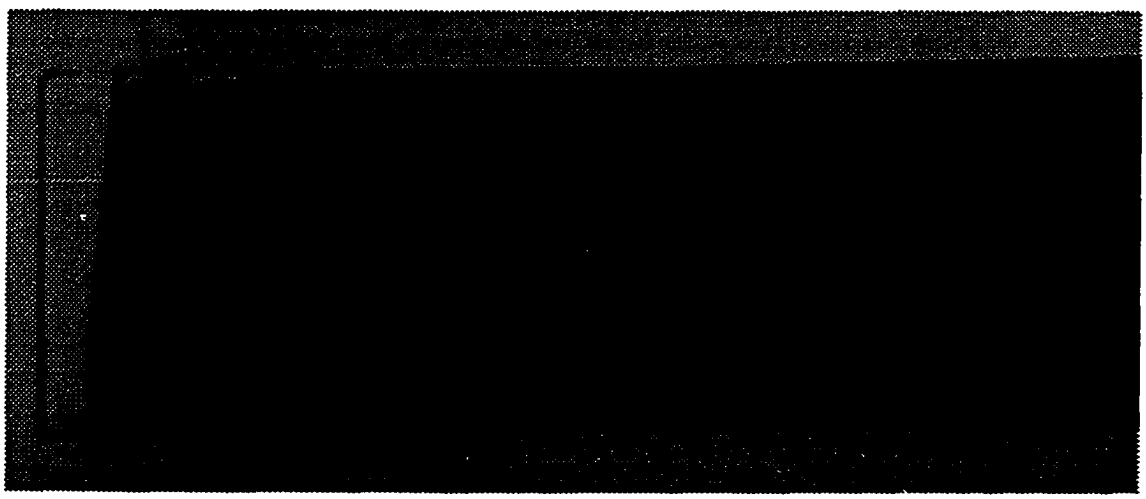

Figure 5.8 **Photograph of Au electrode resulting from adhesion test after modification procedure shown in Figure 5.7.**

different morphology than that observed for the film on bare Au. A very smooth surface was routinely observed by SEM, and higher resolution images revealed the presence of polymer nuclei averaging ca. 80 nm in diameter. The cause and effect relationship between polymer morphology and the resulting tenacious adherence of the poly(pyrrole) films on pyrrole-terminated SAM modified Au substrates is not entirely understood at this time. A likely explanation for the increased adherence is the coupling of surface-confined monomers to solution-phase monomers thereby providing direct covalent linkages between growing polymer chains and the underlying surface. This in turn could provide a smoother, more homogenous surface for the nucleation and growth of poly(pyrrole) chains resulting in a more compact and adherent film. Rubinstein et al. noted an increase in the conductivity of poly(aniline) films deposited on monomer-modified Au electrodes[22] and attributed the changes to the formation of a polymer film with less free volume.

5.7 Conclusions

Microscopic investigation of the pyrrole-terminated monolayers did not achieve the initial goals set for the project, but did provide useful fundamental and technological information. The determination of surface contaminants present on the monomer films has important implications for the fabrication of small features under the ambient conditions employed in this study. Confirmation of the ability of pyrrole-terminated SAMs to effectively increase the adhesion of thick poly(pyrrole) films was a technologically important discovery as adherence of a polymer layer to its underlying substrate is a critical issue in the fabrication of sensors and other thin-film devices.

Figure 5.9 **SEM image of a 1 μm-thick poly(pyrrole) film deposited on a bare Au electrode.**

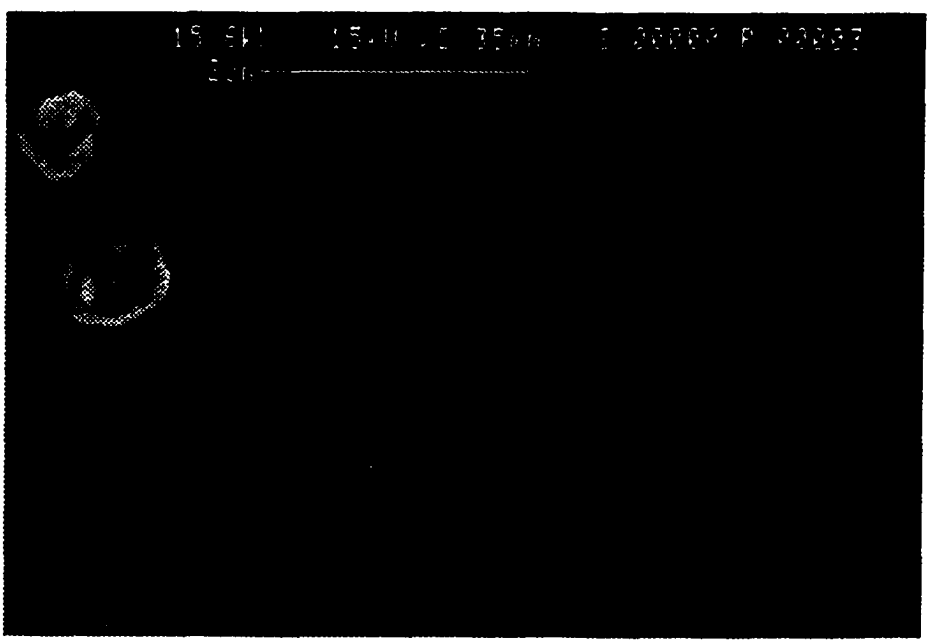

Figure 5.10 **SEM image of a 1μm-thick poly(pyrrole) film on a PyC_6SH-modified Au electrode.**

5.8 References

1) Binnig, G.; Rohrer, H.; Gerber, C.; Weibel, E. *Phys. Rev. Lett.* **1982**, *49*, 57.

2) Jaklevic, R. C.; Lambe, J. *Phys. Rev. Lett.* **1966**, *17*, 1139.

3) Young, R.; Ward, J.; Scire, R. *Rev. Sci. Instrum.* **1972**, *43*, 999.

4) Chidsey, C. E. D.; Liu, G.-Y.; Rowntree, P.; Scoles, G. *J. Chem. Phys.* **1989**, *91*, 4421.

5) Strong, L.; Whitesides, G. M. *Langmuir* **1988**, *4*, 546.

6) Widrig, C. A.; Alves, C. A.; Porter, M. D. *J. Am. Chem. Soc.* **1991**, *113*, 2805.

7) Poirier, G. E.; Pylant, E. D. *Science* **1996**, *272*, 1145.

8) Kim, Y.-T.; McCarley, R. L.; Bard, A. J. *J. Phys. Chem.* **1992**, *96*, 7416.

9) Zhang, H.; Hordon, L. S.; Kuan, S. W. J.; Maccagno, P.; Pease, R. F. W. *J. Vac. Sci. Technol. B.* **1989**, *7*, 1717.

10) Heckl, W. M.; Smith, D. P. E. *J. Vac. Sci. Technol. B* **1991**, *9*, 1159.

11) Tang, S. L.; Alistair, J. M.; Suna, A. *Jpn. J. Appl. Phys.* **1994**, *33*, L466.

12) Sprik, M.; Delamarche, E.; Michel, B.; Röthlisberger, U.; Klein, M. L.; Wolf, H.; Ringsdorf, H. *Langmuir* **1994**, *10*, 4116.

13) Green, J.-B.; McDermott, M. T.; Porter, M. D.; Siperko, L. M. *J. Phys. Chem.* **1995**, *99*, 10960.

14) Chidsey, C. E. D.; Loiacono, D. N.; Sleater, T.; Nakahara, S. *Surf. Sci.* **1988**, *200*, 45.

15) McCarley, R. L.; Dunaway, D. J.; Willicut, R. W. *Langmuir* **1993**, *9*, 2775.

16) Edinger, K.; Gölzhäuser, A.; Demota, K.; Wöll, C.; Grunze, M. *Langmuir* **1993**, *9*, 4.

17) Salmeron, M.; Folch, A.; Neubauer, G.; Tomitori, M.; Ogletree, D. F. *Langmuir* **1992**, *8*, 2832.

18) Hayes, W. A.; Kim, H.; Yue, X.; Perry, S. S.; Shannon, C. *Langmuir* **1997**, *13*, 2511.

19) Meyer, G.; Amer, N. M. *Appl. Phys. Lett.* **1990**, *57*, 2089.

20) Frisbie, C. D.; Rozsnyai, L. F.; Noy, A.; Wrighton, M. S.; Lieber, C. M. *Science* **1994**, *265*, 2071.

21) Simon, R. A.; Ricco, A. J.; Wrighton, M. S. *J. Am. Chem. Soc.* **1982**, *104*, 2031.

22) Rubinstein, I.; Rishpon, J.; Sabatani, E.; Redondo, A.; Gottesfeld, S. *J. Am. Chem. Soc.* **1990**, *112*, 6135.

23) Kumar, A.; Biebuyck, H.; Abbott, N. L. *J. Am. Chem. Soc.* **1992**, *114*, 9188.

Chapter 6

Conclusions and Future Directions

The successful synthesis, characterization, and application of a new class of self assembling molecules has been realized in this thesis. Modification of pyrrole at the *N*-position with an ω-bromoalkane followed by conversion of the bromide to a thiol was performed using thiourea as a nucleophile. This method resulted in a clean, efficient route to the formation of several ω-(*N*-pyrrolyl)alkanethiol analogues while avoiding concurrent formation of unwanted disulfides. The analogues contained different numbers of carbon atoms (methylene groups) between the pyrrole tailgroup and the thiol headgroup so as to allow examination of the effects of increased order in the monolayer films on Au due to differences in the degree of van der Waals interactions.

The new monomer-containing molecules were tested for their ability to form self-assembled monolayers (SAMs) on Au electrode surfaces. Initial studies of the surface-confined monomers were carried out using electrochemical techniques. Cyclic voltammetry first confirmed the ability of the bulk *N*-substituted pyrrole thiols to undergo electrochemical oxidation in non-aqueous electrolyte solution to form a conducting organic polymer - proof that the substituted monomer was still capable of polymerization. Electrochemistry was performed on SAM films of all the various chain length pyrrole thiol analogues on Au. Voltammograms from those experiments indicated irreversible electrochemical oxidation of the monomer units in the film. Analysis of the polymer doping/de-doping region for the electrochemically oxidized monolayers using carefully dried electrolytes revealed the presence of currents

attributable to polymer doping and de-doping. This was the first report of a conducting organic polymer formed from a monolayer of monomer-containing molecules attached to a Au surface through self-assembly.

Three additional electrochemical studies lent strength to the proposed coupling of monomer units in the monolayers to form polymer films. The first experiment established the fact that electrochemically oxidized ω-(*N*-pyrrolyl)alkanethiol monolayers were much more resistant to desorption from the Au surface than pristine monolayers. Second, oxidation of the monomer was possible even at low surface concentrations and in the presence of electroinactive, surface-confined molecules while polymer formation was readily quenched by high concentrations of these diluents. Finally, electrochemical oxidation of the surface-confined monomer monolayer in the presence of the potent nucleophile pyridine resulted in no polymer formation. Such observations have been noted in experiments involving oxidation of pyrrole monomer in the presence of pyridine.[1] These studies indicated that pyridine could couple with the pyrrole radical cations electrochemically generated in solution to form nonconductive polymer films through several mechanisms. On the basis of this latter result and the first two experiments, it was concluded that monomeric units in the film indeed couple together to give conducting organic polymer or oligomer.

After electrochemical characterization, infrared reflection-absorption spectroscopy (IRRAS) and X-ray photoelectron spectroscopy (XPS) techniques were utilized to elucidate the structure of the pyrrole units in the monolayers before and after polymerization. Comparison of reflection-absorption (RA) and transmission IR spectra was performed and indicated that the pyrrole rings confined to the surface were very

isotropic. IRRAS studies demonstrated that all absorbance bands associated with the pyrrole ring appeared to disappear upon complete electrochemical oxidation of the monolayers. It was expected that band shifts and intensity changes for the pyrrole modes would occur, not the complete loss in band intensity that was observed. A possible explanation for the complete loss of intensity of the pyrrole bands was sought. The desorption of the monomers from the electrode surface (which would yield no infrared absorption intensity) was examined by collecting infrared spectra of electrochemically oxidized pyrrole-terminated monolayers that were subsequently exposed to oxygen. The presence of a large infrared absorption in the region of the spectrum expected for a carbonyl mode was noted. The presence of this band is contraindicative of monomer desorption because this band could only result from oxidation of aromatic C-H groups present on the pyrrole ring in the monolayer. X-ray photoelectron spectra confirmed the presence of the pyrrole monolayer after electrochemical oxidation. No loss was noted for either the N_{1s} or S_{2p} photoelectron bands for pyrrole-terminated thiol monolayers on Au after complete electrochemical oxidation.

Another explanation for the complete loss of all infrared absorbtion based on orientational changes of the pyrrole ring with respect to the substrate was proposed and subsequently discarded. Due to the infrared surface selection rules for reflection-absorption spectroscopy (Chapter 4), certain orientations of the pyrrole ring could result in no observable absorption intensity for transitions that are intense when probed with transmission IR. This was not the case for the pyrrole-terminated monolayer systems described here. As previously mentioned, comparison of transmission

(isotropic) and reflectance spectra indicated the same relative band ratios pointing to a very randomly-ordered system. In addition, IR modes that are orthogonal to each other on the pyrrole ring were found to decrease in intensity to the same degree. This is strong evidence that orientational changes are not responsible for the observed intensity losses.

Arguments were developed to explain the decrease in infrared band intensities in terms of differences in conductivity of short vs. long polymer chains. It was assumed that perhaps the extended charge delocalization present in long polymer strands could result in a decreased infrared absorption cross-section for the individual pyrrole units. Partial electrochemical oxidation of the pyrrole-terminated monolayers was performed to generate oligomeric species. These oligomers showed the expected blue-shifted $\omega_{C\text{-}H}$ band for the pyrrole groups while undoped oligomers (similarly prepared) did not. In addition, an α,α'-dimethyl-blocked pyrrole alkanethiol monolayer was synthesized and used to establish a spectroscopic benchmark for molecules incapable of forming long chains (short oligomers). Spectroscopic behavior virtually identical to that previsouly noted for the unblocked oligomer monolayers was observed.

Spectroscopic data was unable to provide direct, conclusive evidence of monomer-coupling in the pyrrole-terminated SAMs. All the experimental data was, however, consistent with this type of mechanism. All the possible alternate mechanisms that could explain the electrochemical data were evaluated and found not to be in accord with the data.

Future spectroscopic analyses of these systems could be improved by using a combination of IRRAS and attenuated total reflectance infrared (ATR-IR) techniques.

A report by Dimilla et al.[2] has shown the ability of alkanethiol SAMs to form high-quality films on thin (5-10 nm) Au films. Liley et al.[3] recently reported the application of such ultrathin Au films coated on a germanium internal reflection element in the study of a novel thiol SAM. They were able to determine the orientation of several vibrational modes of the surface-confined molecules. One particularly important advantage of the use of ATR-IR in the analysis of organic thin films is its ability to probe vibrational modes parallel to the plane of the surface,[4] transitions which are unobservable using IRRAS. Using this complementary spectroscopic approach, the previously mentioned possibility of chain reorientation parallel to the Au surface (causing complete intensity loss in the IRRAS experiment) could be effectively discounted. In addition, ATR-IR is very amenable to in-situ analyses. The application of in-situ ATR-IR to the electrochemical oxidation of the pyrrole monolayers could be useful for monitoring the change in the pyrrole endgroup as a function of polymerization conditions.

Another way to address the question regarding surface-confined polymer formation would be to use mass spectroscopic techniques. McCarley and McCarley[5] have recently reported the electrospray ionization mass spectroscopy (ESIM) spectra of ω-terminated alkanethiolates in solution. Successful development of this methodology could enable the quantitative analysis of polymeric SAM films. Electrochemical desorption of our pyrrole-based polymer[6] followed by mass spectral analysis could confirm monolayer polymerization and give a molecular weight distribution.

Microscopic investigations of the SAMs were also carried out but were found to be less fruitful than initially hoped. Scanning probe microscopy (SPM) methods were unable to resolve the molecular structure of the SAMs. Surface contamination of the air-sensitive monomeric and polymeric monolayers was proposed as the problem due in no small part to the fact that both ambient and inert atmosphere conditions yielded identical images. Through the use of scanning tunneling microscopy (STM) and lateral force microscopy (LFM), surface contamination was found to exist and was determined to be the probable cause of our inability to characterize SAMs on the molecular scale using these methods. Contamination also precluded the use of these SAMs as templates for small conducting feature, i.e. "molecular wire", formation *in air* using the STM. It is our belief that achievement of these microscopic goals is still possible using SPM techniques. The use of STM under liquids has been demonstrated by others and could be used both to keep the surface clean and provide an environment for solution-phase redox mediators useful for the surface-confined electrochemical polymerization reaction.

In addition the fundamental investigations described above, a technological use of ω-(*N*-pyrrolyl)alkanethiol monolayers on Au surfaces was developed. These monolayers were found to increase the adhesion of thick poly(pyrrole) films on Au surfaces. This represents an improvement in our ability to create novel, stable surfaces using thick conducting polymer films. A possible future application of these monolayers could be as selective barriers to solution-phase anions. Hsueh and Brajter-Toth[7] have shown that relatively thin films (several monolayers thick) of overoxidized poly(pyrrole) on carbon and platinum electrodes could selectively bar anions from

entering the film (and thus approaching the underlying surface). Overoxidation of the thin pyrrole-containing films described in this work has been readily accomplished and could thus lead to the thinnest permselective coating for the retardation of anion approach on a Au substrate.

6.1 References

1) Rosseinsky, D. R.; Morse, N. J.; Slade, R. C. T.; Hix, G. B.; Mortimer, R. J.; Walton, D. J. *Electrochim. Acta* **1991**, *36*, 733.

2) DiMilla, P. A.; Folkers, J. P.; Biebuyck, H. A.; Härter, R.; López, G. P.; Whitesides, G. M. *J. Am. Chem. Soc.* **1994**, *116*, 2225.

3) Liley, M.; Keller, T. A.; Duschl, C.; Vogel, H. *Langmuir* **1997**, *13*, 4190.

4) Ulman, A. *An Introduction to Ultrathin Organic Films from Langmuir-Blodgett to Self-Assembly*; Academic: San Diego, 1991.

5) McCarley, T. D.; McCarley, R. L. *Anal. Chem.* **1997**, *69*, 130.

6) Walczak, M. M.; Popenoe, D. D.; Deinhammer, R. S.; Lamp, B. D.; Chung, C.; Porter, M. D. *Langmuir* **1991**, *7*, 2687.

7) Hsueh, C.; Brajter-Toth, A. *Anal. Chem.* **1994**, *66*, 2458.

Vita

Robert J. Willicut was born on Shepherd Air Force Base in Wichita Falls, Texas. After brief tours of duty in Turkey and Washington as a child, he spent his grade-school years in Wichita Falls. He went to junior high and high school in Odessa, Texas, and attended college at Angelo State University where he earned a Bachelor of Science degree in Chemistry in May 1992. He is currently at Louisiana State University completing the requirements to receive his Doctor of Philosophy degree in Chemistry. He is married to a lovely wife, Jennifer, and has the world's most wonderful little boy, Jeffrey Ryan.

DOCTORAL EXAMINATION AND DISSERTATION REPORT

Candidate: Robert J. Willicut

Major Field: Chemistry

Title of Dissertation: Characterization of Monomer-Containing Monolayer Films on Au Surfaces

Approved:

Major Professor and Chairman

Dean of the Graduate School

EXAMINING COMMITTEE:

Date of Examination:

October 7, 1997

IMAGE EVALUATION TEST TARGET (QA-3)

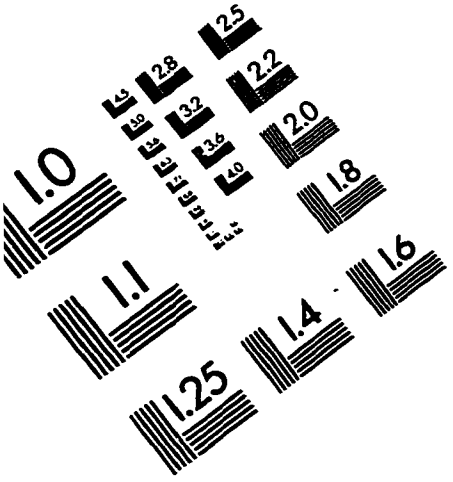

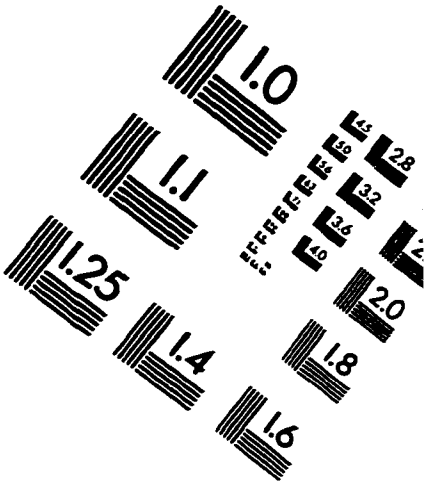

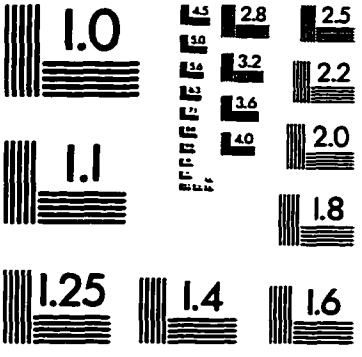

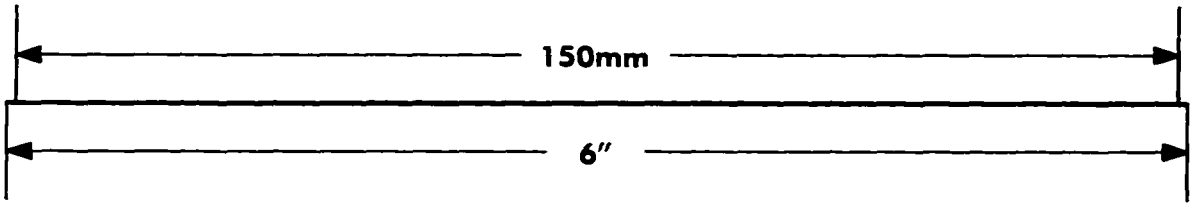

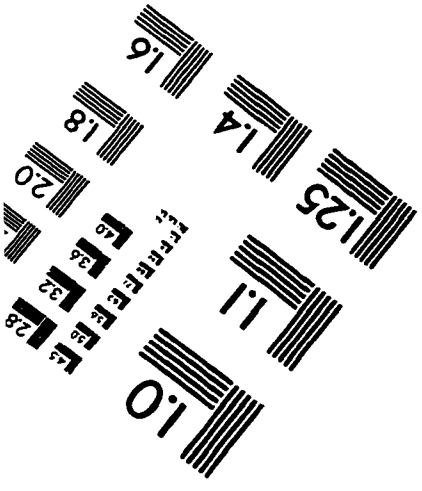

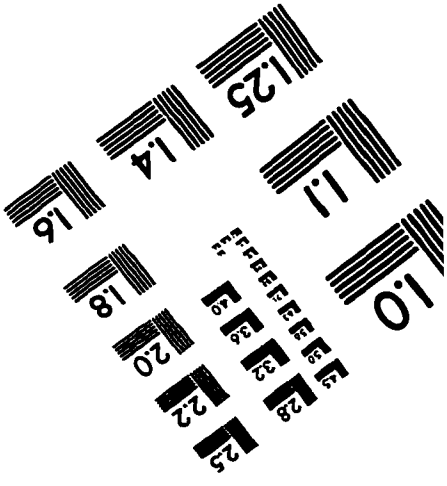

APPLIED IMAGE, Inc
1653 East Main Street
Rochester, NY 14609 USA
Phone: 716/482-0300
Fax: 716/288-5989